Diffusion and Stress Driven Flow in Polymers

Thesis by

Catherine Kent Hayes

In Partial Fulfillment of the Requirements

for the Degree of

Doctor of Philosophy

California Institute of Technology

Pasadena, California

1990

(Submitted April 20, 1990)

Acknowledgments

I would like to thank my adviser, Dr. Donald Cohen, for his unfailing help and encouragement. I must also thank Robert McLachlan, Rachel Shinn-Mendoza, Vidyadhar Mudkavi, Dana Hobson, and Vered Rom for their many helpful suggestions.

I am grateful to Bob Cox for permission to use the material in an unpublished paper.

Caltech has supported me throughout my time in graduate school with Graduate Teaching and Research Assistantships. I am grateful for the Institute's support.

I would like to dedicate this thesis jointly to my parents, Ellen and Thomas Hayes, for their unfailing love and support, and to my husband, Jeffrey Yu, who has been both an encouragement and an example to me during all my (many) years at Caltech.

Abstract

A recently proposed model for non-Fickian diffusion of penetrants into polymers is adapted and used to study a drug-delivery problem. The model modifies Fick's diffusion equation by the addition of stress-induced flux and a bimolecular reaction term. A stress evolution equation incorporating aspects of the Maxwell and Kelvin-Voigt viscoelastic stress models completes the model. The diffusivity and relaxation time in the polymer are taken as functions of the penetrant concentration.

The system is first studied on a doubly infinite domain under the assumption that the penetrant's saturation concentration is small. When the diffusivity and relaxation time are taken to be constant, a perturbation analysis is used to show the form and the region of stability of traveling-wave solutions. When the diffusivity and relaxation time are taken as specified functions of the concentration, the shapes of traveling-wave solutions are predicted by perturbation analysis and found to be different when the equations are diffusion-driven than when they are stress-driven. The predictions are verified by numerical integration for specified parameter values.

The system is also studied on a finite domain under the assumption that the diffusivity is large. A perturbation analysis is used to demonstrate that the concentration and stress evolve according to a Fickian diffusion equation on a short time scale. After longer time has elapsed, the concentration and stress are shown to exhibit steep fronts in a narrow region within the domain. These predictions are verified numerically. Finally, the equations are studied in the steady state and are found to predict the evolution of shocks.

Work done on Fisher's equation is presented in an appendix. When the diffusivity is taken in the same nonlinear form as was used in the polymer-penetrant model, a qualitatively new solution of Fisher's equation is found, using a method which is also applied to the polymer-penetrant system.

Contents

List of Figures

List of Tables

Chapter 1

Introduction

Systems in which molecules diffuse through polymers exhibit interesting and varied behavior. In many cases, the evolution of these systems cannot be described accurately by Fick's familiar diffusion equation,

$$\frac{\partial C}{\partial T} = \nabla \cdot (D \nabla C).$$

Since growing numbers of real-world uses for non-Fickian systems are being found [1,7,8,12], understanding these non-Fickian systems is increasingly important. To study such a system, one must first determine what physical mechanisms are causing its non-Fickian behavior. One then designs a mathematical model incorporating the physical mechanisms, and uses analytical and numerical methods to examine the model.

One area in which polymer-penetrant systems have been and continue to be used is that of controlled delivery of drugs therapeutic to humans [17]. Such systems, in which a specified amount of the drug diffuses through a polymer into the bloodstream, have great advantages over the more common drug-delivery systems. Controlled-delivery systems allow the optimum concentration of the drug to circulate through the body for a long period of time, while pills and injections release a burst of medicine when they are swallowed or injected, followed by a rapid drop-off

in concentration. In this thesis, we will study a set of equations that model some of the principal characteristics of polymer-penetrant drug-delivery systems.

1.1 Derivation of Equations

If we let $C(\underline{X},T)$ be the concentration of a given substance in a medium at position $\underline{X}$ and time T, then the flux $\underline{J}$ at $\underline{X}$ is

$$\underline{J}(\underline{X},T) = -D\nabla C, \tag{1.1}$$

where D is the diffusivity of the substance in the medium. This flux is balanced by the change in concentration in time,

$$\frac{\partial C}{\partial T} = -\nabla \cdot \underline{J}.$$

If we combine these two equations, we find a single equation for $C(\underline{X},T)$:

$$\frac{\partial C}{\partial T} = \nabla \cdot (D\nabla C). \tag{1.2}$$

Equation (1.2), known as Fick's diffusion equation, is based on the postulate that the flux is simply proportional to the concentration gradient, as in (1.1). Systems described by equation (1.2) are called Fickian systems, and equation (1.2) provides an accurate description of a system if the medium itself offers no encouragement or impediment to the diffusing substance. In the case when the medium is a polymer with a complicated internal structure of twisting channels, equation (1.2) may no longer be accurate [1,7,8,12,22,23]. Many polymer-penetrant drug-delivery systems exhibit non-Fickian behavior [17], so we must alter equation (1.2) in order to better describe these systems.

Thomas and Windle [22,23] have made the fundamental observation that in many polymer-penetrant systems, especially at or near the glass transition, the diffusive

process is coupled to a mechanical viscoelastic response. Based on this observation, a mathematical model has been proposed by Cohen, Cox, and White [4,5,6]. We adopt that model here, with appropriate modifications for our problem. A brief presentation of their model follows.

As penetrant molecules crowd into a section of the polymer, they exert pressure at various sites, and penetrant is pushed toward less-crowded areas of the polymer. The effect of this stress-induced flux is to modify the Fickian flux (1.1), so that the total flux J becomes

$$J = -(DC_X + E\sigma_X). \tag{1.3}$$

Here $\sigma \geq 0$ is the viscoelastic stress and E is a viscoelasticity coefficient. A subscript is used to denote partial differentiation. Both D and E can take on widely varying functional forms. Note that expression (1.3) contains derivatives with respect to X only; throughout this work, we will look for planar motion, with change occurring in the X-direction only.

The interaction of penetrant molecule and polymer is taken to be a reversible bimolecular reaction: an empty site in the polymer "reacts" with a molecule of penetrant to form a site-molecule complex. If the molecule is large and the site small, the site-molecule complex may be quite a stable construct. Since a large increase in concentration behind the complex will push the molecule out, the reaction is a reversible one. The bimolecular reaction is modeled on a macroscopic level by

$$R(C) = \mu C(k - C), \tag{1.4}$$

where k is the saturation concentration of the penetrant in the polymer and the parameter μ controls the strength of the "reaction."

If we substitute the two expressions (1.3) and (1.4) into the mass balance equation

$$C_T = -J_X + R(C),$$

we obtain an evolution equation for $C(X,T)$:

$$C_T = (DC_X + E\sigma_X)_X + \mu C(k - C). \tag{1.5}$$

We now need an evolution equation for the viscoelastic stress σ. If we model the polymer as a system of springs and dashpots, we can complete the mathematical system with the fairly general equation

$$\sigma_T + \beta\sigma = F(\varepsilon, \varepsilon_T),$$

where ε is the strain and $1/\beta$ is the relaxation time of the system. This equation combines the standard Maxwell and Kelvin-Voigt viscoelasticity models [18]. If we take $\varepsilon \propto C$, we find

$$\sigma_T + \beta\sigma = f(C, C_T). \tag{1.6}$$

The function $f(C, C_T)$ can take on many forms, simple or complicated, depending on the geometric configuration of the polymer, the type of penetrant, and other physical attributes of the system. Since we are defining σ as a scalar quantity, we require

$$\sigma(X,T) \geq 0 \ \forall X, T.$$

Equations (1.5) and (1.6), taken together, form a complete system of evolution equations for $C(X,T)$ and $\sigma(X,T)$.

β, the inverse of the relaxation time, is in many important cases a function of the penetrant concentration C. When the concentration is below a certain threshold value, the polymer is said to be in a *glassy* state. When it is in this state, the effects of any disturbance take a long time to die away; the disturbed polymer relaxes to its undisturbed state very slowly. At concentrations above the threshold value, the polymer relaxes quickly to its undisturbed state after a disturbance and is said to be in a *rubbery* state. The relaxation time $1/\beta$ is accordingly large for C below

threshold and small for C above threshold. In many polymer-penetrant systems the rubbery and glassy relaxation times differ by several orders of magnitude.

Equations (1.5) and (1.6), together with appropriate initial and boundary conditions, constitute a well-posed system of differential equations. We note that it is possible to eliminate the stress σ from these equations and write a single integrodifferential equation for C,

$$C_T = (DC_X)_X + \left[E\left(\int_0^T e^{-\int_\tau^T \beta(C(X,q))dq} f(C, C_\tau)d\tau\right)_X\right]_X + \mu C(k - C).$$

We see explicitly from this equation that when β is large (the system is in its rubbery state), the effects of a disturbance disappear rapidly; when β is small so that the system is in its glassy state, the effects of a disturbance linger for some time.

1.2 Discussion of Equations

We will study equations (1.5) and (1.6) in two different domains. In Chapter 2, we will look for traveling-wave solutions of the equations on the domain $-\infty < X < +\infty$. In Chapter 3, we will examine the equations on a finite domain.

Traveling-wave solutions of the equations are solutions of the form $C = C(Z)$, $\sigma = \sigma(Z)$, where $Z \equiv X - VT$ and V is the (constant) speed of the wave. We are interested in these solutions for two reasons. Because ideally a polymer-penetrant drug-delivery system should send out a constant concentration of drug at a constant speed to be most effective, we would like our model to have solutions that travel as a set profile at a constant speed. Furthermore, if we consider a dry, finite block of polymer into which a wavefront of penetrant at saturation concentration is moving from one end, we see that it is very likely that all the complicated and interesting behavior takes place at the front, with the regions behind and ahead of the front simply in saturated, rubbery state and dry, glassy state respectively. In this case, one

method of analysis at the front would be to define locally a new length variable ξ so that the front region would be stretched over the domain $-\infty < \xi < +\infty$. We would then seek traveling-wave solutions as functions of ξ and T, with boundary conditions that would match the solutions at the front to the conditions outside the front when the distance variable was shrunk to the original X. In the context of singular perturbation theory, the traveling wave in stretched variables often constitutes the so-called boundary layer expansion.

In Chapter 2, we will use a perturbation analysis to study equations (1.5) and (1.6). The small parameter we will use is the nondimensionalized saturation concentration. We will find that traveling waves which satisfy $C(-\infty) = k$ and $C(+\infty) = 0$ exist for a variety of special cases of the equations if the nondimensionalized saturation concentration is small enough.

The first and simplest case we will examine is one in which all three of the coefficients D, E, and β are taken to be constant. We will examine two different models for the stress evolution: Model A,

$$\sigma_T + \beta\sigma = aC_T, \; a \text{ a constant},$$

and Model B,

$$\sigma_T + \beta\sigma = bC, \; b \text{ a constant},$$

and will obtain qualitatively different solution curves for the two models. In addition, we will examine the stability of the solution curves to small perturbations. We will then study both models under the more realistic conditions

$$D(C) = \frac{D_R + D_G}{2} + \frac{D_R - D_G}{2} \tanh \frac{C - C_{RG}}{\Delta C},$$

as shown in Figure 1.1, and

$$\beta(C) = \frac{\beta_R + \beta_G}{2} + \frac{\beta_R - \beta_G}{2} \tanh \frac{C - C_{RG}}{\Delta C},$$

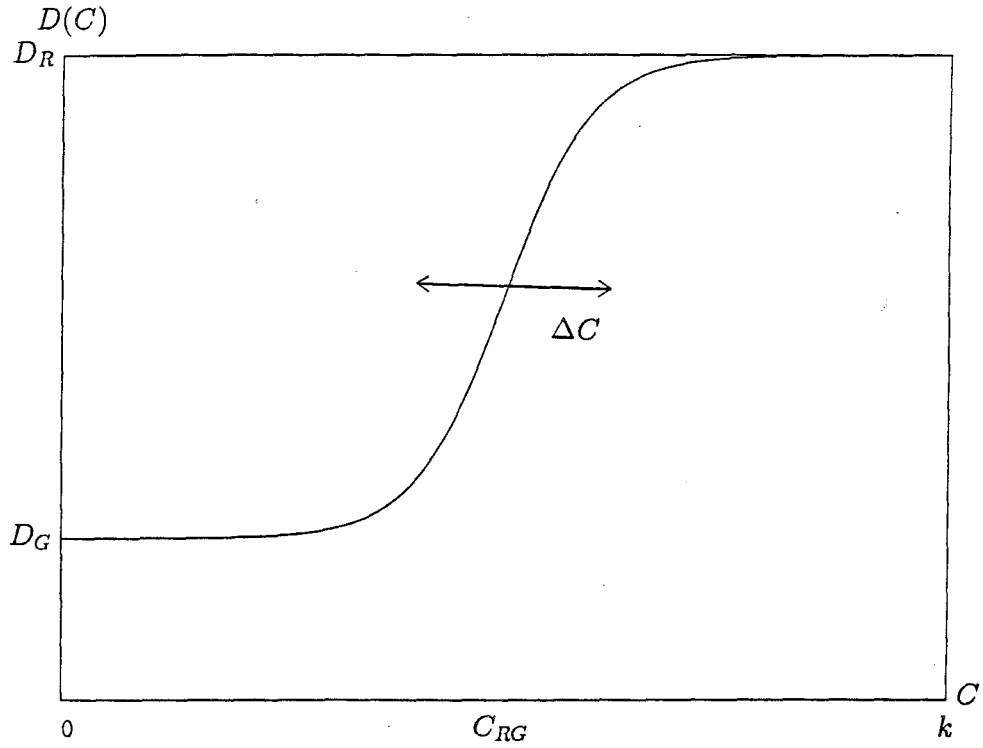

Figure 1.1: Diffusivity $D(C) = \frac{D_R+D_G}{2} + \frac{D_R-D_G}{2} \tanh \frac{C-C_{RG}}{\Delta C}$

as shown in Figure 1.2. Here the positive parameter ΔC is taken to be very small with respect to C_{RG}. The quantity C_{RG} is the concentration around which the polymer undergoes its glass–rubber transition; we take $C_{RG} < k$. Use of the profile for β shown in Figure 1.2 has been justified above. It seems feasible to take a similar form for D since we are considering a physical system in which very little happens except at the transition between the polymer's rubbery and glassy states; thus, we set the diffusivity to be nearly constant except near the critical value of C, C_{RG}. We will study equations (1.5) and (1.6) using perturbation methods and solve them numerically for various parameter values, and we will note the effects on the solutions of *stress driving*, in which, after nondimensionalization, $E \gg D_R$, and of *diffusion driving*, in which, after nondimensionalization, $E \ll D_R$.

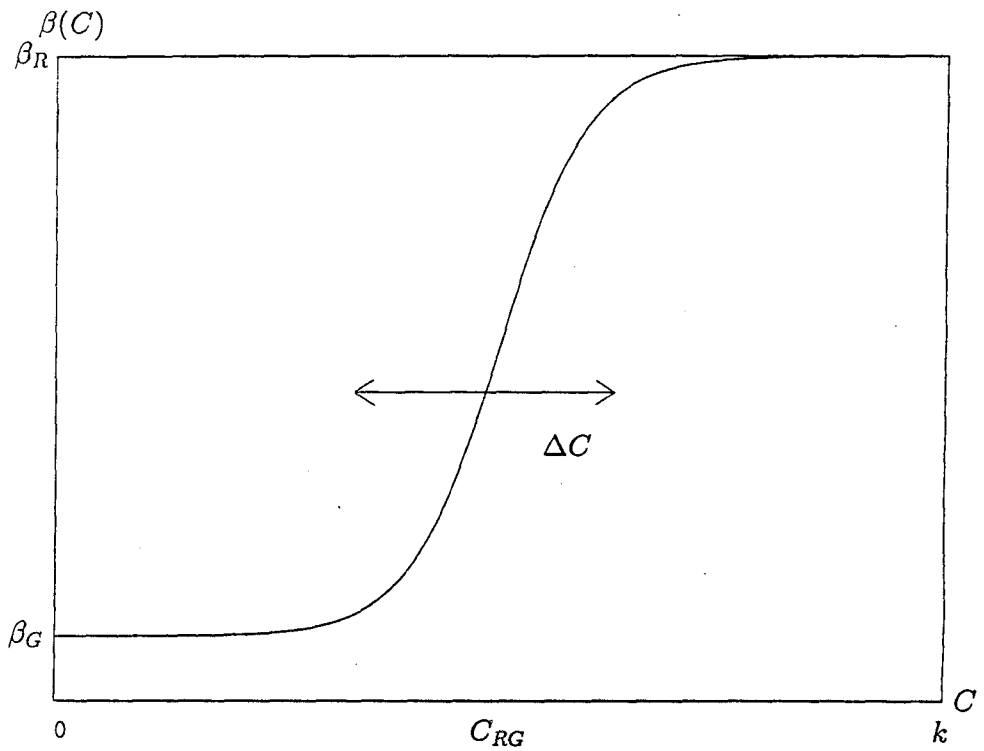

Figure 1.2: (Relaxation time)$^{-1}$ $\beta(C) = \frac{\beta_R+\beta_G}{2} + \frac{\beta_R-\beta_G}{2} \tanh \frac{C-C_{RG}}{\Delta C}$

In Chapter 3, we will consider the behavior of the equations on a finite domain $0 < X < L$, with the initial conditions $C(X,0) = \sigma(X,0) = 0$ and the boundary conditions $C(0,T) = C_0$, $C(L,T) = C_1$. This model covers polymer-penetrant drug-delivery systems in which a reservoir of the drug is placed at one end of a dry block of polymer and the drug diffuses through the block. If the drug is carried quickly away in the blood as soon as it leaves the end of the polymer block opposite the reservoir, then this opposite end of the block can be thought of as drawing on a "reservoir" of drug with zero concentration. If, on the other hand, the bloodstream carries the drug away so slowly that there is always drug built up at the end of the block opposite the reservoir, then we can consider a system with reservoirs of nonzero concentration at both ends of the block as a step towards a good model of the physical system.

Our intention in Chapter 3 is to discover the concentration and stress profiles that emerge when $\beta(C)$ is as in Figure 1.2 and the function $f(C, C_T)$ in equation (1.6) is chosen to combine C and $\partial C/\partial T$, so that σ evolves according to

$$\sigma_T + \beta\sigma = aC_T + bC,$$

where a and b are constants. This model allows σ to exhibit different responses to rapid change and gradual change in C. If C rises swiftly to a value C_0, (as will happen for small times in our system near $X = 0$ and $X = L$ when the penetrant starts to flow through the dry polymer), the terms σ_T and aC_T will dominate, so σ will rise swiftly to aC. If C continues to evolve, more slowly, after its initial rapid rise, σ will evolve gradually to $bC/\beta(C)$ [5,9].

For our analysis in Chapter 3, we take $\mu = 0$ in equation (1.5) in order that we may compare our results to the solutions found by Cohen and White [4], who examined this system with $a = 0$. As in their paper, we will take D and E as constants, and we will scale the equations so that the nondimensionalized analogue of both D and E is a single parameter, d. We will study the equations for large d. Using perturbation expansion in the small parameter $1/d$ as well as numerical integration of the equations, we will show that the concentration and stress originally obey a Fickian diffusion law, but that, after a short time elapses, their profiles exhibit a sharp jump at an interior value of X. In addition to finding the time-dependent profiles of C and σ, we will find explicit long-time and steady-state solutions in the limiting case $\Delta C = 0$. These solutions are very easily obtained and are qualitatively similar to the solutions of the equations with $\Delta C \neq 0$ but $\Delta C \ll C$, found using numerical and perturbation-method techniques.

Chapter 4 contains conclusions and possible directions for future research.

In Appendix A we present analysis of Fisher's equation,

$$u_t = (d(u)u_x)_x + u(1-u),$$

where

$$d(u) = \frac{1+\omega}{2} + \frac{1-\omega}{2} \tanh \frac{u-u_0}{\Delta u}; \; \omega < 1; \; 0 < \Delta u \ll 1.$$

This function $d(u)$ is similar in shape to the function $D(C)$ shown in Figure 1.1. Fisher's equation is used in modeling biological systems [10,11,19] and has been studied with various functional forms for $d(u)$, although not, to our knowledge, with the form for $d(u)$ mentioned above. We find that, when the equation contains our form for $d(u)$, a qualitatively new traveling-wave solution u emerges. Our analysis of the equation makes use of the technique of setting $\Delta u = 0$ to gain information about the case $0 < \Delta u \ll 1$. The success of this analysis of Fisher's equation led us to try the same simplifying technique on equations (1.5) and (1.6).

Chapter 2

Traveling-Wave Solutions

We seek solutions of the form $C = C(Z)$, $\sigma = \sigma(Z)$, where $Z \equiv X - VT$ and the velocity V is constant, of the following system of equations:

$$\frac{\partial C}{\partial T} = \frac{\partial}{\partial X}\left(D(C)\frac{\partial C}{\partial X} + E\frac{\partial \sigma}{\partial X}\right) + \mu C(k - C) \tag{2.1}$$

$$\frac{\partial \sigma}{\partial T} = -\beta(C)\sigma + f\left(C, \frac{\partial C}{\partial T}\right). \tag{2.2}$$

Here

$C \equiv$ concentration

$\sigma \equiv$ stress

$D(C) \equiv$ diffusion coefficient

$E \equiv$ viscoelasticity coefficient

$k \equiv$ (small) amplitude of traveling wave
and saturation concentration of polymer

$\beta(C) \equiv$ inverse of polymer relaxation time

$\mu \equiv$ proportionality constant

$T \equiv$ time

$X \equiv$ distance.

In those sections of this chapter where we study the behavior of C and σ for D and β not constant, we take the functional forms

$$D(C) = \frac{D_R + D_G}{2} + \frac{D_R - D_G}{2} \tanh \frac{C - C_{RG}}{\Delta C}$$

and

$$\beta(C) = \frac{\beta_R + \beta_G}{2} + \frac{\beta_R - \beta_G}{2} \tanh \frac{C - C_{RG}}{\Delta C},$$

which were discussed in Chapter 1.

We are interested in traveling-wave solutions that drop monotonically from full solute saturation $C = k$ at $Z = -\infty$, to zero concentration at $Z = +\infty$. In order to compare concentration-forced and concentration rate-forced stress models, we will look at the two cases $f(C, C_T) = aC_T$ (Model A) and $f(C, C_T) = bC$ (Model B). These two models predict qualitatively different stress profiles. We will find small-amplitude (k small) traveling waves for each model with the diffusivity and relaxation time held constant (in which case we analyze the stability of the solutions we find), and also with the diffusivity and relaxation time varying with C.

2.1 Model A: Evolution of σ Forced by C_T

We begin by studying Model A, in which $f(C, C_T) = aC_T$. We first put equations (2.1) and (2.2) in nondimensional form. Using

$$\begin{aligned} C(X,T) &\equiv \frac{\beta_R}{\mu} u(x,t) \\ \sigma(X,T) &\equiv \frac{a\beta_R}{\mu} s(x,t) \\ x &\equiv \sqrt{\frac{\beta_R}{D_R}} X \\ t &\equiv \beta_R T, \end{aligned}$$

we find

$$u_t = (\delta(u)u_x)_x + \kappa s_{xx} + u(\gamma - u) \tag{2.3}$$

$$s_t = -B(u)s + u_t, \tag{2.4}$$

where subscripts are used to denote partial differentiation, and

$$\kappa \equiv \frac{Ea}{D_R}$$

$$\gamma \equiv \frac{\mu k}{\beta_R}.$$

Here

$$\delta(u) \equiv \frac{D(\beta_R u/\mu)}{D_R} = \frac{1+\omega_\delta}{2} + \frac{1-\omega_\delta}{2}\tanh\frac{u-\theta\gamma}{\gamma\Delta u}$$

and

$$B(u) \equiv \frac{\beta(\beta_R u/\mu)}{\beta_R} = \frac{1+\omega_B}{2} + \frac{1-\omega_B}{2}\tanh\frac{u-\theta\gamma}{\gamma\Delta u},$$

where

$$\omega_\delta \equiv \frac{D_G}{D_R} < 1;\ \omega_B \equiv \frac{\beta_G}{\beta_R} < 1;\ \theta \equiv \frac{C_{RG}}{k} < 1;\ \Delta u \equiv \frac{\Delta C}{k} \ll 1.$$

The functions $\delta(u)$ and $B(u)$ are sketched in Figure 2.1. Setting

$$z \equiv x - vt$$

with v a constant velocity, we find the system of ordinary differential equations

$$(\delta(u)u')' + \kappa s'' + vu' + u(\gamma - u) = 0 \tag{2.5}$$

$$vs' - vu' - B(u)s = 0, \tag{2.6}$$

where a prime denotes differentiation with respect to z. We seek a solution which drops from $u = \gamma$ at $z = -\infty$ to $u = 0$ at $z = +\infty$.

In all of the analysis in both this section and § 2.2, we will consider γ to be small. For the perturbation analysis of § 2.1.1 and § 2.2.1, γ is the small parameter. When we solve the equations numerically in § 2.1.2 and § 2.2.2, we take $\gamma = 0.1$.

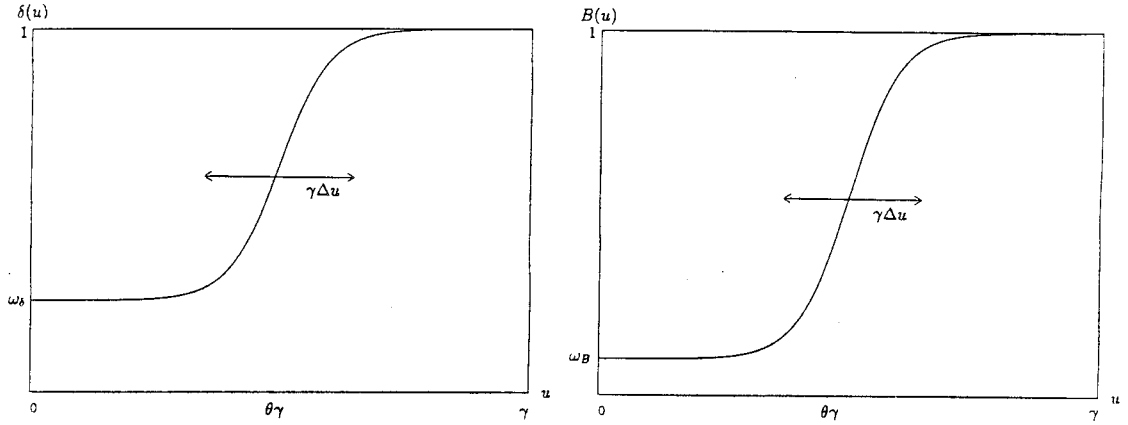

a: $\delta(u) = \frac{1+\omega_\delta}{2} + \frac{1-\omega_\delta}{2} \tanh \frac{u-\theta\gamma}{\gamma\Delta u}$ b: $B(u) = \frac{1+\omega_B}{2} + \frac{1-\omega_B}{2} \tanh \frac{u-\theta\gamma}{\gamma\Delta u}$

Figure 2.1: Coefficient functions $\delta(u)$ and $B(u)$

2.1.1 Case of Constant Coefficients

The first and simplest case we consider is the case in which $\delta(u) \equiv 1$ and $B(u) \equiv 1$. (In the original variables, this case corresponds to the polymer's diffusivity and relaxation time being held constant at their rubbery values.) We seek solutions $u_c(z)$ and $s_c(z)$ of

$$u_c'' + \kappa s_c'' + v u_c' + u_c(\gamma - u_c) = 0 \tag{2.7}$$

and

$$v s_c' - v u_c' - s_c = 0, \tag{2.8}$$

where the subscript c refers to the fact that $B(u)$ and $\delta(u)$ are now constant. We will find that, for γ small enough, we can solve equations (2.7) and (2.8) analytically, finding traveling-wave solutions for u_c and s_c as power series in γ.

To this end, we rescale equations (2.7) and (2.8) as follows:

$$\xi \equiv \gamma z, \; u_c(z) \equiv \gamma p(\xi), \; s_c(z) \equiv \gamma g(\xi). \tag{2.9}$$

The resulting equations are

$$\gamma p'' + \gamma\kappa g'' + v p' + p(1-p) = 0 \tag{2.10}$$

and

$$\gamma v g' - g - \gamma v p' = 0, \tag{2.11}$$

with boundary conditions

$$p(-\infty) = 1,\ p(+\infty) = 0,$$

where a prime now denotes differentiation with respect to ξ. We look for a solution expressed as a series in powers of the small quantity γ:

$$p(\xi) = p_0(\xi) + \gamma p_1(\xi) + \gamma^2 p_2(\xi) + \cdots = \sum_{n=0} \gamma^n p_n(\xi)$$

$$g(\xi) = g_0(\xi) + \gamma g_1(\xi) + \gamma^2 g_2(\xi) + \cdots = \sum_{n=0} \gamma^n g_n(\xi).$$

We insert these expansions into equations (2.10) and (2.11) and combine terms in like powers of γ:

$$v p_0' + p_0(1 - p_0) + \gamma[v p_1' + (1 - 2p_0)p_1 + p_0'' + \kappa g_0''] + O(\gamma^2) = 0$$

$$g_0 + \gamma(g_1 + v p_0' - v g_0) + O(\gamma^2) = 0.$$

If we set the coefficient of each power of γ separately to zero and apply the boundary conditions, we can solve the resulting equations for p_0, p_1, g_0, and g_1. We find

$$\begin{aligned} p_0(\xi) &= \frac{1}{1 + C_0 e^{\xi/v}},\ (C_0 > 0 \text{ a constant}) \\ g_0(\xi) &= 0 \end{aligned}$$

and

$$\begin{aligned} p_1(\xi) &= \frac{C_0 e^{\xi/v}}{v^2(1 + C_0 e^{\xi/v})^2}\left[\ln \frac{C_0 e^{\xi/v}}{(1 + C_0 e^{\xi/v})^2} + C_1\right],\ C_1 \text{ a constant} \\ g_1(\xi) &= \frac{C_0 e^{\xi/v}}{(1 + C_0 e^{\xi/v})^2}. \end{aligned}$$

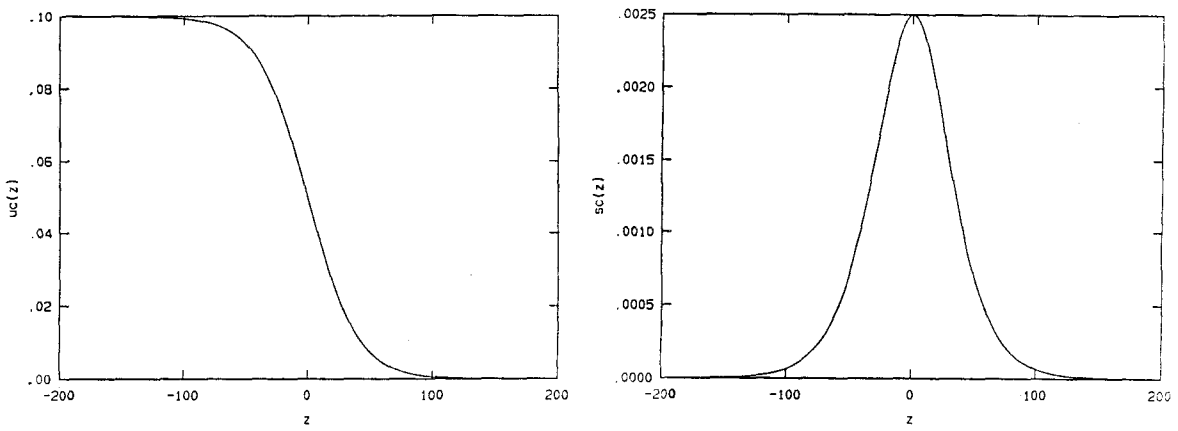

a: $u_c(z)$ b: $s_c(z)$

Figure 2.2: Constant-coefficient solutions $u_c(z)$ and $s_c(z)$

As functions of z, these solutions of equations (2.7) and (2.8) are

$$u_c(z) = \frac{\gamma}{1 + C_0 e^{\gamma z/v}} + \frac{\gamma^2 C_0 e^{\gamma z/v}}{v^2(1 + C_0 e^{\gamma z/v})^2}\left[\ln \frac{C_0 e^{\gamma z/v}}{(1 + C_0 e^{\gamma z/v})^2} + C_1\right] + O(\gamma^3) \qquad (2.12)$$

$$s_c(z) = \frac{\gamma^2 C_0 e^{\gamma z/v}}{(1 + C_0 e^{\gamma z/v})^2} + O(\gamma^3). \qquad (2.13)$$

Note that κ plays no role in the solutions before $O(\gamma^3)$. The solutions are graphed in Figure 2.2 with the parameter values $\gamma = 0.1$, $v = 2$, $C_0 = 1$, and $C_1 = \ln 4$.

We see that $u_c(z)$ drops monotonically from γ to 0, exactly as we wished. We see, also, that $s_c(z)$, the nondimensionalized stress, is localized to the relatively small domain in which $u_c(z)$ is noticeably different from γ or 0. As the wave of penetrant moves through the polymer, stress builds up at the front of the wave. Behind the wavefront, where the polymer is essentially saturated, the polymer will relax to a practically unstressed state. In addition, we see that, for all z,

$$s_c(z) \ll u_c(z).$$

In the original variables,

$$\frac{\sigma(X,T)}{aC(X,T)} \leq A\frac{\mu k}{\beta_R} = A\gamma,$$

where $A = O(1)$ is a constant.

We wish to examine the stability of the solutions above for increasing time; in particular, we would like to know if the solutions are stable to small perturbations for some values of κ and v and unstable for others. The functions found above,

$$u_c(x,t) \approx \frac{\gamma}{1 + C_0 e^{\gamma(x-vt)/v}} \tag{2.14}$$

$$s_c(x,t) \approx \frac{\gamma^2 C_0 e^{\gamma(x-vt)/v}}{(1 + C_0 e^{\gamma(x-vt)/v})^2}, \tag{2.15}$$

are solutions, to $O(\gamma)$ and $O(\gamma^2)$ respectively, of equations (2.7) and (2.8). We will carry out a linearized stability analysis of these solutions for t large, using a Laplace transform method [13].

With $B(u) \equiv \delta(u) \equiv 1$, equations (2.3) and (2.4) become

$$(u_c)_t = (u_c)_{xx} + \kappa(s_c)_{xx} + u_c(\gamma - u_c) \tag{2.16}$$

$$(s_c)_t = -s_c + (u_c)_t. \tag{2.17}$$

We first solve equation (2.17) for $s_c(x,t)$ to produce

$$s_c(x,t) = \int_0^t e^{-(t-\tau)} \frac{\partial}{\partial \tau} u_c(x,\tau) d\tau.$$

We substitute this solution into equation (2.16) and find

$$\kappa \frac{\partial^2}{\partial x^2} \left\{ \int_0^t e^{-(t-\tau)} \frac{\partial}{\partial \tau} u_c(x,\tau) d\tau \right\} = (u_c)_t - (u_c)_{xx} - u_c(\gamma - u_c). \tag{2.18}$$

If we differentiate equation (2.18) once with respect to t and substitute the right-hand side of equation (2.18) into the result, we find a third-order equation for $u_c(x,t)$:

$$(1+\kappa)(u_c)_{xxt} + (u_c)_{xx} - (u_c)_{tt} - (1-\gamma)(u_c)_t - 2u_c(u_c)_t + u_c(\gamma - u_c) = 0. \tag{2.19}$$

We find it easier to work in the traveling-wave frame, so we substitute

$$z \equiv x - vt,\ u_c(x,t) \equiv \overline{u}_c(z,t)$$

into equation (2.19) to find

$$-v(1+\kappa)(\overline{u}_c)_{zzz} + (1+\kappa)(\overline{u}_c)_{zzt} + (1-v^2)(\overline{u}_c)_{zz} + 2v(\overline{u}_c)_{zt} - (\overline{u}_c)_{tt}$$

$$+ v(1-\gamma)(\overline{u}_c)_z - (1-\gamma)(\overline{u}_c)_t + 2v\overline{u}_c(\overline{u}_c)_z - 2\overline{u}_c(\overline{u}_c)_t + \overline{u}_c(\gamma - \overline{u}_c) = 0. \quad (2.20)$$

If we transform (2.14) into the traveling-wave frame, we find, as before, that an approximate solution of equation (2.20), for small γ, is

$$u_c^{(0)}(z) = \frac{\gamma}{1 + C_0 e^{\gamma z/v}},$$

(where we have dropped the bar from $\overline{u}_c$). We say that $u_c^{(0)}$ is a stable solution of equation (2.20) if a small disturbance to it decays exponentially in time; that is, if we define

$$u_c(z,t) \equiv u_c^{(0)}(z) + f(z,t),$$

$$|f(z,0)| \ll |u_c^{(0)}(z,0)|,$$

where $u_c(z,t)$ is a solution of equation (2.20), we require that

$$\lim_{t\to\infty} |e^{at} f(z,t)| \leq M(z) \text{ for some } a > 0. \quad (2.21)$$

Since $u_c^{(0)}(z)$ satisfies the boundary conditions $u_c(-\infty) = \gamma$, $u_c(+\infty) = 0$ for all t, we must set the conditions

$$f(-\infty,t) = 0,\ f(+\infty,t) = 0;$$

in fact, we will require that f and all its t- and z-derivatives decay at least exponentially as $|z| \to \infty$.

Substitution of $u_c(z,t)$ into equation (2.20) leads to

$$-v(1+\kappa)(u_c^{(0)})_{zzz}+(1+\kappa)f_{zzt}-v(1+\kappa)f_{zzz}+(1-v^2)(u_c^{(0)})_{zz}+(1-v^2)f_{zz}+2vf_{zt}$$
$$-f_{tt}+v(1-\gamma)(u_c^{(0)})_z+v(1-\gamma)f_z-(1-\gamma)f_t+2vu_c^{(0)}(u_c^{(0)})_z+2vu_c^{(0)}f_z$$
$$+2v(u_c^{(0)})_zf+2vff_z-2u_c^{(0)}f_t-2ff_t+\gamma u_c^{(0)}+\gamma f-(u_c^{(0)})^2-2u_c^{(0)}f-f^2=0.$$

We find from this equation that we must have

$$f(z,t)=O(\gamma^2)$$

and that the leading-order equation for $f(z,t)$ is

$$\begin{aligned} v(1+\kappa)f_{zzz}-(1+\kappa)f_{zzt}+(v^2-1)f_{zz}-2vf_{zt}-vf_z+f_{tt}+f_t &= \\ v(u_c^{(0)})_z+u_c^{(0)}(\gamma-u_c^{(0)}) &= 0. \quad (2.22) \end{aligned}$$

We present a stability analysis of the leading-order equation, equation (2.22). Straightforward perturbation expansion [16] can be used to show that the results obtained from analysis of equation (2.22) hold to all orders in γ.

We take a Laplace transform in t of equation (2.22), leading to

$$v(1+\kappa)F'''+(v^2-1-(1+\kappa)s)F''-v(1+2s)F'+(s+s^2)F=g(z;s), \quad (2.23)$$

where

$$g(z;s)\equiv(1+s)f(z,0)+f_t(z,0)-(1+\kappa)f_{zz}(z,0)-2vf_z(z,0)$$

and a prime denotes differentiation with respect to z. Here

$$F(z;s)\equiv\int_0^\infty f(z,t)e^{-st}dt;\ f(z,t)\equiv\frac{1}{2\pi i}\int_{c-i\infty}^{c+i\infty}F(z;s)e^{ts}ds$$

are the usual Laplace-transform pair, with c a real number greater than the greatest real part among the singularities of $F(z;s)$ as a function of s. Our stability condition, equation (2.21), will hold if and only if $c<0$; that is,

$$\lim_{t\to\infty}|e^{at}f(z,t)|\le M(z)\iff\exists\delta>0\ni c\le-\delta. \quad (2.24)$$

Since equation (2.23) is a linear differential equation with constant coefficients, we can solve it and determine explicitly whether any of the singularities of $F(z;s)$ has positive real part. We first note that we can easily solve the homogeneous equation

$$v(1+\kappa)F_h''' + (v^2 - 1 - (1+\kappa)s)F_h'' - v(1+2s)F_h' + (s+s^2)F_h = 0 \qquad (2.25)$$

to find the three solutions

$$F_h(z;s) = e^{y_1(s)z},\ e^{y_2(s)z},\ \text{and}\ e^{y_3(s)z},$$

where y_1, y_2, and y_3 are the roots of

$$y^3 + \frac{v^2 - 1 - (1+\kappa)s}{v(1+\kappa)}y^2 - \frac{1+2s}{1+\kappa}y + \frac{s+s^2}{v(1+\kappa)} = 0. \qquad (2.26)$$

Using the formula for the roots of a cubic equation, we find that, for s large and positive, two of the functions $y_1(s)$, $y_2(s)$, and $y_3(s)$ are real and positive, with the other real and negative. Using variation of parameters, we can then construct a solution of equation (2.23) which satisfies the boundary conditions $F(\pm\infty;s) = 0$:

$$\begin{aligned} F(z;s) \;=\; & -\frac{1}{(y_1-y_2)(y_1-y_3)}\int_z^{+\infty} g(\zeta;s)e^{-y_1(\zeta-z)}d\zeta \\ & -\frac{1}{(y_1-y_2)(y_2-y_3)}\int_{-\infty}^{z} g(\zeta;s)e^{y_2(z-\zeta)}d\zeta \\ & -\frac{1}{(y_1-y_3)(y_2-y_3)}\int_z^{+\infty} g(\zeta;s)e^{-y_3(\zeta-z)}d\zeta, \end{aligned} \qquad (2.27)$$

where we have chosen y_2 as the label of the root of equation (2.26) which is negative when s is large and positive. The chosen limits of integration ensure that $F(\pm\infty;s) = 0$ if $g(z;s) \to 0$ sufficiently fast as $|z| \to \infty$. Since $g(z;s)$ is defined in terms of $f(z,0)$ and its derivatives, and we are requiring exponential decay as $|z| \to \infty$ for $f(z,t)$ and its derivatives, $g(z;s)$ does decay fast enough to ensure that $F(\pm\infty;s) = 0$.

We must find the locations of the singularities of $F(z;s)$ in the complex s-plane. We see from (2.27) that $F(z;s)$ exhibits singularities at points $s(\kappa,v)$ at which one

or more of $y_1(s)$, $y_2(s)$, $y_3(s)$ are singular, or at which any two of $y_1(s)$, $y_2(s)$, $y_3(s)$ are equal. We use the cubic formula to find that the only singularities of the y_i are branch points. These branch points occur at points s which satisfy

$$\lambda^2 s^2 + (4\lambda v^2 + 2\lambda)s + (v^4 + (3\lambda - 2)v^2 + 1) = 0 \tag{2.28}$$

or

$$\lambda^3 s^5 + (\lambda^2 v^2/4 + \lambda^3 + 3\lambda^2)s^4 + [(-2\lambda^2 + 5\lambda)v^2 + 3\lambda^2 + 3\lambda]s^3$$
$$+ [(-\lambda/2 + 1)v^4 + (-2\lambda^2 + 19\lambda/2 - 2)v^2 + 3\lambda + 1]s^2 + [(\lambda + 1)v^4 + (5\lambda - 2)v^2 + 1]s$$
$$+ [v^6/4 + (\lambda - 1/2)v^4 + v^2/4] = 0, \tag{2.29}$$

(where we have set $\lambda \equiv 1 + \kappa$). The values of s for which two of the y_i are equal are the roots of equation (2.29).

Since the singularities of $F(z;s)$ occur at the roots of equations (2.28) and (2.29), the stability condition (2.24) requires that these roots lie in $\Re s < 0$. To study these roots, we apply the Routh-Hurwitz criteria [14] to the polynomials (2.28) and (2.29). These criteria are a chain of successively more restrictive conditions on the polynomials: If all of the zeros of the polynomial

$$P(s) \equiv P_0 + P_1 s + \cdots + P_{n-1}s^{n-1} + P_n s^n$$

are to lie in the left half of the complex s-plane, we first require that $P(s)$ have positive coefficients. Furthermore, defining the "even" polynomial

$$P_{\text{even}}(s) \equiv P_0 + P_2 s^2 + \cdots + \text{term with highest even power in } P(s),$$

with roots $a_1(v,\lambda)$, $a_2(v,\lambda)$, ..., and the "odd" polynomial

$$P_{\text{odd}}(s) \equiv P_1 s + P_3 s^3 + \cdots + \text{term with highest odd power in } P(s),$$

with roots $b_1(v,\lambda)$, $b_2(v,\lambda)$, ..., we then require that all of the roots a_i and b_i be pure imaginary and simple. If this condition holds, we can order the roots by imaginary part, defining

$$(\text{root})_j < (\text{root})_k \text{ if } \mathcal{I}(\text{root})_j < \mathcal{I}(\text{root})_k.$$

Having ordered the a_i and b_i in this manner, we apply the final requirement, that the a_i and b_i mutually separate each other:

$$a_1 < b_1 < a_2 < b_2 < \cdots$$

if n is even;

$$b_1 < a_1 < b_2 < a_2 < \cdots$$

if n is odd. If and only if this chain of conditions holds will the zeros of $P(s)$ lie in $\Re s < 0$.

The Routh-Hurwitz criteria impose no restrictions on κ and v for equation (2.28); the roots are all in $\Re s < 0$. For equation (2.29), the criteria were examined numerically. The region of stability is shown in a (κ, v)-plot in Figure 2.3.

2.1.2 Solution for Variable $B(u)$ and $\delta(u)$

We hope to find a traveling-wave solution of equations (2.5) and (2.6) for nonconstant $B(u)$ and $\delta(u)$. If we first take γ to be small and apply the change of variables (2.9) used in § 2.1.1, we find that the leading-order solutions for $u(z)$ and $s(z)$ are

$$u(z) = \frac{\gamma}{1 + C_0 e^{\gamma z/v}} + O(\gamma^2) \tag{2.30}$$

$$s(z) = \frac{\gamma^2 C_0 e^{\gamma z/v}}{B(u_0(z))(1 + C_0 e^{\gamma z/v})^2} + O(\gamma^3), \tag{2.31}$$

$$\text{where } u_0(z) \equiv \frac{\gamma}{1 + C_0 e^{\gamma z/v}}.$$

The equation for the $O(\gamma^2)$ term of $u(z)$ cannot be solved in closed form. We note that this solution $u(z)$ is the same through $O(\gamma)$ as the solution $u_c(z)$ found in § 2.1.1,

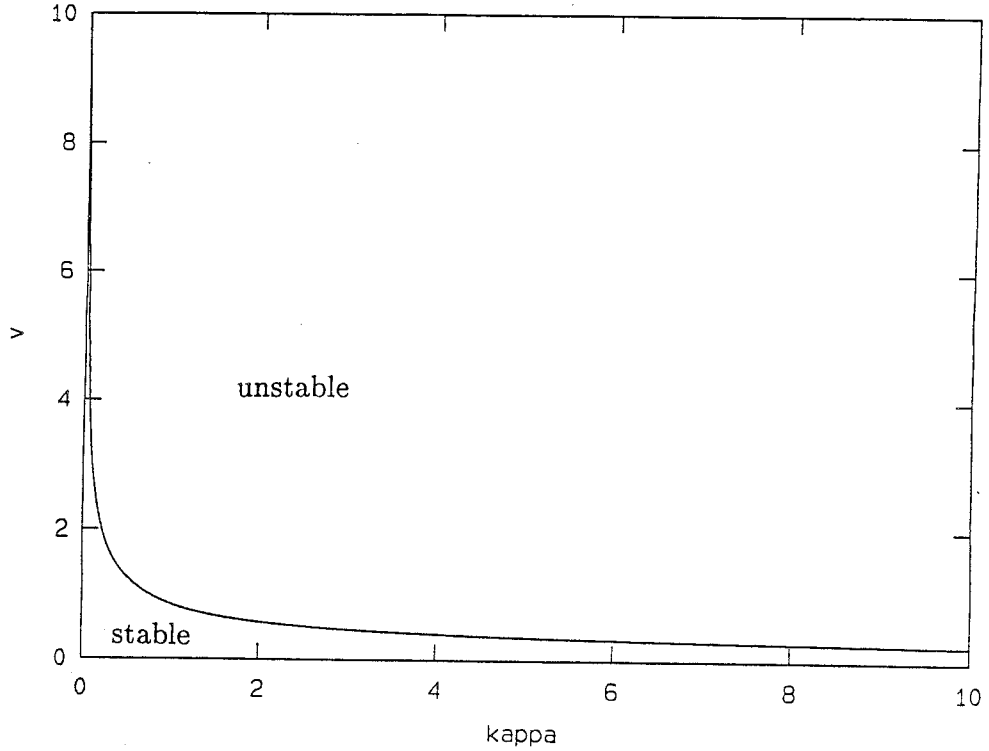

Figure 2.3: Region of stability for $u_c(z)$ in (κ, v)-space

while

$$s(z) \approx \frac{s_c(z)}{B(u_0(z))},$$

where $s_c(z)$ is the constant-coefficient ($\delta(u) \equiv 1$, $B(u) \equiv 1$) solution found in § 2.1.1. For those z large enough that $u_0(z) < \theta\gamma$, we know that $B(u_0(z)) < 1$; therefore $s(z) > s_c(z)$ in this region. Sketches of $s(z)$ and $s_c(z)$ are compared in Figure 2.4.

We must realize before we continue that the system (2.5), (2.6), with its variable coefficients, is qualitatively different from the constant-coefficient system that we were able to solve with a regular perturbation expansion in § 2.1.1. Near $u = \theta\gamma$ (the concentration at which $B(u)$ and $\delta(u)$ are in the middle of their transition from glassy to rubbery values), $\delta(u)$ and $B(u)$ are changing rapidly; hence, we cannot assume that the expression $(\delta(u)u' + \kappa s')'$ which appears in equation (2.5) is negligible with respect to the other terms in the equation. The nature of the system is not regular,

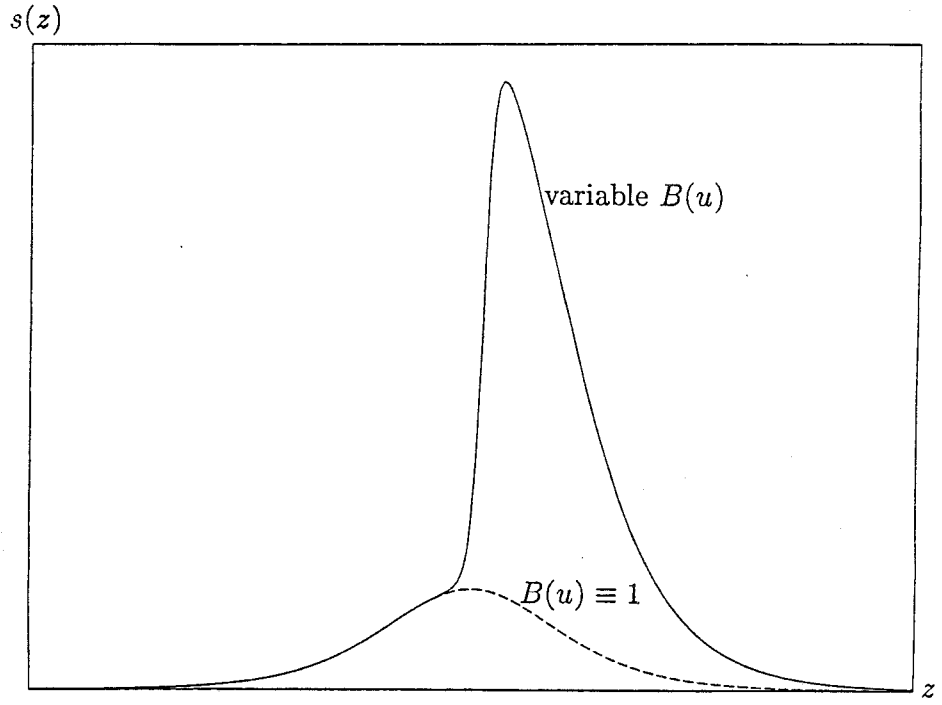

Figure 2.4: Comparison of $s_c(z)$ and $s(z)$

but singular, and the regular perturbation technique which we used to produce (2.30) and (2.31) breaks down.

In order to find the full effects of variable $B(u)$ and $\delta(u)$ on $u(z)$, we must examine equations (2.5) and (2.6) numerically. We can, however, make a rough prediction about the behavior of $u(z)$ near $u(z) = \theta\gamma$ by assuming that $\Delta u = 0$, so that $B(u)$ and $\delta(u)$ are piecewise constant. We used this technique to obtain new solutions of Fisher's equation; these results are presented in Appendix A. Our success in solving Fisher's equation led us to use the same technique here.

In the range $u > \theta\gamma$, $B(u) \equiv 1$ and $\delta(u) \equiv 1$ if $\Delta u = 0$. Therefore, $u(z)$ and $s(z)$ will be identical, in $u > \theta\gamma$, to the functions $u_c(z)$ and $s_c(z)$ defined in § 2.1.1. We assume that $s(z)$ will be continuous across $u = \theta\gamma$ and find the relationship between u' (as u approaches $\theta\gamma$ from $u > \theta\gamma$) and u' (as u approaches $\theta\gamma$ from $u < \theta\gamma$) by

requiring that the penetrant flux be continuous. The flux J is defined by

$$J = -(\delta(u)u_x + \kappa s_x),$$

or, in the traveling-wave frame,

$$J = -(\delta(u)u' + \kappa s').$$

Using equation (2.6), we find

$$J = -(\delta(u)u' + \kappa B(u)s/v + \kappa u').$$

With $\delta(u)$ and $B(u)$ piecewise constant, we have

$$\begin{aligned} u > \theta\gamma : -J_R &= (1+\kappa)u'_R + \kappa s/v \\ u < \theta\gamma : -J_G &= (\omega_\delta + \kappa)u'_G + \kappa\omega_B s/v, \end{aligned}$$

where the subscripts R and G are used to refer respectively to the rubbery state of the polymer ($u > \theta\gamma$) and its glassy state ($u < \theta\gamma$). If we require

$$J_R = J_G \text{ at } u = \theta\gamma,$$

we find

$$u'_G = \frac{1+\kappa}{\omega_\delta + \kappa}u'_R + \frac{\kappa(1-\omega_B)}{v(\omega_\delta+\kappa)}s \text{ at } u = \theta\gamma. \tag{2.32}$$

This formula shows the effects on u of *stress driving* (κ large) and *diffusion driving* (κ small). Since we are assuming that u drops monotonically from γ to 0 (so that u' is always negative) and that s is always positive, we see from equation (2.32) that

$$|u'_G| < |u'_R| \Longleftrightarrow u'_G > u'_R \text{ for large enough } \kappa,$$

but

$$|u'_G| > |u'_R| \Longleftrightarrow u'_G < u'_R \text{ for small enough } \kappa.$$

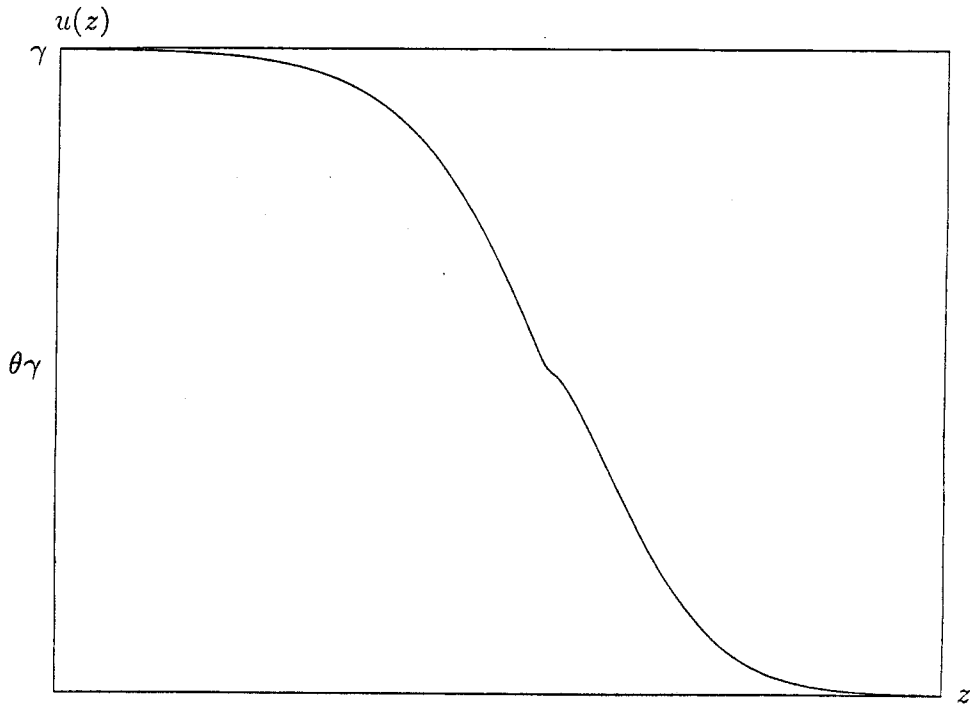

Figure 2.5: Predicted shape of $u(z)$ when κ is large

The sketches in Figures 2.5 and 2.6 show the behavior of u predicted by equation (2.32) for large and small κ. We expect that profiles of u similar to those in Figures 2.5 and 2.6 will appear in the numerical solution of equations (2.5) and (2.6) when Δu is very small.

This analysis shows the limitations of the simple reasoning that leads to the functions (2.30) and (2.31) as first-order solutions of equations (2.5) and (2.6). If $u'(z)$ is discontinuous or has a steep gradient at a point z_0, we cannot assume that $u''(z_0)$ is negligible, as we do in deriving (2.30); the problem becomes a singular perturbation problem. These formulas are still useful, however, because they provide an easily obtainable "feel" for the general trend of $u(z)$ and $s(z)$, although they are not numerically accurate.

In order to solve equations (2.5) and (2.6) numerically, we transform them into

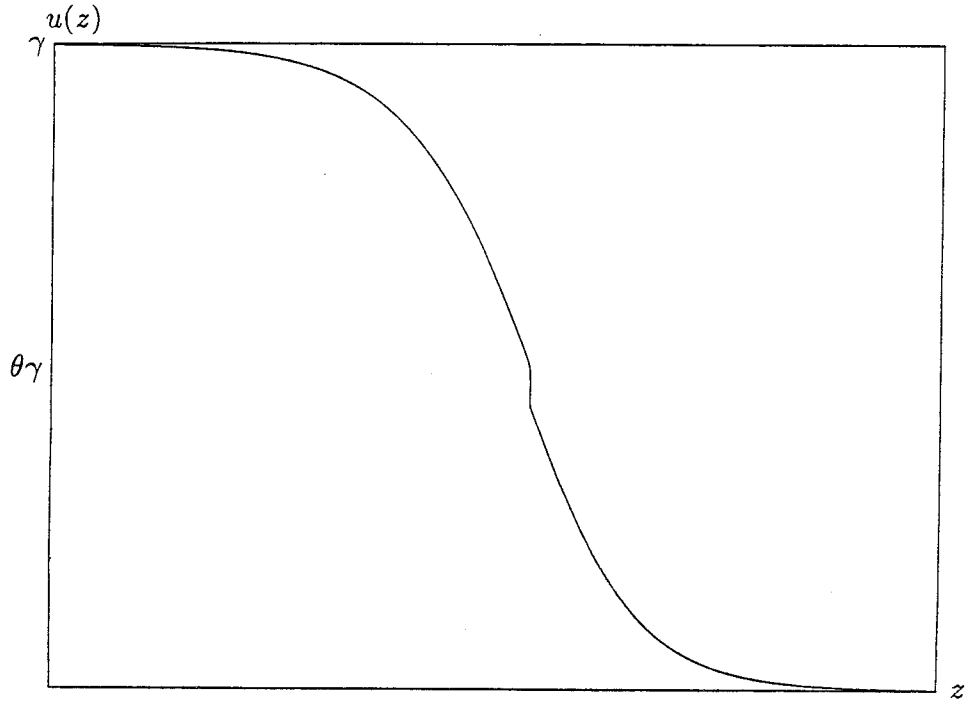

Figure 2.6: Predicted shape of $u(z)$ when κ is small

a system of three first-order equations. By defining

$$u - \gamma \equiv q, \; u' \equiv w,$$

we find the system

$$q' = w \tag{2.33}$$

$$w' = \frac{1}{\delta(q+\gamma)+\kappa}\{-\kappa[B(q+\gamma)]^2 s/v^2 - \kappa B'(q+\gamma)ws/v - (v+\kappa B(q+\gamma)/v)w - \delta'(q+\gamma)w^2 + q(q+\gamma)\} \tag{2.34}$$

$$s' = B(q+\gamma)s/v + w, \tag{2.35}$$

which we solve using a fourth-order accurate Runge-Kutta method [2]. In these variables, the solution we want travels from the fixed point $(q, w, s) = (0, 0, 0)$ to the fixed point $(q, w, s) = (-\gamma, 0, 0)$.

Equation (2.35) presents a problem in numerical solution. It has an exponentially increasing homogeneous solution

$$s_h(z) = A_h e^{\frac{1}{v}\int B(\gamma+q(z))dz}, \ A_h \text{ a constant},$$

which will increase (or decrease, if A_h is negative) without bound. We require $A_h = 0$ for a bounded solution, but any initial conditions we choose for q, w, and s will lead to a solution with a nonzero value of A_h because of the limited accuracy of the computer.

To counteract the problem of exponentially increasing s, we use a multiple shooting method. We first linearize the equations about the initial fixed point $(q, w, s) = (0, 0, 0)$ to find a set of starting values, as described below. Within a small neighborhood of these values we find two sets of initial values for q, w, and s, one leading to a solution (q_+, w_+, s_+) of equations (2.33), (2.34), and (2.35) with a positive value for A_h and one leading to a solution (q_-, w_-, s_-) with a negative value for A_h. Because we have chosen the initial values from the same small neighborhood, the two solutions start out close together. We set a threshold ε, integrate the equations forward, using both sets of initial values, to find the two vectors $(q_+(z), w_+(z), s_+(z))$ and $(q_-(z), w_-(z), s_-(z))$, and accept solution values over the range $(s_+(z) - s_-(z)) < \varepsilon$. We then integrate forward a test solution which starts midway between our two old solutions, find out whether it blows up positively or negatively, and repeat the first process with the test solution and the appropriate old solution. In this way, we find bounded solutions for $u(z) = \gamma + q(z)$ and $s(z)$.

We study the equations numerically using the parameter values $\theta = 0.5$ and $\Delta u = 0.01$. To find the initial values for w and s, we assume that near $q = 0$ $(u \approx \gamma)$, we can approximate w and s as

$$w \approx \alpha q, \ s \approx \beta q, \tag{2.36}$$

		κ					
γ		0.001	0.01	0.1	1	10	100
0.1	α	0.049	0.049	0.049	0.049	0.050	none
	β	−0.108	−0.108	−0.108	−0.109	−0.112	none
0.3	α	0.140	0.140	0.141	0.144	none	none
	β	−0.390	−0.390	−0.391	−0.404	none	none
0.5	α	0.225	0.225	0.227	0.250	none	none
	β	−0.817	−0.818	−0.828	−1.000	none	none
0.7	α	0.304	0.304	0.310	none	none	none
	β	−1.550	−1.556	−1.629	none	none	none
0.9	α	0.379	0.380	0.402	none	none	none
	β	−3.117	−3.169	−4.124	none	none	none

Table 2.1: Roots $\alpha > 0$ and $\beta < 0$ for $v = 2$

where α and β are constants. We are looking for a concentration profile which drops monotonically from $q = 0$ ($u = \gamma$) to $q = -\gamma$ ($u = 0$) as z increases, and for a stress profile which is nonnegative for all z. Since $q < 0$, we thus require $\alpha > 0$ and $\beta < 0$. We find α and β from plugging (2.36) into equations (2.33), (2.34), and (2.35), leading to

$$\alpha^3 + \frac{v^2 - \delta(\gamma)B(\gamma)}{v(\delta(\gamma)+\kappa)}\alpha^2 - \frac{B(\gamma)+\gamma}{\delta(\gamma)+\kappa}\alpha + \frac{\gamma B(\gamma)}{v(\delta(\gamma)+\kappa)} = 0$$

and

$$\beta = \frac{v\alpha}{v\alpha - B(\gamma)}.$$

In Tables 2.1 ($v = 2$) and 2.2 ($v = 2.75$), we display the real roots α and β with the desired signs for several values of γ and κ. For fixed γ and v, there is a cutoff value for κ above which no roots α and β with the desired signs exist. This cutoff decreases as γ increases for fixed v, and increases as v increases for fixed γ.

We have taken γ to be "small," but not fixed, in order to obtain the analytical results presented in § 2.1. The entries in Tables 2.1 and 2.2 indicate that, for fixed v

γ		κ = 0.001	0.01	0.1	1	10	100
0.1	α	0.036	0.036	0.036	0.036	0.036	0.050
	β	−0.110	−0.110	−0.110	−0.110	−0.111	−0.158
0.3	α	0.105	0.105	0.105	0.107	none	none
	β	−0.406	−0.407	−0.407	−0.415	none	none
0.5	α	0.171	0.171	0.172	0.182	none	none
	β	−0.889	−0.890	−0.898	−1.000	none	none
0.7	α	0.235	0.235	0.238	none	none	none
	β	−1.818	−1.824	−1.891	none	none	none
0.9	α	0.296	0.297	0.314	none	none	none
	β	−4.327	−4.431	−6.353	none	none	none

Table 2.2: Roots $\alpha > 0$ and $\beta < 0$ for $v = 2.75$

and κ, there is no monotonically decreasing traveling-wave solution $u(z)$ if γ is too large. The requirement that γ be small is a necessary condition for the existence of u.

In order to show the effects of stress driving and diffusion driving, we use widely varying values of κ and the fixed values $\gamma = 0.1$, $\omega_B = 0.01$, $\omega_S = 0.25$, and $v = 2$ in our numerical solutions. In Figure 2.7 we display diffusion-driven $u(z)$ and $s(z)$ profiles with $\kappa = 0.001$ and $\kappa = 0.01$, and, in Figure 2.8, stress-driven $u(z)$ and $s(z)$ profiles with $\kappa = 1$ and $\kappa = 10$. The effect on $u(z)$ of increasing κ is as predicted by equation (2.32), and the behavior of $s(z)$ is as predicted by equation (2.31).

2.2 Model B: Evolution of σ Forced by C

In this section we will study Model B, for which we take $f(C, C_T) = bC$ in equation (2.2). As before, we will put equations (2.1) and (2.2) in nondimensional form.

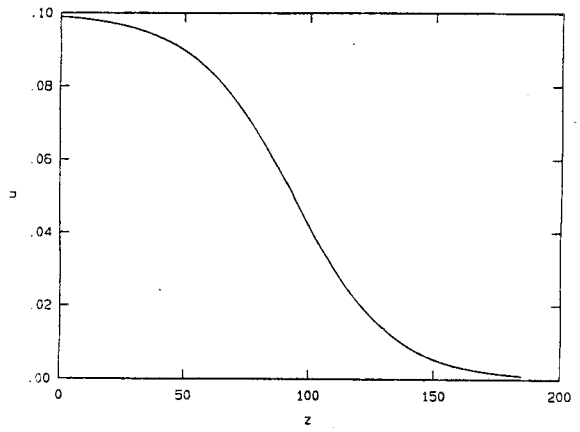

a: $u(z)$ with $\kappa = 0.001$

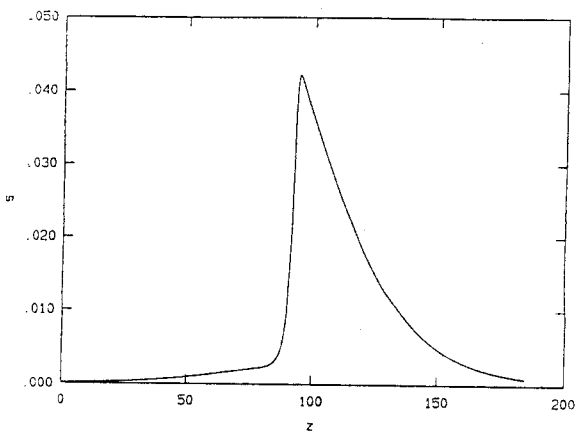

b: $s(z)$ with $\kappa = 0.001$

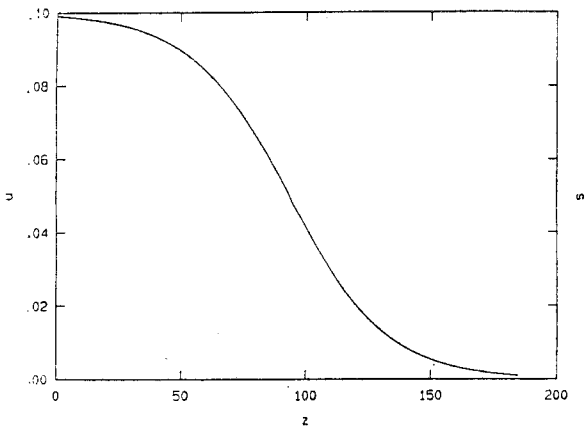

c: $u(z)$ with $\kappa = 0.01$

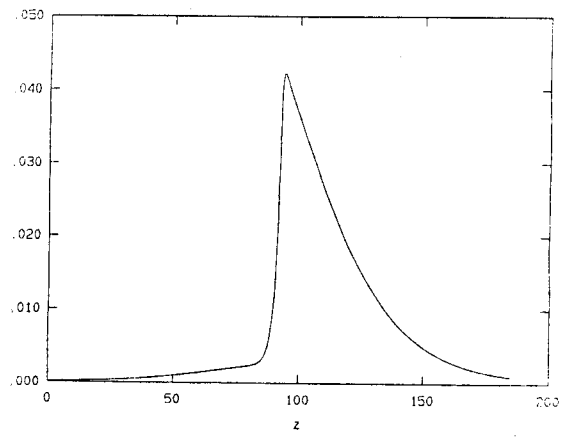

d: $s(z)$ with $\kappa = 0.01$

Figure 2.7: Profiles of diffusion-driven $u(z)$ and $s(z)$; $\kappa = 0.001$ and 0.01

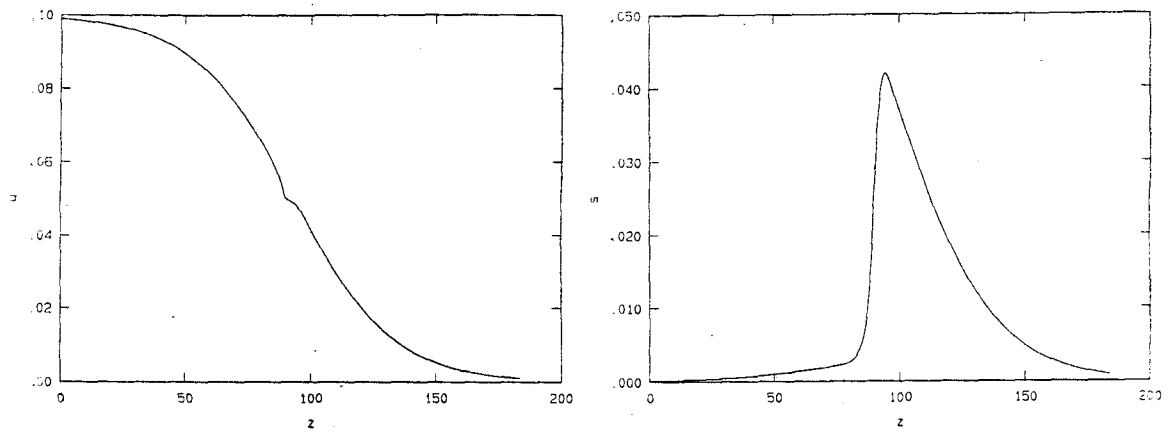

a: $u(z)$ with $\kappa = 1$ b: $s(z)$ with $\kappa = 1$

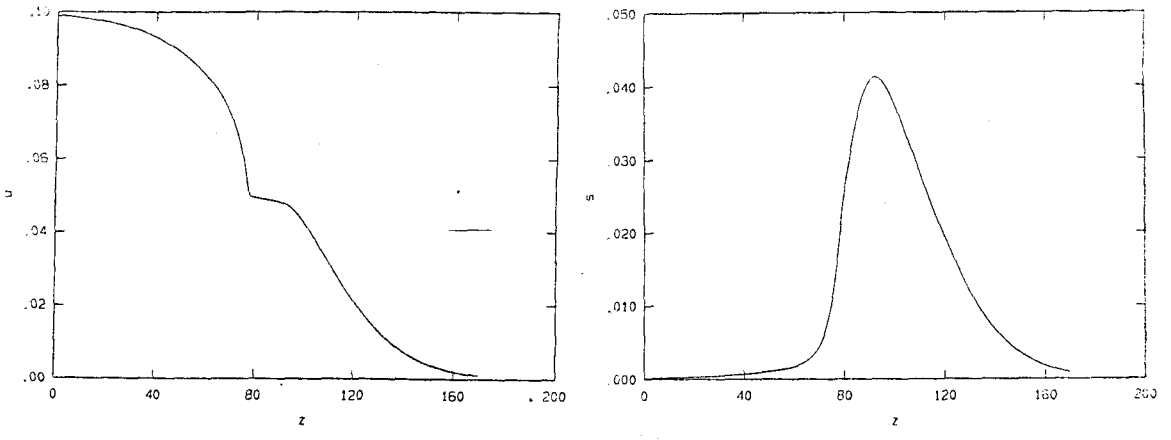

c: $u(z)$ with $\kappa = 10$ d: $s(z)$ with $\kappa = 10$

Figure 2.8: Profiles of stress-driven $u(z)$ and $s(z)$; $\kappa = 1$ and 10

Using

$$\begin{aligned} C(X,T) &\equiv \frac{\beta_R}{\mu} u(x,t) \\ \sigma(X,T) &\equiv \frac{b}{\mu} s(x,t) \\ x &\equiv \sqrt{\frac{\beta_R}{D_R}} X \\ t &\equiv \beta_R T, \end{aligned}$$

we find

$$u_t = (\delta(u)u_x)_x + \rho s_{xx} + u(\gamma - u) \tag{2.37}$$

$$s_t = -B(u)s + u, \tag{2.38}$$

where

$$\rho \equiv \frac{Eb}{\beta_R D_R},$$

and γ, $\delta(u)$, and $B(u)$ are as in § 2.1. Setting

$$z \equiv x - vt$$

we find the system of ordinary differential equations

$$(\delta(u)u')' + \rho s'' + vu' + u(\gamma - u) = 0 \tag{2.39}$$

$$vs' + u - B(u)s = 0. \tag{2.40}$$

Again, we take γ small and seek a solution which drops monotonically from $u = \gamma$ at $z = -\infty$ to $u = 0$ at $z = +\infty$.

2.2.1 Case of Constant Coefficients

We find some of the basic properties of the solutions of equations (2.39) and (2.40) by looking at the simple case in which $\delta(u) \equiv 1$ and $B(u) \equiv 1$. We seek solutions $u_c(z)$ and $s_c(z)$ of

$$u_c'' + \rho s_c'' + v u_c' + u_c(\gamma - u_c) = 0 \tag{2.41}$$

and

$$vs_c' + u_c - s_c = 0, \tag{2.42}$$

where the subscript c refers to the fact that $B(u)$ and $\delta(u)$ are now constant. We will find, as before, that for γ small enough we can find solutions to equations (2.41) and (2.42) as power series in γ.

We first apply the rescaling (2.9) to equations (2.41) and (2.42):

$$\xi \equiv \gamma z,\ u_c(z) \equiv \gamma p(\xi),\ s_c(z) \equiv \gamma g(\xi)$$

leading to

$$\gamma p'' + \gamma \rho g'' + vp' + p(1-p) = 0 \tag{2.43}$$

$$\gamma v g' + p - g = 0 \tag{2.44}$$

$$p(-\infty) = 1,\ p(+\infty) = 0,$$

where a prime now denotes differentiation with respect to ξ. We assume that γ is a small parameter and look for solutions as power series in γ:

$$p(\xi) = p_0(\xi) + \gamma p_1(\xi) + \gamma^2 p_2(\xi) + \cdots = \sum_{n=0} \gamma^n p_n(\xi)$$

$$g(\xi) = g_0(\xi) + \gamma g_1(\xi) + \gamma^2 g_2(\xi) + \cdots = \sum_{n=0} \gamma^n g_n(\xi).$$

We insert these expansions into equations (2.43) and (2.44) and combine terms in like powers of γ:

$$vp_0' + p_0(1-p_0) + \gamma[vp_1' + (1-2p_0)p_1 + p_0'' + \rho g_0''] + O(\gamma^2) = 0$$

$$p_0 - g_0 + \gamma(p_1 - g_1 + vg_0') + O(\gamma^2) = 0.$$

If we set the coefficient of each power of γ separately to zero and apply the boundary conditions, we can solve the resulting equations for p_0, p_1, g_0, and g_1. We find

$$p_0(\xi) = \frac{1}{1 + C_0 e^{\xi/v}},\ (C_0 > 0 \text{ a constant})$$

$$g_0(\xi) = \frac{1}{1 + C_0 e^{\xi/v}}$$

and

$$p_1(\xi) = \frac{(1+\rho)C_0e^{\xi/v}}{v^2(1+C_0e^{\xi/v})^2}\left[\ln\frac{C_0e^{\xi/v}}{(1+C_0e^{\xi/v})^2}+C_1\right],\ C_1 \text{ a constant}$$

$$g_1(\xi) = \frac{(1+\rho)C_0e^{\xi/v}}{v^2(1+C_0e^{\xi/v})^2}\left[\ln\frac{C_0e^{\xi/v}}{(1+C_0e^{\xi/v})^2}+C_1-\frac{v^2}{1+\rho}\right].$$

As functions of z, these solutions of equations (2.41) and (2.42) are

$$u_c(z) = \frac{\gamma}{1+C_0e^{\gamma z/v}} + \frac{(1+\rho)\gamma^2C_0e^{\gamma z/v}}{v^2(1+C_0e^{\gamma z/v})^2}\left[\ln\frac{C_0e^{\gamma z/v}}{(1+C_0e^{\gamma z/v})^2}+C_1\right]+O(\gamma^3) \qquad (2.45)$$

$$s_c(z) = \frac{\gamma}{1+C_0e^{\gamma z/v}} + \frac{(1+\rho)\gamma^2C_0e^{\gamma z/v}}{v^2(1+C_0e^{\gamma z/v})^2}\left[\ln\frac{C_0e^{\gamma z/v}}{(1+C_0e^{\gamma z/v})^2}+C_1-\frac{v^2}{1+\rho}\right] + O(\gamma^3). \qquad (2.46)$$

Both $u_c(z)$ and $s_c(z)$ are equal, to first order in γ, to the function graphed in Figure 2.2a.

We note several differences between these solutions (2.45) and (2.46) and the constant-coefficient solutions (2.12) and (2.13) of the model which we studied in § 2.1, Model A. In Model B, the nondimensionalized concentration and stress are equal to first order. In the dimensional variables,

$$\frac{\sigma(X,T)}{C(X,T)} \approx \frac{b}{\beta_R}.$$

Furthermore, in Model B, the wave of penetrant moving into the polymer induces a stress at the wavefront, and the region of polymer behind the wavefront remains stressed. Finally, the parameter ρ, analogous to the parameter κ of Model A, appears in the $O(\gamma^2)$ terms of $u_c(z)$ and $s_c(z)$. Variations in ρ will have more impact on $u_c(z)$ and $s_c(z)$ when Model B holds than will variations in κ in Model A.

We wish to examine the stability of the $O(\gamma)$ solutions

$$u_c(x,t) \approx \frac{\gamma}{1+C_0 e^{\gamma(x-vt)/v}} \tag{2.47}$$

$$s_c(x,t) \approx \frac{\gamma}{1+C_0 e^{\gamma(x-vt)/v}} \tag{2.48}$$

for t large. We use the Laplace transform method of § 2.1 to study the stability of (2.47) and (2.48) [13]. With $B(u) \equiv \delta(u) \equiv 1$, equations (2.37) and (2.38) are

$$(u_c)_t = (u_c)_{xx} + \rho(s_c)_{xx} + u_c(\gamma - u_c) \tag{2.49}$$

$$(s_c)_t = -s_c + u_c. \tag{2.50}$$

We first solve equation (2.50) for $s_c(x,t)$ and find

$$s_c(x,t) = \int_0^t e^{-(t-\tau)} u_c(x,\tau) d\tau.$$

We substitute this solution into equation (2.49) and find

$$\rho \frac{\partial^2}{\partial x^2} \left\{ \int_0^t e^{-(t-\tau)} u_c(x,\tau) d\tau \right\} = (u_c)_t - (u_c)_{xx} - u_c(\gamma - u_c). \tag{2.51}$$

If we differentiate equation (2.51) once with respect to t and substitute the right-hand side of equation (2.51) into the result, we find a third-order equation for $u_c(x,t)$:

$$(u_c)_{xxt} + (1+\rho)(u_c)_{xx} - (u_c)_{tt} - (1-\gamma)(u_c)_t - 2u_c(u_c)_t + u_c(\gamma - u_c) = 0. \tag{2.52}$$

In the traveling-wave frame, with

$$z \equiv x - vt,\ u_c(x,t) \equiv \overline{u}_c(z,t)$$

equation (2.52) becomes

$$-v(\overline{u}_c)_{zzz} + (\overline{u}_c)_{zzt} + (1+\rho-v^2)(\overline{u}_c)_{zz} + 2v(\overline{u}_c)_{zt} - (\overline{u}_c)_{tt} + v(1-\gamma)(\overline{u}_c)_z$$

$$- (1-\gamma)(\overline{u}_c)_t + 2v\overline{u}_c(\overline{u}_c)_z - 2\overline{u}_c(\overline{u}_c)_t + \overline{u}_c(\gamma - \overline{u}_c) = 0. \tag{2.53}$$

If we transform (2.47) into the traveling-wave frame, we find, as before, that an approximate solution of equation (2.53), for small γ, is

$$u_c^{(0)}(z) = \frac{\gamma}{1 + C_0 e^{\gamma z/v}},$$

(where we have dropped the bar from $\overline{u}_c$). For $u_c^{(0)}$ to be a stable solution of equation (2.53), if we define

$$u_c(z,t) \equiv u_c^{(0)}(z) + f(z,t),$$

$$|f(z,0)| \ll |u_c^{(0)}(z,0)|,$$

where $u_c(z,t)$ is a solution of equation (2.53), we require that

$$\lim_{t\to\infty} |e^{at} f(z,t)| \leq M(z) \text{ for some } a > 0, \tag{2.54}$$

and that $f(z,t)$ and its t- and z-derivatives decay toward zero at least exponentially as $|z| \to \infty$. Substitution of $u_c(z,t)$ into equation (2.53) leads to

$$-v(u_c^{(0)})_{zzz} + f_{zzt} - v f_{zzz} + (1+\rho-v^2)(u_c^{(0)})_{zz} + (1+\rho-v^2) f_{zz} + 2v f_{zt}$$

$$- f_{tt} + v(1-\gamma)(u_c^{(0)})_z + v(1-\gamma) f_z - (1-\gamma) f_t + 2v u_c^{(0)} (u_c^{(0)})_z + 2v u_c^{(0)} f_z$$

$$+ 2v(u_c^{(0)})_z f + 2v f f_z - 2u_c^{(0)} f_t - 2 f f_t + \gamma u_c^{(0)} + \gamma f - (u_c^{(0)})^2 - 2u_c^{(0)} f - f^2 = 0.$$

We find from this equation that we must have

$$f(z,t) = O(\gamma^2)$$

and that the leading-order equation for $f(z,t)$ is

$$\begin{aligned} v f_{zzz} - f_{zzt} + (v^2 - 1 - \rho) f_{zz} - 2v f_{zt} - v f_z + f_{tt} + f_t &= \\ v(u_c^{(0)})_z + u_c^{(0)}(\gamma - u_c^{(0)}) &= 0. \end{aligned} \tag{2.55}$$

As in § 2.1, we will present analysis of only the leading-order equation, equation (2.55). Just as in § 2.1, standard perturbation expansion indicates that the

leading-order results hold to all orders in γ [16]. We take a Laplace transform in t as before, leading to

$$vF''' + (v^2 - 1 - \rho - s)F'' - v(1 + 2s)F' + (s + s^2)F = g(z; s), \tag{2.56}$$

where

$$g(z; s) \equiv (1 + s)f(z, 0) + f_t(z, 0) - f_{zz}(z, 0) - 2vf_z(z, 0).$$

Here

$$F(z; s) \equiv \int_0^\infty f(z, t)e^{-st}dt;\ f(z, t) \equiv \frac{1}{2\pi i}\int_{c-i\infty}^{c+i\infty} F(z; s)e^{ts}ds$$

are the Laplace-transform pair, with c a real number greater than the greatest real part among the singularities of $F(z; s)$ as a function of s. Our stability condition, equation (2.54), will hold if and only if $c < 0$; that is,

$$\lim_{t\to\infty} |e^{at}f(z, t)| \leq M(z) \Longleftrightarrow \exists \delta > 0 \ni c \leq -\delta. \tag{2.57}$$

As in § 2.1, we find that $F(z; s)$ can be expressed in terms of the three solutions

$$F_h(z; s) = e^{y_1(s)},\ e^{y_2(s)}, \text{ and } e^{y_3(s)}$$

of the homogeneous equation

$$vF_h''' + (v^2 - 1 - \rho - s)F_h'' - v(1 + 2s)F_h' + (s + s^2)F_h = 0. \tag{2.58}$$

Here y_1, y_2, and y_3 are the roots of

$$y^3 + \frac{v^2 - 1 - \rho - s}{v}y^2 - (1 + 2s)y + \frac{s + s^2}{v} = 0. \tag{2.59}$$

We find from the cubic formula that, for s large and positive, y_1 and y_3 are real and positive and y_2 is real and negative. Therefore, a solution of equation (2.56) satisfying $F(\pm\infty; s) = 0$ is

$$
\begin{aligned}
F(z;s) \;=\; & -\frac{1}{(y_1-y_2)(y_1-y_3)}\int_z^{+\infty} g(\zeta;s)e^{-y_1(\zeta-z)}d\zeta \\
& -\frac{1}{(y_1-y_2)(y_2-y_3)}\int_{-\infty}^{z} g(\zeta;s)e^{y_2(z-\zeta)}d\zeta \\
& -\frac{1}{(y_1-y_3)(y_2-y_3)}\int_z^{+\infty} g(\zeta;s)e^{-y_3(\zeta-z)}d\zeta. \qquad (2.60)
\end{aligned}
$$

We must locate the singularities of $F(z;s)$ in the complex s-plane. These singularities occur at the singularities of the y_i and at any point s at which two of the y_i are equal. Using the formula for the roots of a cubic equation, we find that the functions y_1, y_2, and y_3 have no singularities but branch points, and that these branch points lie at points s which satisfy

$$s^2 + (4v^2 + 2\lambda)s + (v^4 + (3-2\lambda)v^2 + \lambda^2) = 0 \qquad (2.61)$$

or

$$
\begin{aligned}
& s^5 + (v^2/4 + 3\lambda + 1)s^4 + [(5\lambda - 2)v^2 + 3\lambda^2 + 3\lambda]s^3 \\
& + [(\lambda - 1/2)v^4 + (-2\lambda^2 + 19\lambda/2 - 2)v^2 + \lambda^3 + 3\lambda^2]s^2 + [(\lambda+1)v^4 + (-2\lambda^2 + 5\lambda)v^2 + \lambda^3]s \\
& + [v^6/4 + (-\lambda/2 + 1)v^4 + \lambda^2 v^2/4] = 0, \qquad (2.62)
\end{aligned}
$$

(where we have set $\lambda \equiv 1+\rho$). We find also that two of the y_i will be equal when and only when s is a root of equation (2.62). Therefore, the stability condition (2.57) requires that the roots of equations (2.61) and (2.62) lie in $\Re s < 0$. To study these roots, we use the Routh-Hurwitz criteria, as before [14]. We find that the criteria impose no restrictions at all on v and ρ, either for equation (2.61) or for equation (2.62); therefore, the functions (2.47) and (2.48) are stable solutions of equations (2.49) and (2.50) for all v and ρ.

2.2.2 Solution for Variable $B(u)$ and $\delta(u)$

We hope to find a traveling-wave solution of equations (2.39) and (2.40) for non-constant $B(u)$ and $\delta(u)$. If we first take γ to be small and apply the change of variables (2.9) used in § 2.2.1, we find that the leading-order solutions for $u(z)$ and $s(z)$ are

$$u(z) = \frac{\gamma}{1 + C_0 e^{\gamma z/v}} + O(\gamma^2) \tag{2.63}$$

$$s(z) = \frac{\gamma}{B(u_0(z))(1 + C_0 e^{\gamma z/v})} + O(\gamma^2), \tag{2.64}$$

$$\text{where } u_0(z) \equiv \frac{\gamma}{1 + C_0 e^{\gamma z/v}}.$$

The equations for the $O(\gamma^2)$ terms of $u(z)$ and $s(z)$ cannot be solved analytically. We note that, as when Model A holds, this solution $u(z)$ is the same through $O(\gamma)$ as the solution $u_c(z)$ found in § 2.2.1, while

$$s(z) \approx \frac{s_c(z)}{B(u_0(z))},$$

where $s_c(z)$ is the constant-coefficient solution found in § 2.2.1. Sketches of $s(z)$ and $s_c(z)$ are compared in Figure 2.9.

We must realize that the system (2.39), (2.40) cannot be solved throughout $-\infty < z < +\infty$ by a regular perturbation method; the problem is a singular perturbation problem, as was the analogous problem solved in § 2.1. Near $u = \theta\gamma$, the term $(\delta(u)u' + \rho s')'$ is not negligible compared to the rest of the terms in equation (2.39), and the results (2.63), (2.64) are invalid. In order to get a rough idea of the behavior of $u(z)$ near $u = \theta\gamma$, we use the approach of setting $\Delta u = 0$, as in § 2.1.2. In the range $u > \theta\gamma$, $B(u) \equiv 1$ and $\delta(u) \equiv 1$ if $\Delta u = 0$; in $u < \theta\gamma$, $B(u) = \omega_B$ and $\delta(u) = \omega_\delta$. We assume, as before, that $s(z)$ will be continuous across $u = \theta\gamma$ and find the relationship between u' (as u approaches $\theta\gamma$ from $u > \theta\gamma$) and u' (as u approaches $\theta\gamma$ from $u < \theta\gamma$) by requiring that the penetrant flux J be continuous.

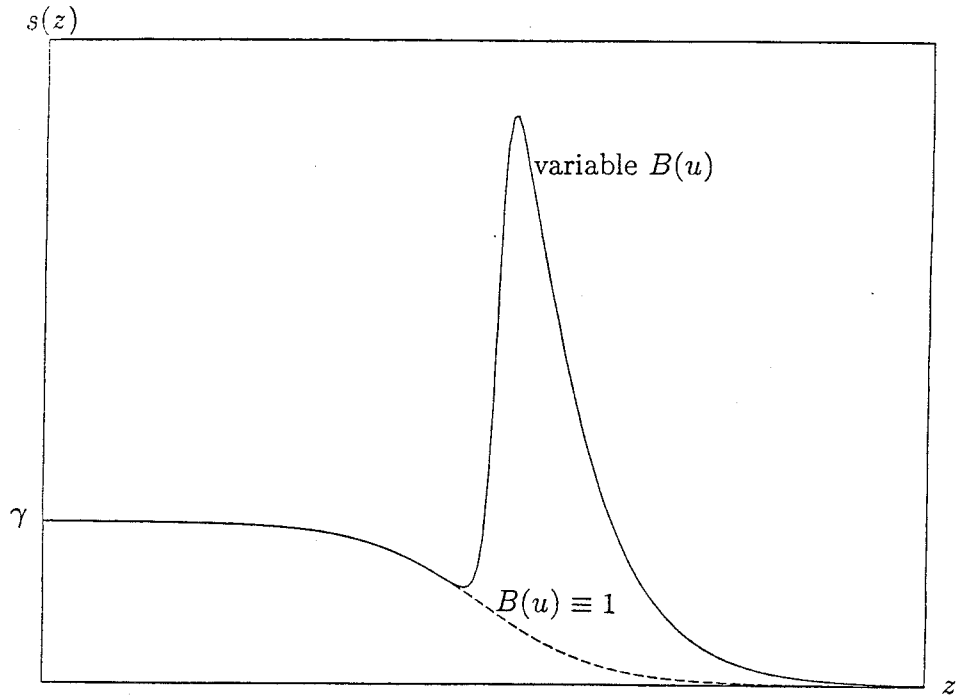

Figure 2.9: Comparison of $s_c(z)$ and $s(z)$

Using equation (2.40), we find

$$J = -(\delta(u)u' + \rho B(u)s/v - \rho u/v).$$

With $\delta(u)$ and $B(u)$ piecewise constant, we have

$$\begin{aligned} u > \theta\gamma : -J_R &= u'_R + \rho s/v - \rho u/v \\ u < \theta\gamma : -J_G &= \omega_\delta u'_G + \rho\omega_B s/v - \rho u/v, \end{aligned}$$

where the subscripts R and G are used to refer respectively to the rubbery state of the polymer ($u > \theta\gamma$) and its glassy state ($u < \theta\gamma$). If we require

$$J_R = J_G \text{ at } u = \theta\gamma$$

we find

$$u'_G = \frac{1}{\omega_\delta} u'_R + \frac{\rho(1-\omega_B)}{v\omega_\delta} s \text{ at } u = \theta\gamma. \tag{2.65}$$

This formula again shows the effects on u of stress driving and diffusion driving. Since we are assuming that u' is always negative and that s is always positive, we see from equation (2.65) that

$$|u'_G| < |u'_R| \Longleftrightarrow u'_G > u'_R \text{ for large enough } \rho,$$

but

$$|u'_G| > |u'_R| \Longleftrightarrow u'_G < u'_R \text{ for small enough } \rho.$$

These relations are similar to those found by the same method in § 2.1.2. When Δu is very small, we expect $u(z)$ to look like the sketch in Figure 2.5 when ρ is large, and like the sketch in Figure 2.6 when ρ is small.

In order to find the full behavior of the solutions of equations (2.39) and (2.40) for variable $B(u)$ and $\delta(u)$, we solve the equations numerically. We first transform them into a system of three first-order equations by setting $u' \equiv w$. We find

$$\begin{aligned} u' &= w \\ w' &= \frac{1}{\delta(u)}\{-\rho[B(u)]^2 s/v^2 - \rho B'(u)ws/v + (\rho/v - v)w - \delta'(u)w^2 \\ &\quad + \rho B(u)u/v^2 - u(\gamma - u)\} \\ s' &= \frac{1}{v}\{B(u)s - u\}. \end{aligned}$$

The fixed points of this system are $(u, w, s) = (\gamma, 0, \gamma/B(\gamma))$ and $(u, w, s) = (0, 0, 0)$. (Note that $B(\gamma) \approx 1$ for Δu small, so $\gamma/B(\gamma) \approx \gamma$.) We now define

$$u - \gamma \equiv q, \; s - \mu \equiv r,$$

where

$$\mu \equiv \frac{\gamma}{B(\gamma)},$$

and find the system

$$q' = w \tag{2.66}$$

$$w' = \frac{1}{\delta(q+\gamma)}\{-\rho[B(q+\gamma)]^2(r+\mu)/v^2 - \rho B'(q+\gamma)w(r+\mu)/v + (\rho/v - v)w - \delta'(q+\gamma)w^2 + \rho(q+\gamma)B(q+\gamma)/v^2 + q(q+\gamma)\} \tag{2.67}$$

$$r' = \frac{1}{v}\{B(q+\gamma)(r+\mu) - (q+\gamma)\}, \tag{2.68}$$

which we solve with the same fourth-order accurate Runge-Kutta method used in § 2.1.2 [2]. In these variables, the solution we want travels from the fixed point $(q, w, r) = (0, 0, 0)$ to the fixed point $(q, w, r) = (-\gamma, 0, -\mu)$. As in § 2.1.2, we must use a multiple shooting method to counteract the unbounded tendency of the homogeneous solution of equation (2.68),

$$r_h(z) = A_h e^{\frac{1}{v}\int B(\gamma+q(z))dz}, \ A_h \text{ a constant.}$$

The method used on these equations is precisely the same as the one used on Model A.

We study the equations numerically using the parameter values $\theta = 0.5$ and $\Delta u = 0.05$. To find the initial values for w and r, we assume as before that near $q = 0$ $(u \approx \gamma)$, we can approximate w and r as

$$w \approx \alpha q, \ r \approx \beta q, \tag{2.69}$$

where α and β are constants. We are looking for concentration and stress profiles which decrease initially from the fixed point $q = r = 0$. Since $q < 0$, we require $\alpha > 0$ and $\beta > 0$. We find α and β from plugging (2.69) into equations (2.66), (2.67), and (2.68), leading to

$$\alpha^3 + \frac{v^2 - \rho - \delta(\gamma)B(\gamma) + \rho B'(\gamma)\mu}{v\delta(\gamma)}\alpha^2 - \frac{B(\gamma)+\gamma}{\delta(\gamma)}\alpha + \frac{\gamma B(\gamma)}{v\delta(\gamma)} = 0$$

and

$$\beta = \frac{1 - \mu B'(\gamma)}{B(\gamma) - v\alpha}.$$

		κ					
γ		0.001	0.01	0.1	1	10	100
0.1	α	0.049	0.049	0.049	0.048	0.040	0.022
	β	1.108	1.108	1.108	1.105	1.088	1.048
0.3	α	0.140	0.140	0.139	0.130	0.093	0.044
	β	1.390	1.389	1.385	1.352	1.228	1.096
0.5	α	0.225	0.224	0.221	0.198	0.129	0.058
	β	1.816	1.814	1.793	1.655	1.348	1.131
0.7	α	0.304	0.303	0.296	0.253	0.157	0.069
	β	2.548	2.537	2.446	2.025	1.459	1.161
0.9	α	0.378	0.376	0.361	0.297	0.180	0.079
	β	4.105	4.043	3.603	2.464	1.563	1.187

Table 2.3: Roots $\alpha > 0$ and $\beta > 0$ for $v = 2$

There is a set of positive roots ($\alpha > 0, \beta > 0$) for all the values of v, γ, and ρ that we consider. We display the roots for $v = 2$ and several values of γ and ρ in Table 2.3.

As we can see from Table 2.3, we cannot rule out the possibility of desirable solutions u and s existing for large γ, as we did when studying Model A, solely on the basis of the behavior of the linearized system near $u = \gamma$. We continue, however, to take γ small, so that we can compare the Model B results to the Model A results.

In order to show the effects of stress driving and diffusion driving, we use the values $\rho = 0.001$ and $\rho = 1$ and the fixed values $\gamma = 0.1$, $\omega_B = 0.01$, $\omega_\delta = 0.25$, and $v = 2$ in our numerical solutions. In Figure 2.10 we display diffusion-driven $u(z)$ and $s(z)$ profiles with $\rho = 0.001$, and, in Figure 2.11, stress-driven $u(z)$ and $s(z)$ profiles with $\rho = 1$. The effect on $u(z)$ of increasing ρ is as predicted by equation (2.65), and the behavior of $s(z)$ is as predicted by equation (2.64).

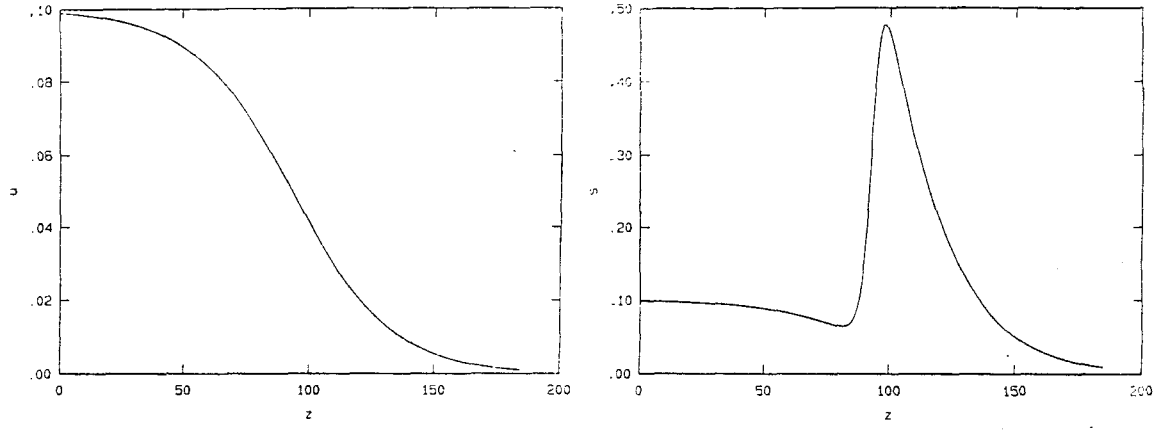

a: $u(z)$ with $\rho = 0.001$ b: $s(z)$ with $\rho = 0.001$

Figure 2.10: Profiles of diffusion-driven $u(z)$ and $s(z)$; $\rho = 0.001$

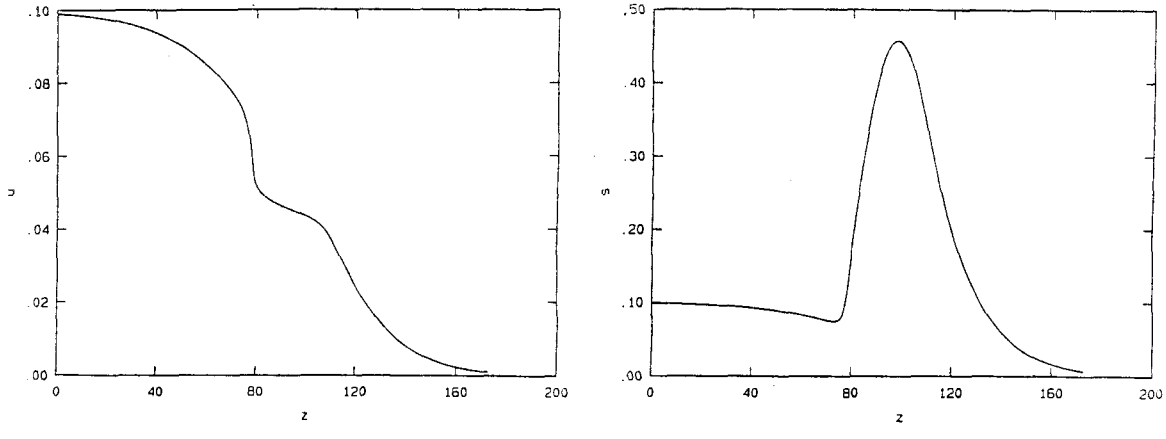

a: $u(z)$ with $\rho = 1$ b: $s(z)$ with $\rho = 1$

Figure 2.11: Profiles of stress-driven $u(z)$ and $s(z)$; $\rho = 1$

2.3 Conclusions

The polymer-penetrant system modeled by equations (2.1) and (2.2) possesses small-amplitude traveling-wave solutions $C(Z)$ and $\sigma(Z)$, where $Z = X - VT$, satisfying the equations and the boundary conditions $C(-\infty) = k$ (k small), $C(+\infty) = 0$, when the diffusivity and relaxation time are taken to be essentially constant in the glassy and rubbery regions of the polymer, varying only at the glass–rubber transition, and the stress evolution model is taken to be either purely concentration-forced or purely concentration rate-forced. When the diffusivity and relaxation time are both taken to be identically constant throughout the polymer, $C(Z)$ and $\sigma(Z)$ can be expressed as power series in the small dimensionless parameter γ. For both stress evolution models, $C(Z)$ simply drops smoothly from k to 0. The stress $\sigma(Z)$ exhibits different forms in the two models. In the concentration rate-forced model, stress builds up at the front of the penetrant wave, but the polymer relaxes quickly back to an unstressed state behind the wavefront. In the concentration-forced model, the section of polymer behind the wavefront never relaxes; in fact, the stress behaves throughout the polymer like the concentration, both variables exhibiting their largest values at $Z = -\infty$.

A stability analysis was performed on the solution $C(Z)$. In the concentration rate-forced model, the first term of the small-γ expansion for $C(Z)$ was found to be stable to small perturbations for a restricted set of parameter values; in the concentration-forced model, the first term of the small-γ expansion for $C(Z)$ was found to be stable for all parameter values.

The equations were also studied for nonconstant diffusivity and relaxation time. A simple approximation showed that the stress σ would reach much larger values when the relaxation time varied than when it was constant. Another approximation indicated that the concentration C would take different forms at the glass–rubber

transition, depending on whether the equations were stress driven or diffusion driven. Both effects were found when the equations were solved numerically.

Chapter 3

Solutions on a Bounded Domain

In this chapter, we turn from the solution of equations (1.5) and (1.6) on an infinite domain to the very different problem of solving the system on a finite domain. We wish to discover how the concentration and stress profiles of an initially dry block of polymer set between two penetrant reservoirs evolve through time. In this model, the flux of penetrant depends linearly on the gradients of both the penetrant concentration C and the induced stress σ:

$$\frac{\partial C}{\partial T} = D\frac{\partial^2 C}{\partial X^2} + E\frac{\partial^2 \sigma}{\partial X^2}, \tag{3.1}$$

where D and E are constants. We take the stress evolution equation

$$\frac{\partial \sigma}{\partial T} = -\beta(C)\sigma + a\frac{\partial C}{\partial T} + bC, \tag{3.2}$$

where a and b are constants and

$$\beta(C) = \frac{\beta_R + \beta_G}{2} + \frac{\beta_R - \beta_G}{2}\tanh\frac{C - C_{RG}}{\Delta C}$$

is the function shown in Figure 1.2. This equation responds differently to a sudden influx of penetrant than to a gradual penetrant buildup. We expect to find that $\sigma \approx aC$ after a sudden penetrant jump, but that $\sigma \approx bC/\beta(C)$ during a gradual penetrant buildup.

We will nondimensionalize the system (3.1), (3.2) so that the nondimensional analogue of D and E is taken to be a single parameter d, and we will assume that d is large. When we analyze the system under this assumption, we will find that there is a short initial time interval during which the stress and concentration obey a Fickian diffusion law. After this interval the solutions become nearly discontinuous, with true discontinuity appearing in the steady state.

We look for solutions $C(x,t)$ and $\sigma(x,t)$ on the domain

$$0 < X < L, T > 0,$$

and apply the initial conditions

$$C(X,0) = \sigma(X,0) = 0$$

and the boundary conditions

$$C(0,T) = C_0, C(L,T) = C_1,$$

where we require

$$C_0 < C_{RG} < C_1.$$

Cohen and White [4] studied the system (3.1), (3.2) in the case $a = 0$. They found solutions $C(X,T)$, $\sigma(X,T)$ which are smooth over most of the range $0 < X < L$, but which exhibit steep gradients in C and σ at one interior point X^*. We will solve equations (3.1) and (3.2) with $a \neq 0$ and compare our results to those of Cohen and White. We will examine a case in which the nondimensional analogue of b dominates the nondimensional analogue of a, and a case in which the opposite is true; in both cases, we will compare the results C and σ obtained when $C_0 = 0$ to those obtained when $C_0 \neq 0$.

We nondimensionalize the problem by defining

$$\begin{aligned} C(X,T) &\equiv C_1 u(x,t) \\ \sigma(X,T) &\equiv \frac{DC_1}{E} s(x,t) \\ x &\equiv \frac{X}{L} \\ t &\equiv \beta_R T, \end{aligned}$$

to obtain the equations

$$\varepsilon u_t = u_{xx} + s_{xx}, \tag{3.3}$$

$$s_t + b(u)s = pu + ru_t, \tag{3.4}$$

which hold on $0 < x < 1$, $t > 0$. The boundary conditions transform to

$$u(0,t) = \alpha,\ u(1,t) = 1, \tag{3.5}$$

and the initial conditions become

$$u(x,0) = s(x,0) = 0. \tag{3.6}$$

Here

$$\varepsilon \equiv \frac{1}{d},\ \text{where } d \equiv \frac{D}{\beta_R L^2},$$

and we will study the system (3.3), (3.4) under the assumption that ε is very small. The nondimensional parameters are defined by

$$\begin{aligned} p &\equiv \frac{bE}{\beta_R D} \\ r &\equiv \frac{aE}{D} \\ \alpha &\equiv \frac{C_0}{C_1} < 1. \end{aligned}$$

The function $b(u)$ is given by

$$b(u) \equiv \frac{\beta(C_1 u)}{\beta_R} = \frac{1+\omega}{2} + \frac{1-\omega}{2} \tanh \frac{u - u_{RG}}{\Delta u},$$

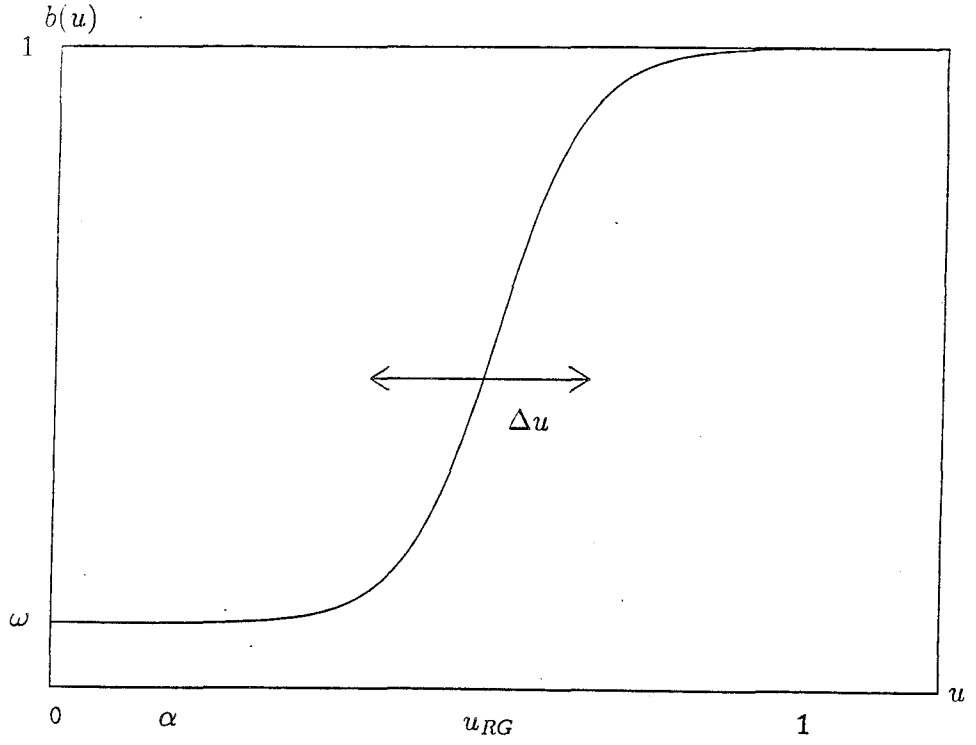

Figure 3.1: $b(u) = \frac{1+\omega}{2} + \frac{1-\omega}{2} \tanh \frac{u-u_{RG}}{\Delta u}$

where

$$\omega \equiv \frac{\beta_G}{\beta_R} < 1;\ u_{RG} \equiv \frac{C_{RG}}{C_1} < 1;\ \Delta u \equiv \frac{\Delta C}{C_1} \ll 1.$$

$b(u)$ is sketched in Figure 3.1. As we did in Chapter 2, we will take ω and Δu to be very small, so that our results will reflect a large and abrupt jump in relaxation time as the polymer changes from its rubbery state to its glassy state.

For later use, we will find it convenient to know the time history of $s(x,t)$ at the boundaries $x = 0$ and $x = 1$. To find this information, we evaluate equation (3.4) at $x = 0$ and at $x = 1$:

$$\begin{aligned} x = 0\text{: } \frac{\partial}{\partial t}s(0,t) &= -b(u(0,t))s(0,t) + pu(0,t) + r\frac{\partial}{\partial t}u(0,t) \\ &= -b(\alpha)s(0,t) + p\alpha \end{aligned}$$

so

$$s(0,t) = \frac{p\alpha}{b(\alpha)} + Ae^{-b(\alpha)t},\ A \text{ a constant.}$$

Similarly, we find

$$s(1,t) = \frac{p}{b(1)} + Be^{-b(1)t},\ B \text{ a constant.}$$

A and B are determined below.

3.1 Perturbation Analysis for ε Small

We begin our analysis by looking for solutions $u(x,t)$ and $s(x,t)$ as perturbation series in the small parameter ε. By the techniques of singular perturbation theory [16], we find that there is an initial layer of thickness $O(\varepsilon)$ near $t = 0$ for all x in $0 < x < 1$. In the outer region away from $t = 0$, we insert the expansions

$$\begin{aligned} u(x,t) &\equiv u_0(x,t) + O(\varepsilon) \\ s(x,t) &\equiv s_0(x,t) + O(\varepsilon) \end{aligned}$$

into equations (3.3), (3.4) to find the $O(1)$ system

$$0 = (u_0)_{xx} + (s_0)_{xx} \tag{3.7}$$

$$(s_0)_t = -b(u_0)s_0 + pu_0 + r(u_0)_t. \tag{3.8}$$

By solving equation (3.7) and using the boundary information for u and s, we find readily that

$$u_0(x,t) + s_0(x,t) = \left[\alpha + \frac{p\alpha}{b(\alpha)} + Ae^{-b(\alpha)t}\right](1-x) + \left[1 + \frac{p}{b(1)} + Be^{-b(1)t}\right]x. \tag{3.9}$$

We solve (3.9) for $s_0(x,t)$ and insert the result into equation (3.8) to find a nonlinear ordinary differential equation for $u_0(x,t)$:

$$\frac{\partial u_0}{\partial t}+\frac{p+b(u_0)}{1+r}u_0-\left\{\left[\alpha+\frac{p\alpha}{b(\alpha)}+Ae^{-b(\alpha)t}\right](1-x)+\left[1+\frac{p}{b(1)}+Be^{-b(1)t}\right]x\right\}\frac{b(u_0)}{1+r}$$
$$=\frac{-b(\alpha)Ae^{-b(\alpha)t}(1-x)-b(1)Be^{-b(1)t}x}{1+r}, \tag{3.10}$$

in which x appears only as a parameter. This equation cannot be solved analytically in general.

Before we examine equation (3.10) further, we find the behavior of u and s in the initial layer. In this layer, equations (3.7) and (3.8) are not good approximations to the full system (3.3), (3.4); we cannot simply neglect the term εu_t in equation (3.3).

We stretch the region near $t = 0$ by setting

$$\tau \equiv \frac{t}{\varepsilon},\ u(x,t) \equiv v(x,\tau), \text{ and } s(x,t) \equiv w(x,\tau).$$

To lowest order, we take

$$v(x,\tau) \equiv v_0(x,\tau) + O(\varepsilon),\ w(x,\tau) \equiv w_0(x,\tau) + O(\varepsilon);$$

equations (3.3)–(3.6) then yield

$$(v_0)_\tau = (v_0)_{xx} + (w_0)_{xx}, \tag{3.11}$$

$$(w_0)_\tau = r(v_0)_\tau, \tag{3.12}$$

$$v_0(0,\tau) = \alpha,\ v_0(1,\tau) = 1, \tag{3.13}$$

$$v_0(x,0) = w_0(x,0) = 0. \tag{3.14}$$

Equation (3.12) and the initial conditions (3.14) for v_0 and w_0 imply that

$$w_0(x,\tau) = rv_0(x,\tau). \tag{3.15}$$

With this form for w_0, equation (3.11) becomes

$$(v_0)_\tau = (1+r)(v_0)_{xx}, \tag{3.16}$$

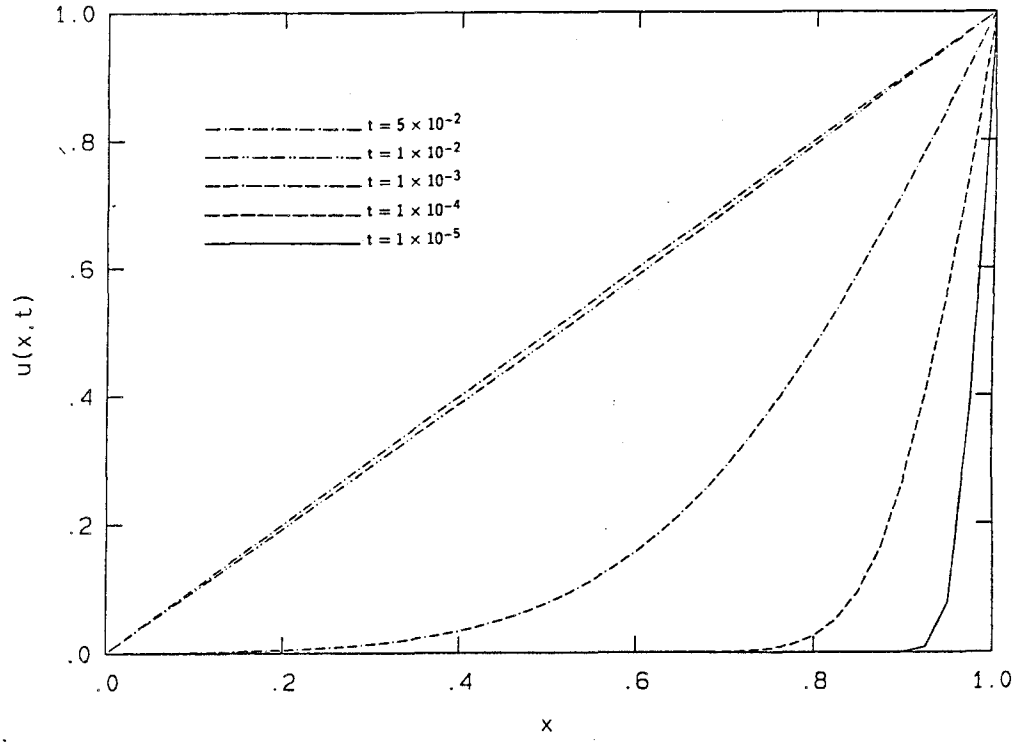

Figure 3.2: First-order $u(x,t) = s(x,t)$ for small t; $\alpha = 0$

a simple diffusion equation. We solve equation (3.16) for v_0 and use (3.15) to determine w_0, finding

$$v_0(x,\tau) = \alpha(1-x) + x + 2\sum_{n=1}^{\infty} \frac{(-1)^n - \alpha}{n\pi} \sin n\pi x \; e^{-n^2\pi^2(1+r)\tau} \tag{3.17}$$

$$\begin{aligned} w_0(x,\tau) &= r v_0(x,\tau) \\ &= r\left\{\alpha(1-x) + x + 2\sum_{n=1}^{\infty} \frac{(-1)^n - \alpha}{n\pi} \sin n\pi x \; e^{-n^2\pi^2(1+r)\tau}\right\}. \end{aligned} \tag{3.18}$$

In Figures 3.2 and 3.3, we display graphs of $v_0(x,\tau)$ for several values of $t = \varepsilon\tau$. We use the values $\varepsilon = 0.05$ and $r = 1$ in both graphs; $\alpha = 0$ in Figure 3.2 and $\alpha = 0.5$ in Figure 3.3. Since $r = 1$, v_0 and w_0 are equal. Note that neither p nor $b(u)$ plays a role, to first order, in v or w. We see that the sudden influx of penetrant has resulted in the relation $w \approx rv$; when transformed back to the dimensional variables, this relation becomes $\sigma \approx aC$, the result we expected to observe.

Since $w_0(x,\tau)$ is completely determined, we must fix the constants A and B to

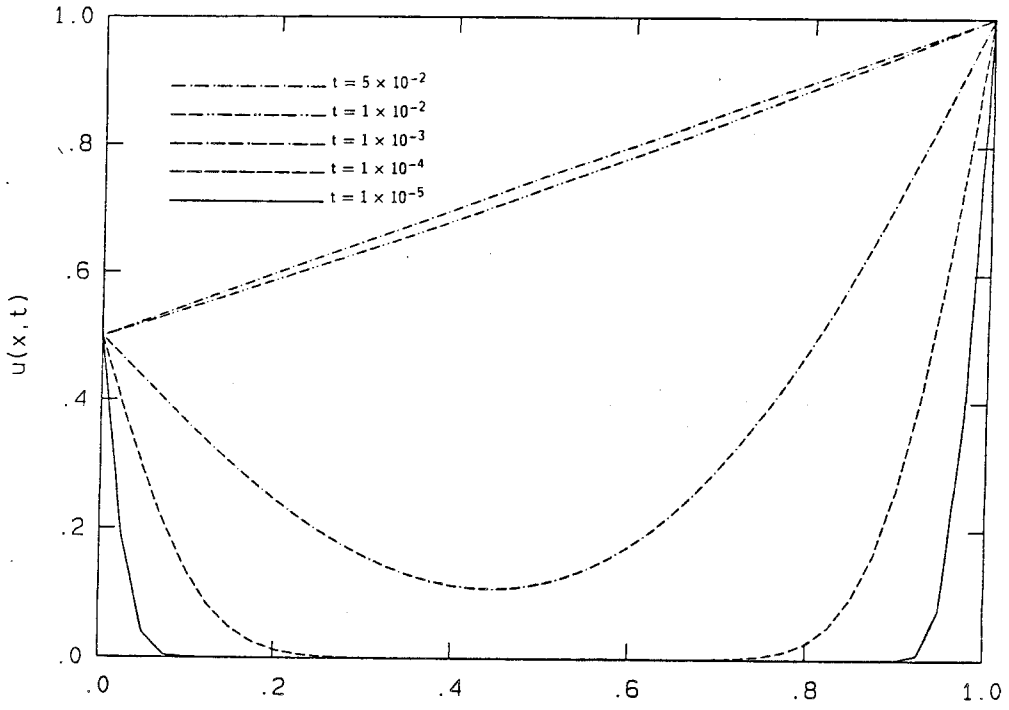

Figure 3.3: First-order $u(x,t) = s(x,t)$ for small t; $\alpha = 0.5$

match the boundary values of w_0; that is,

$$\lim_{\tau\to\infty} w_0(0,\tau) = \lim_{t\to 0} s(0,t)$$

and

$$\lim_{\tau\to\infty} w_0(1,\tau) = \lim_{t\to 0} s(1,t),$$

so that

$$r\alpha = \frac{p\alpha}{b(\alpha)} + A \Longrightarrow A = r\alpha - \frac{p\alpha}{b(\alpha)}$$

and

$$r = \frac{p}{b(1)} + B \Longrightarrow B = r - \frac{p}{b(1)}.$$

Therefore, the fully specified boundary data for s are

$$\begin{aligned} s(0,t) &= r\alpha e^{-b(\alpha)t} + \frac{p\alpha}{b(\alpha)}\left[1 - e^{-b(\alpha)t}\right] \\ s(1,t) &= re^{-b(1)t} + \frac{p}{b(1)}\left[1 - e^{-b(1)t}\right]. \end{aligned}$$

Since $\lim_{t\to 0} s(0,t) = r\alpha$ and $\lim_{t\to 0} s(1,t) = r$, stress begins to build up at the boundaries of the polymer as soon as the penetrant starts to diffuse in.

If we set r equal to zero in (3.17) and (3.18), we obtain the same initial-layer functions that Cohen and White found when they examined the case $r = 0$ [4]. Our results with $r \neq 0$ are quite different from theirs, in that the stress s, rather than simply equaling zero throughout the initial layer, is a nonzero function of x and t with the same shape as the concentration u.

We must verify that the inner functions v_0, w_0 and the outer functions u_0, s_0 are consistent with each other. We do so by evaluating $v_0 + w_0$ and $u_0 + s_0$ on a t-interval where they are both defined: We set $t \equiv \eta t_\eta$, where $\varepsilon < \eta(\varepsilon) \ll 1$ for all ε. As $\varepsilon \to 0$, keeping t_η fixed, $t \to 0$ and $\tau = \eta(\varepsilon)t_\eta/\varepsilon \to \infty$. Therefore, as $\varepsilon \to 0$,

$$\begin{aligned} u_0(x,t) + s_0(x,t) &= u_0(x,\eta t_\eta) + s_0(x,\eta t_\eta) \\ &= \alpha\left[1 + \frac{p}{b(\alpha)} + \left(r - \frac{p}{b(\alpha)}\right) e^{-b(\alpha)\eta t_\eta}\right](1-x) \\ &\quad + \left[1 + \frac{p}{b(1)} + \left(r - \frac{p}{b(1)}\right) e^{-b(1)\eta t_\eta}\right] x \\ &\xrightarrow{\varepsilon\to 0} (1+r)[\alpha(1-x) + x] \end{aligned}$$

and

$$\begin{aligned} v_0(x,\tau) + w_0(x,\tau) &= v_0(x,\eta t_\eta/\varepsilon) + w_0(x,\eta t_\eta/\varepsilon) \\ &= (1+r)[\alpha(1-x) + x] \\ &\quad + 2(1+r)\sum_{n=1}^{\infty} \frac{(-1)^n - \alpha}{n\pi} \sin n\pi x \; e^{-n^2\pi^2(1+r)\eta t_\eta/\varepsilon} \\ &\xrightarrow{\varepsilon\to 0} (1+r)[\alpha(1-x) + x] \\ &= \lim_{\varepsilon\to 0}\{u_0(x,t) + s_0(x,t)\}. \end{aligned}$$

The solutions in the initial layer do indeed match the solutions outside the layer to first order.

We have, in the functions (3.17) and (3.18), analytical expressions for the first-order behavior of u and s for small time. In order to find the first-order behavior of u and s for longer time, we must solve the nonlinear equation (3.10) for u_0 and insert the result into the expression (3.9) to find s_0. We cannot solve equation (3.10) analytically as it stands; however, we can find the approximate behavior of u_0 by solving equation (3.10) in the limiting case $\Delta u \to 0$. In this limit, $b(u)$ is a step function and the equation simplifies into two first-order ordinary differential equations with constant coefficients:

$$\begin{aligned} u_0 < u_{RG}\text{: } (u_0)_t + \frac{\omega+p}{1+r}u_0 &= \frac{\omega(1+p)-\alpha(\omega+p)}{1+r}x + \frac{\alpha(\omega+p)}{1+r} \\ &\quad + \frac{(1-\omega)(p-r)}{1+r}xe^{-t} \qquad (3.19) \\ u_0 > u_{RG}\text{: } (u_0)_t + \frac{1+p}{1+r}u_0 &= \frac{\omega(1+p)-\alpha(\omega+p)}{\omega(1+r)}x + \frac{\alpha(\omega+p)}{\omega(1+r)} \\ &\quad - \frac{\alpha(1-\omega)(p-\omega r)}{\omega(1+r)}(1-x)e^{-\omega t}. \qquad (3.20) \end{aligned}$$

Since these equations are to hold in the outer region away from $t = 0$, we cannot use the initial condition $u(x,0) = 0$. Instead, we use the $\tau \to \infty$ limit of the initial function $v_0(x,\tau)$ as the initial condition for u_0:

$$\lim_{\tau\to\infty} v_0(x,\tau) = \alpha(1-x) + x \equiv u_0(x,0).$$

We see immediately that, when $t = 0$,

$$u_0(x,t) < u_{RG} \Longleftrightarrow x < \frac{u_{RG}-\alpha}{1-\alpha} \equiv x_{RG} \qquad (3.21)$$

and

$$u_0(x,t) > u_{RG} \Longleftrightarrow x > \frac{u_{RG}-\alpha}{1-\alpha}, \qquad (3.22)$$

so that initially there is no ambiguity about the domains on which equations (3.19) and (3.20) hold. We assume that (3.21) and (3.22) hold for all time; this assumption,

based on the lack of a flux mechanism in equation (3.10), will be shown to be valid when we solve the system numerically below. We can easily integrate equations (3.19) and (3.20) to find

$$x < x_{RG}\text{: } u_0(x,t) = \alpha(1-x) + x\left\{\frac{\omega(1+p)}{\omega+p} + \frac{(1-\omega)(p-r)}{p-r-(1-\omega)}e^{-t} - \frac{(1-\omega)(p-\omega r)}{(\omega+p)[p-r-(1-\omega)]}e^{-\frac{\omega+p}{1+r}t}\right\} \tag{3.23}$$

$$x > x_{RG}\text{: } u_0(x,t) = x + \alpha(1-x)\left\{\frac{\omega+p}{\omega(1+p)} - \frac{(1-\omega)(p-\omega r)}{\omega[p-\omega r+1-\omega]}e^{-\omega t} + \frac{(1-\omega)(p-r)}{(1+p)[p-\omega r+1-\omega]}e^{-\frac{1+p}{1+r}t}\right\}. \tag{3.24}$$

$s_0(x,t)$ is obtained from $u_0(x,t)$ via equation (3.9).

We are interested in the cases $p > r$, in which u dominates u_t in the stress evolution equation (3.4), and $p < r$, in which u_t dominates u. In Figures 3.4 and 3.5, we show u_0 and s_0, for several values of t, for the case $p > r$. In these figures we use the parameter values $p = 1.5$, $u_{RG} = (1+\alpha)/2$, $\omega = 0.01$, and $r = 1$. We take $\alpha = 0$ in Figure 3.4 and $\alpha = 0.5$ in Figure 3.5, so that we can see the results for both zero and nonzero penetrant concentration incoming at $x = 0$. The $p < r$ results are displayed in Figures 3.6 and 3.7 where, again, $\alpha = 0$ and $\alpha = 0.5$ respectively, and the parameter values are $p = 0.001$, $u_{RG} = (1+\alpha)/2$, $\omega = 0.01$, and $r = 1$.

We see that these outer solutions are very different from the diffusive solutions in the inner layer near $t = 0$. In all cases, the outer solutions display a steep front at the interior point x_{RG}. When $p \ll r$, the height of the front reaches a maximum at finite time and then collapses down; when $p > r$, the height of the front is still increasing at $t = 50$. We note also that the position of the front is determined by the parameters u_{RG} and α, and does not vary with t. Finally, we observe that the slopes of the line segments composing u_0 in $x < x_{RG}$ and $x > x_{RG}$ are negative for large time when $\alpha = 0.5$ and $p = 1.5$, and positive in the other cases. This characteristic

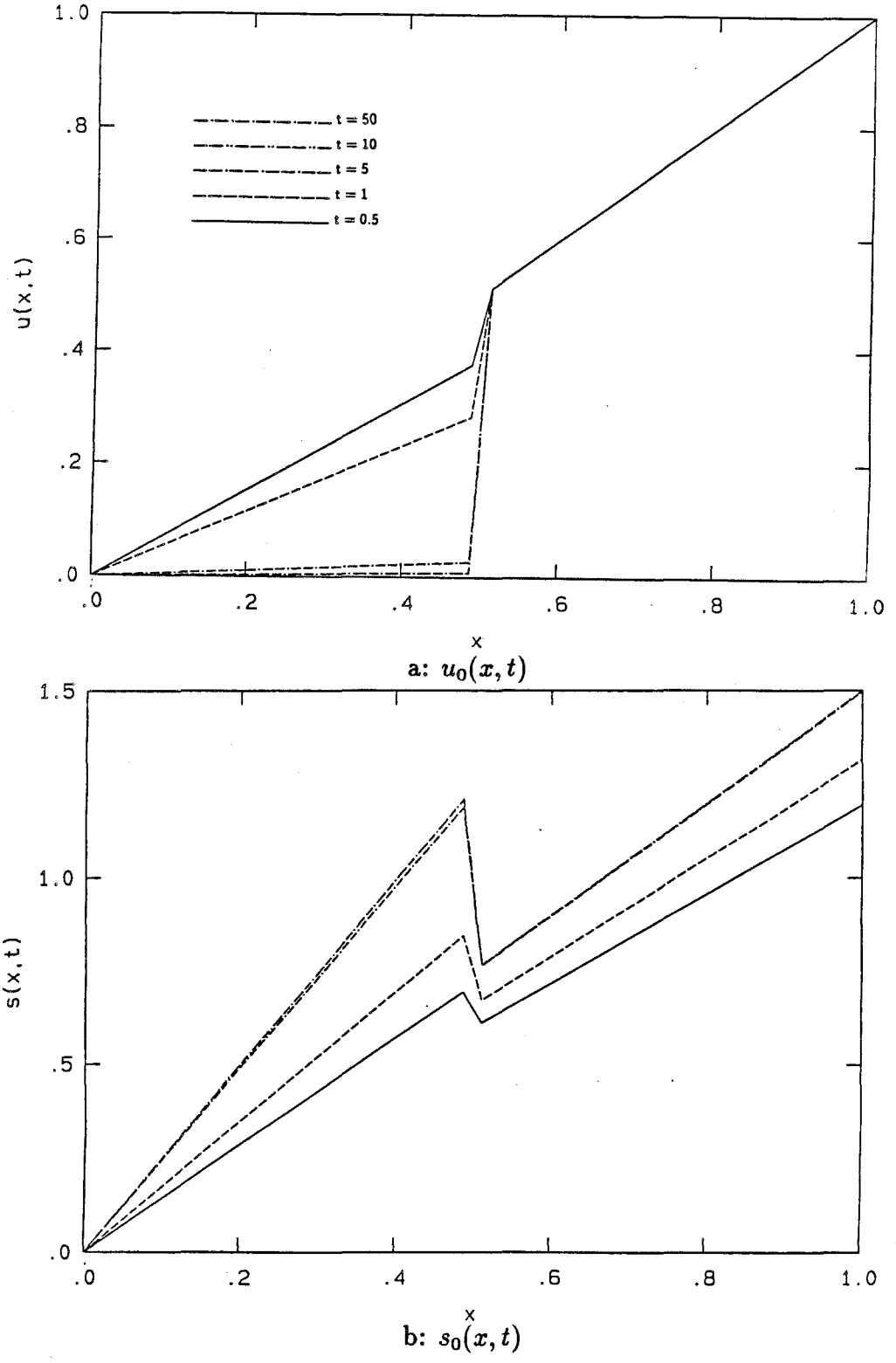

Figure 3.4: Profiles of u_0 and s_0 for large t; $p = 1.5$; $\alpha = 0$; $\Delta u = 0$

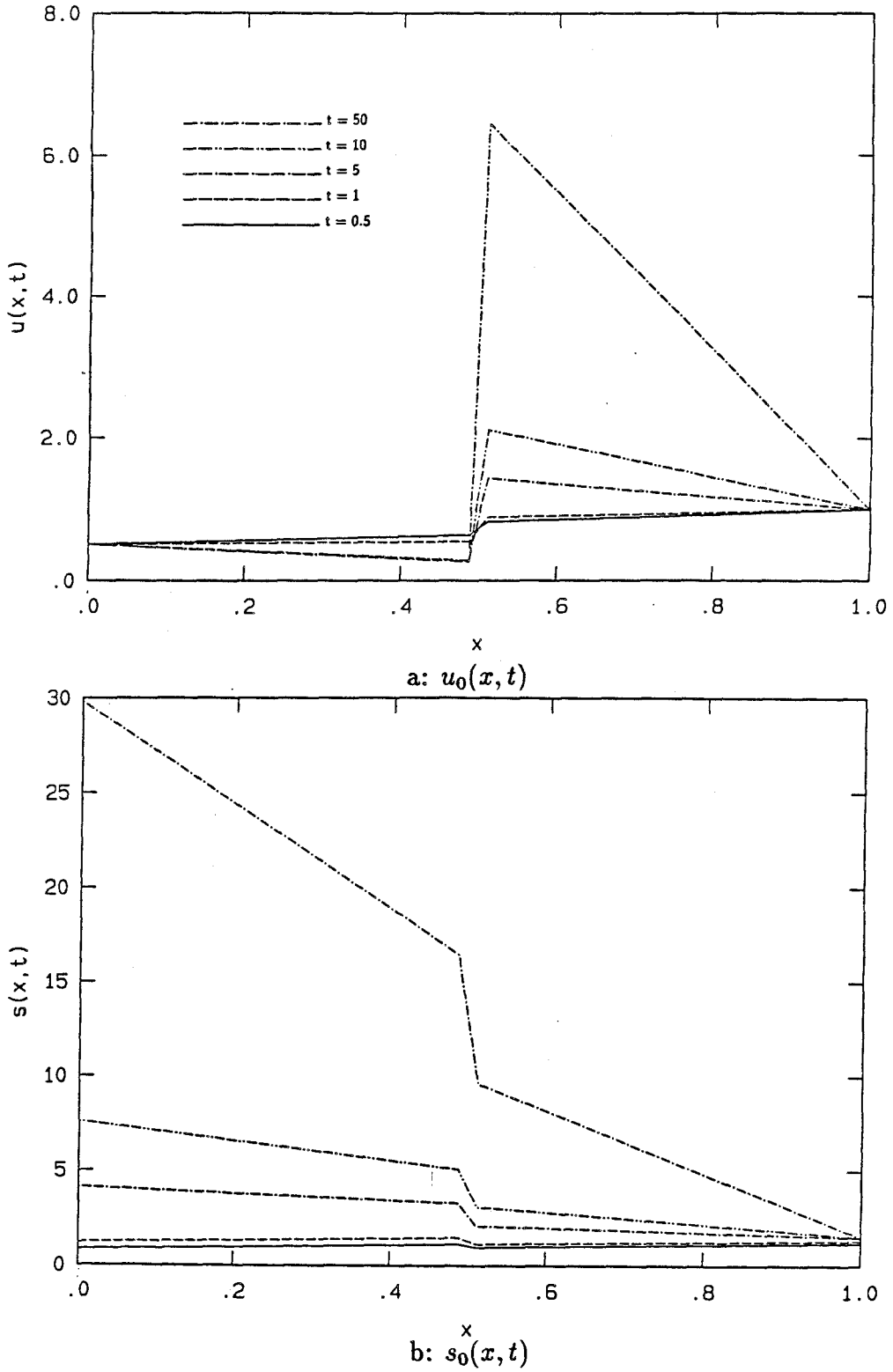

Figure 3.5: Profiles of u_0 and s_0 for large t; $p = 1.5$; $\alpha = 0.5$; $\Delta u = 0$

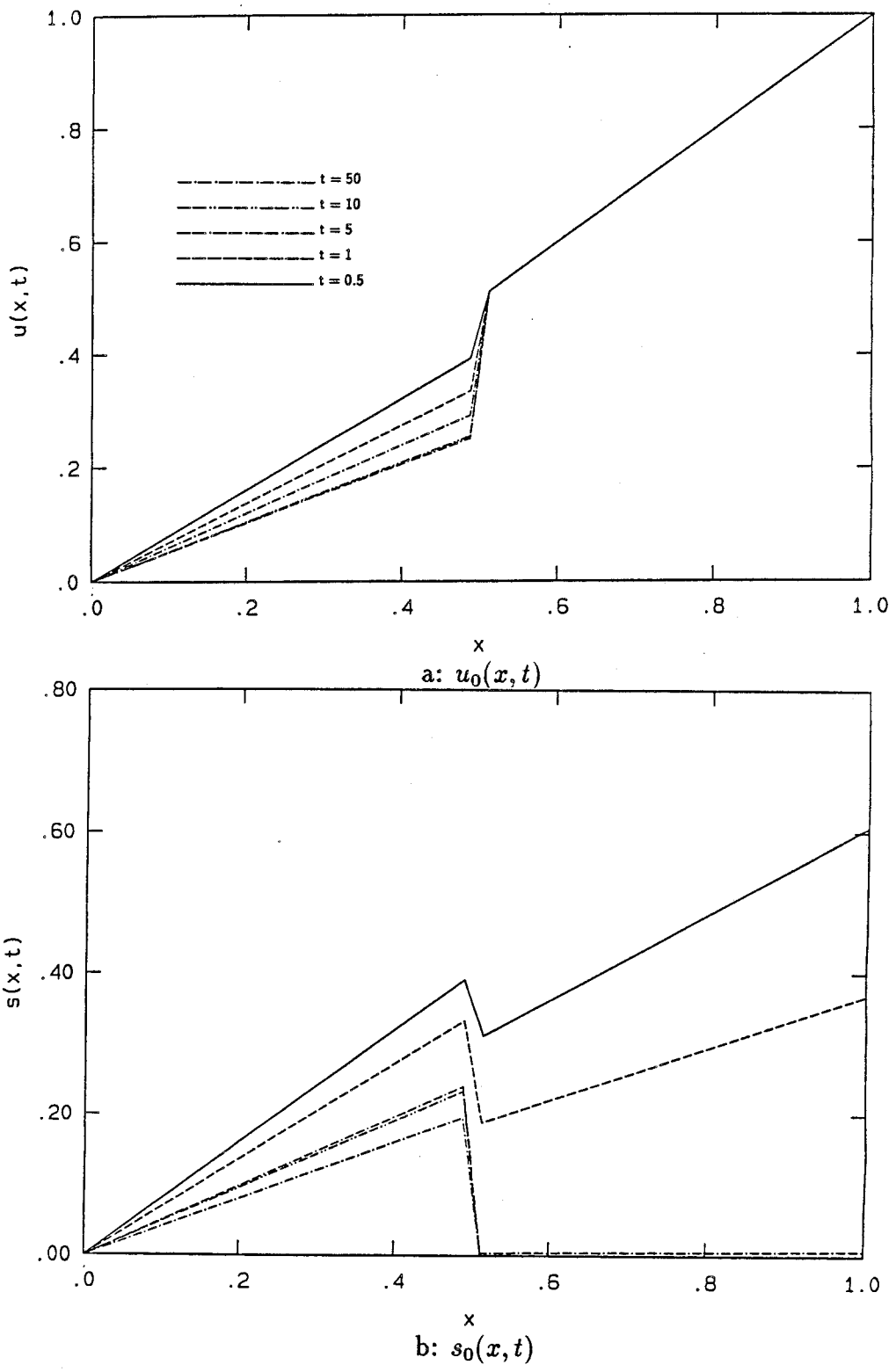

Figure 3.6: Profiles of u_0 and s_0 for large t; $p = 0.001$; $\alpha = 0$; $\Delta u = 0$

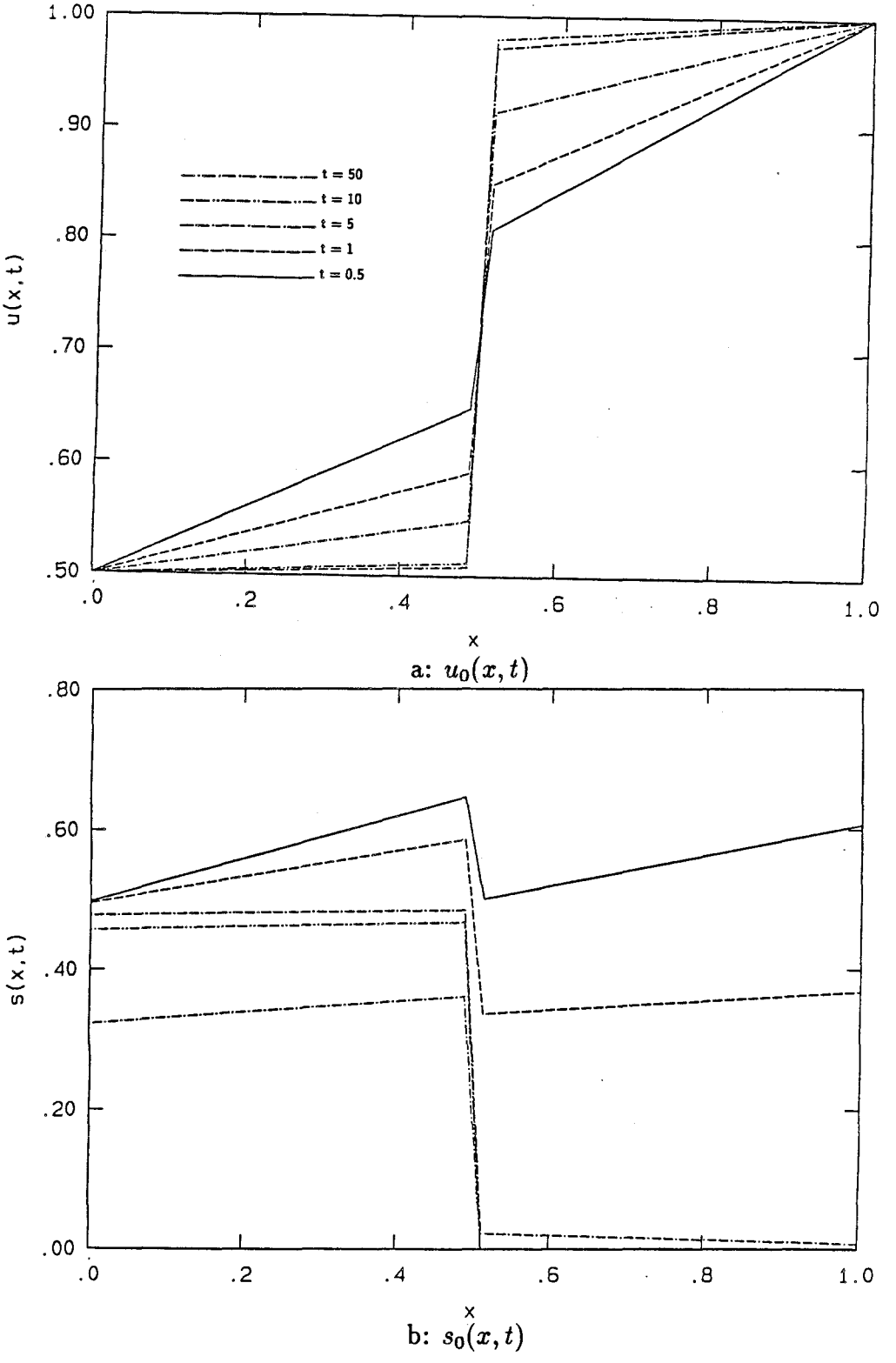

Figure 3.7: Profiles of u_0 and s_0 for large t; $p = 0.001$; $\alpha = 0.5$; $\Delta u = 0$

will be further explored in § 3.3 when we carry out a steady-state analysis of the equations.

When Δu is not equal to zero, but is very small, equation (3.10) must be solved numerically. Since it is a first-order ordinary differential equation in t, we compute its solutions easily using a fourth-order accurate Runge-Kutta method [2]. Our results are presented in Figures 3.8 ($\alpha = 0$) and 3.9 ($\alpha = 0.5$) with the parameter values $p = 1.5$, $u_{RG} = (1 + \alpha)/2$, $\Delta u = 0.01$, $\omega = 0.01$, and $r = 1$, and in Figures 3.10 ($\alpha = 0$) and 3.11 ($\alpha = 0.5$) with $p = 0.001$, $u_{RG} = (1 + \alpha)/2$, $\Delta u = 0.01$, $\omega = 0.01$, and $r = 1$. These functions are all very similar to the corresponding $\Delta u = 0$ solutions.

In the two sets of functions (3.17), (3.18) and (3.23), (3.24), (3.9), we have explicit asymptotic approximations to $u(x,t)$ and $s(x,t)$, for small and large times respectively. Figures 3.2 to 3.7 comprise solutions computed from these asymptotic approximations. We will now compare them to the actual solutions, which we find from numerical analysis of the full system (3.3)–(3.6).

3.2 Solutions of Full Equations

We wish to solve the full system (3.3)–(3.6) so that we can verify the perturbation analysis of § 3.1 and also find the behavior of $u(x,t)$ and $s(x,t)$ beyond $O(1)$ in ε. Because we cannot solve the equations analytically, we analyze them numerically.

We need a numerical method that will resolve both the initial layer in t and the steep front near $x = x_{RG}$. In the spirit of Kálnay de Rivas [15], we perform a cubic transformation on both independent variables, setting

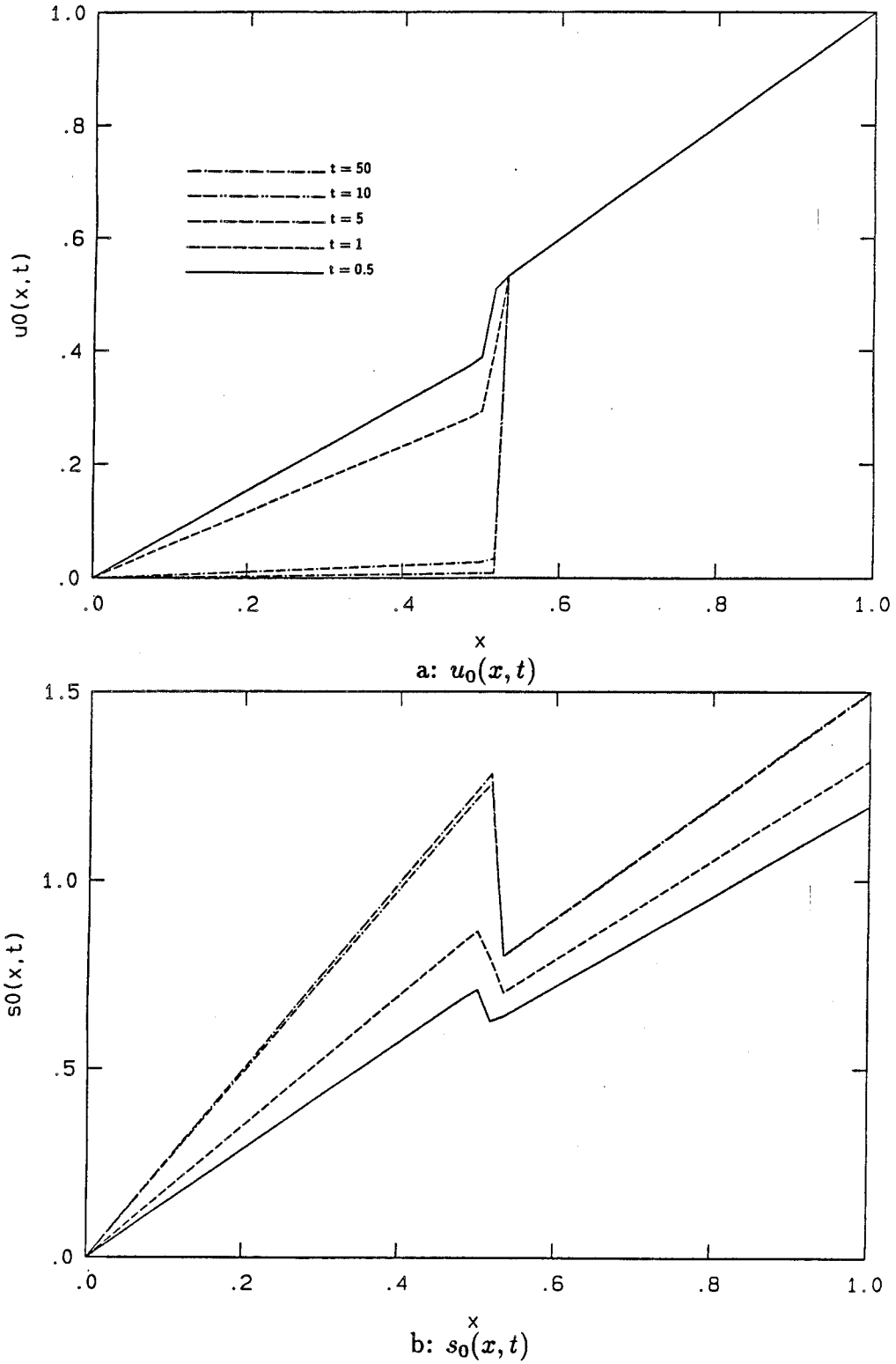

Figure 3.8: Profiles of u_0 and s_0 for large t; $p = 1.5$; $\alpha = 0$

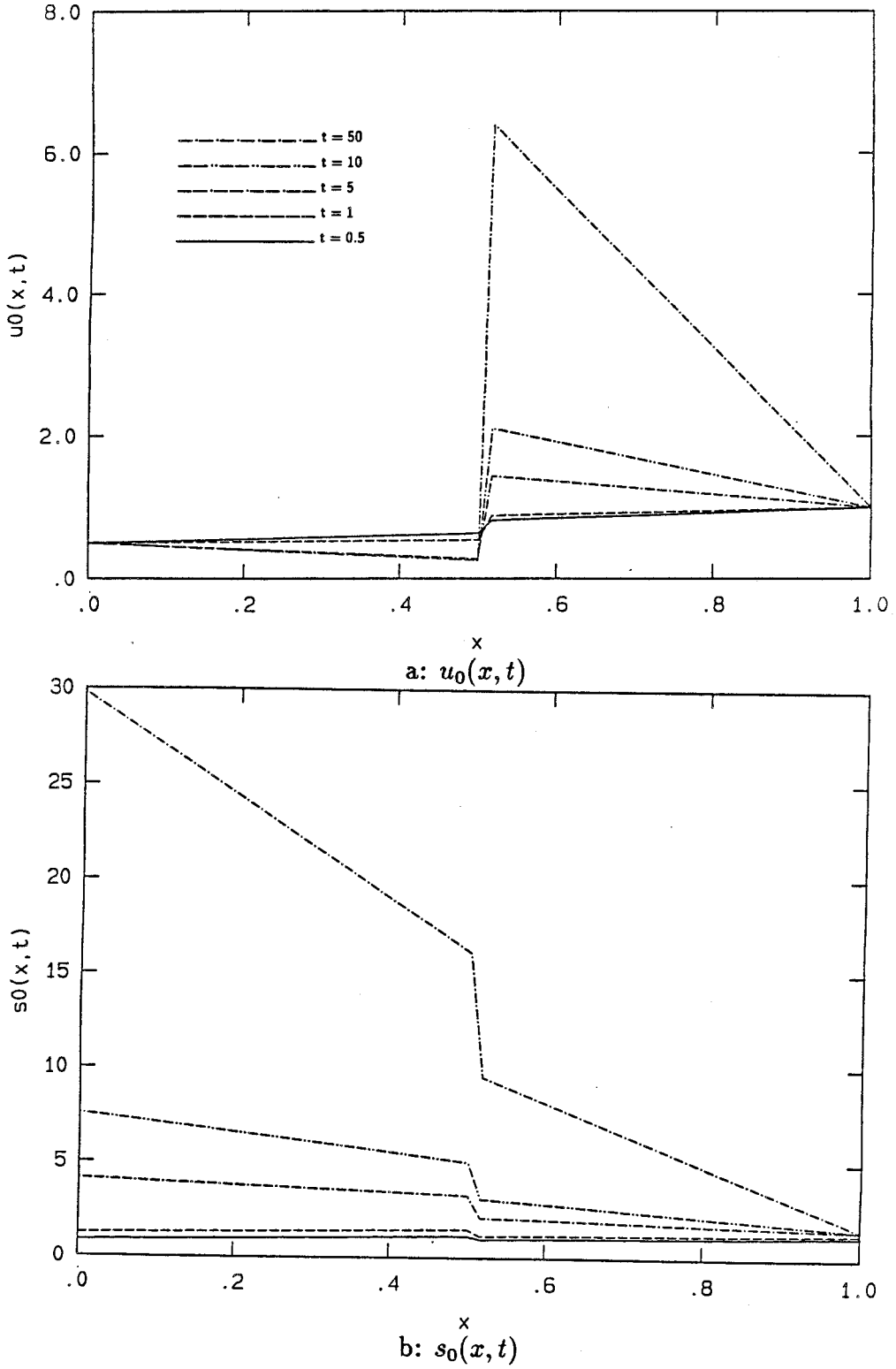

a: $u_0(x,t)$

b: $s_0(x,t)$

Figure 3.9: Profiles of u_0 and s_0 for large t; $p = 1.5$; $\alpha = 0.5$

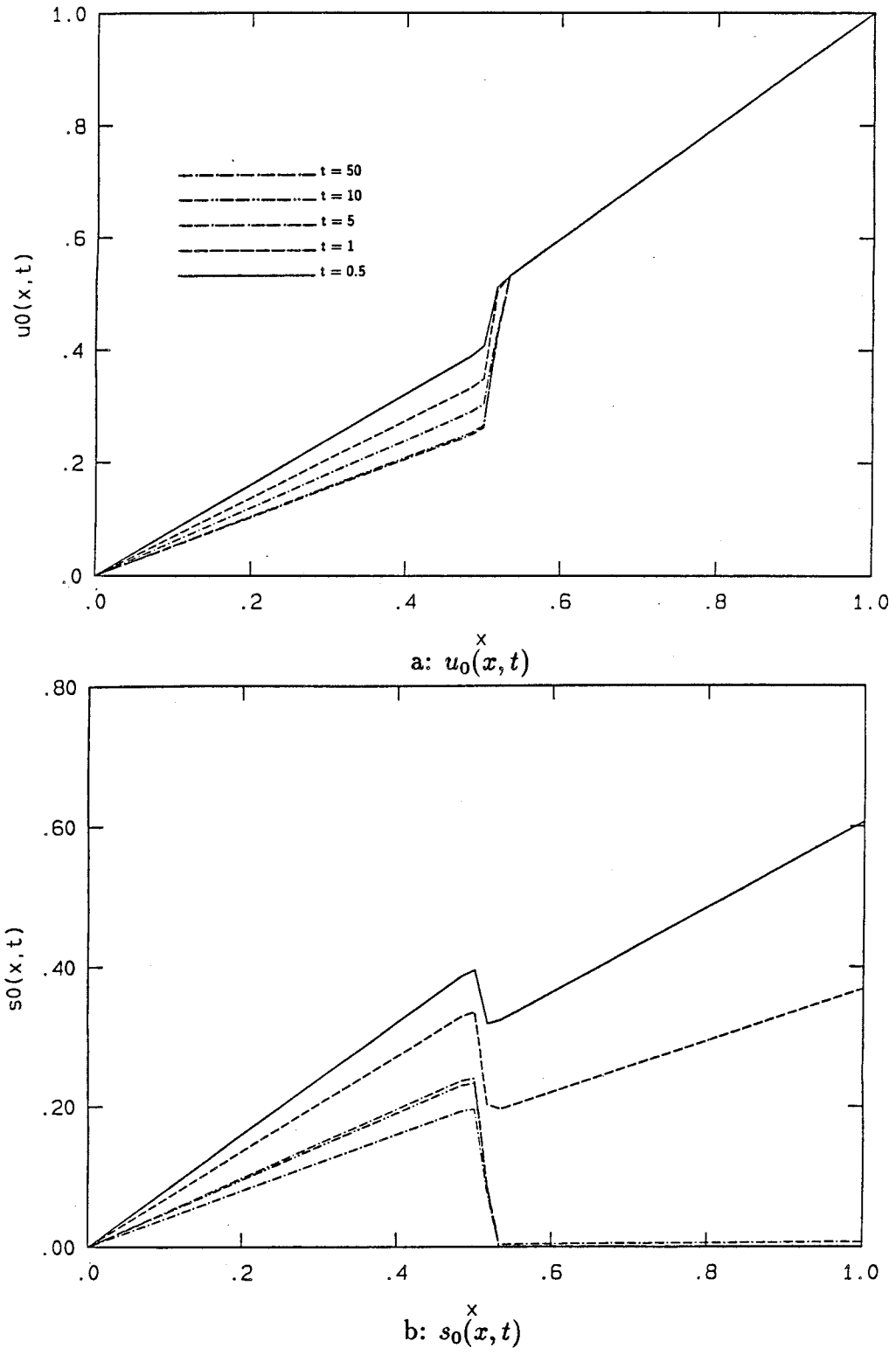

Figure 3.10: Profiles of u_0 and s_0 for large t; $p = 0.001$; $\alpha = 0$

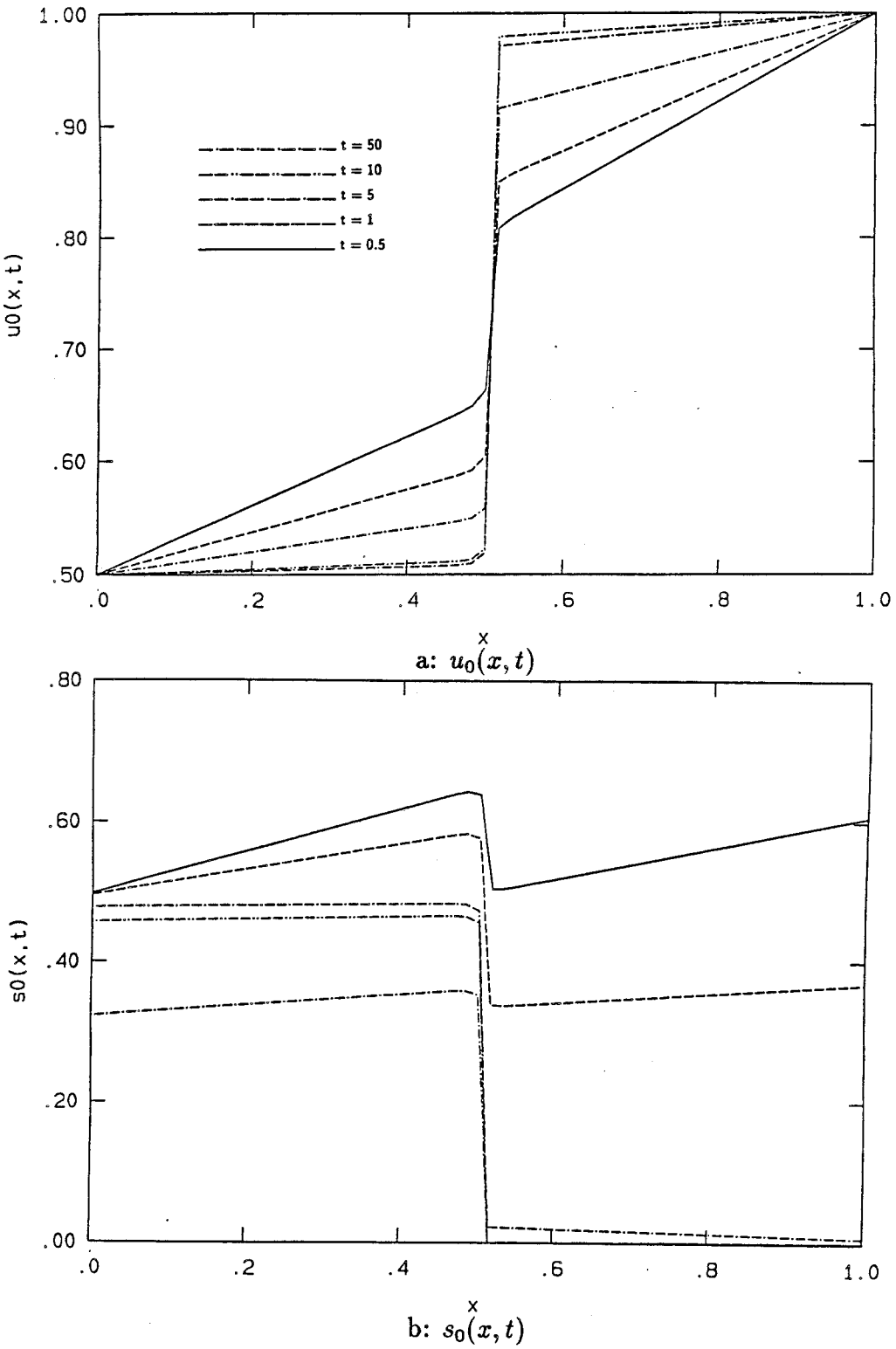

Figure 3.11: Profiles of u_0 and s_0 for large t; $p = 0.001$; $\alpha = 0.5$

$$\xi^3 \equiv x - x_{RG}$$
$$\tau^3 \equiv t$$

and

$$u(x,t) \equiv \overline{u}(\xi,\tau);\ s(x,t) \equiv \overline{s}(\xi,\tau).$$

Near $t = 0$, $dt/d\tau = 3\tau^2 = 3t^{2/3}$ is very small, so a uniform mesh in τ corresponds to a very small mesh spacing in t. Similarly, $dx/d\xi = 3(x - x_{RG})^{2/3}$ is very small near $x = x_{RG}$, so a uniform mesh in ξ corresponds to a small mesh spacing in x.

The equations change under these independent-variable transformations to

$$3\varepsilon\xi^5\frac{\partial\overline{u}}{\partial\tau} = \tau^2\left[\xi\left(\frac{\partial^2\overline{u}}{\partial\xi^2} + \frac{\partial^2\overline{s}}{\partial\xi^2}\right) - 2\left(\frac{\partial\overline{u}}{\partial\xi} + \frac{\partial\overline{s}}{\partial\xi}\right)\right] \tag{3.25}$$

$$r\frac{\partial\overline{u}}{\partial\tau} - \frac{\partial\overline{s}}{\partial\tau} = 3\tau^2[b(\overline{u})\overline{s} - p\overline{u}], \tag{3.26}$$

which hold on the range

$$\xi_0 < \xi < \xi_1,\ \tau > 0,$$

where

$$\xi_0 \equiv -\left(\frac{u_{RG} - \alpha}{1 - \alpha}\right)^{1/3}$$
$$\xi_1 \equiv \left(\frac{1 - u_{RG}}{1 - \alpha}\right)^{1/3}.$$

$\overline{u}$ satisfies the boundary conditions

$$\overline{u}(\xi_0,\tau) = \alpha,\ \overline{u}(\xi_1,\tau) = 1; \tag{3.27}$$

$\overline{u}$ and $\overline{s}$ satisfy the initial conditions

$$\overline{u}(\xi,0) = \overline{s}(\xi,0) = 0. \tag{3.28}$$

Since equation (3.25) is stiff, we use an implicit method to solve it [2]. The method used to solve equation (3.26) is also implicit, except that the nonlinear term $b(\overline{u})$ is modeled explicitly. We integrate the equations over the range $\tau = 0$ to $\tau = 4.642$, corresponding to the range $t = 0$ to $t \approx 100$, checking for accuracy at τ-intervals of 0.05.

We present the results, as functions of x and t, in Figures 3.12 through 3.15. As in § 3.1, in all cases we use the parameter values $\varepsilon = 0.05$, $u_{RG} = (1 + \alpha)/2$, $\omega = 0.01$, $\Delta u = 0.01$, and $r = 1$. The four graphs cover the cases $\alpha = 0$, $p = 1.5$; $\alpha = 0.5$, $p = 1.5$; $\alpha = 0$, $p = 0.001$; and $\alpha = 0.5$, $p = 0.001$. We find solutions which look diffusive for very small t ($t = 10^{-5}$ and 10^{-3}) and shocklike for larger t ($t = 1$, 10, and 100). In all cases of the parameters α and p, the solutions are almost identical to the corresponding functions found by perturbation techniques in § 3.1. Due to the higher-order ε terms, u and s are not composed of line segments for large t, but of smooth curves away from $x \approx x_{RG}$ and steep curves near $x \approx x_{RG}$.

3.3 Steady-State Solutions

We conclude our analysis by looking for the steady-state behavior of u and s. Noting that the solutions found in the previous sections are shocklike at long times, we expect to find shocks in the steady-state solutions [24].

If we let $u_s(x)$ and $s_s(x)$ be the steady-state solutions of equations (3.3) and (3.4), we see immediately that u_s and s_s satisfy

$$(u_s + s_s)_{xx} = 0 \tag{3.29}$$

$$b(u_s)s_s = pu_s \tag{3.30}$$

and that u_s satisfies the boundary conditions

$$u_s(0) = \alpha,\ u_s(1) = 1. \tag{3.31}$$

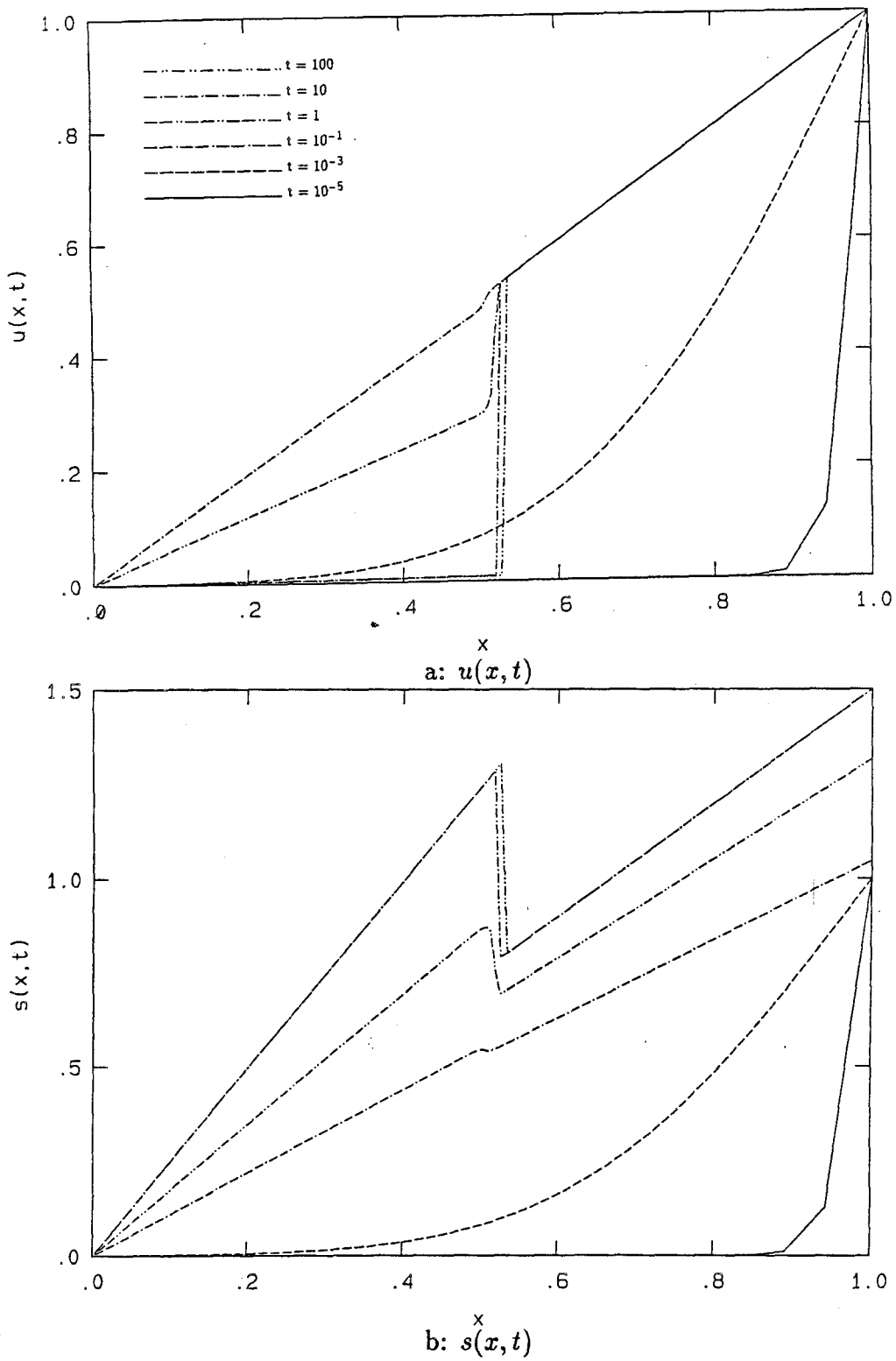

Figure 3.12: Profiles of u and s for small and large t; $p = 1.5$; $\alpha = 0$

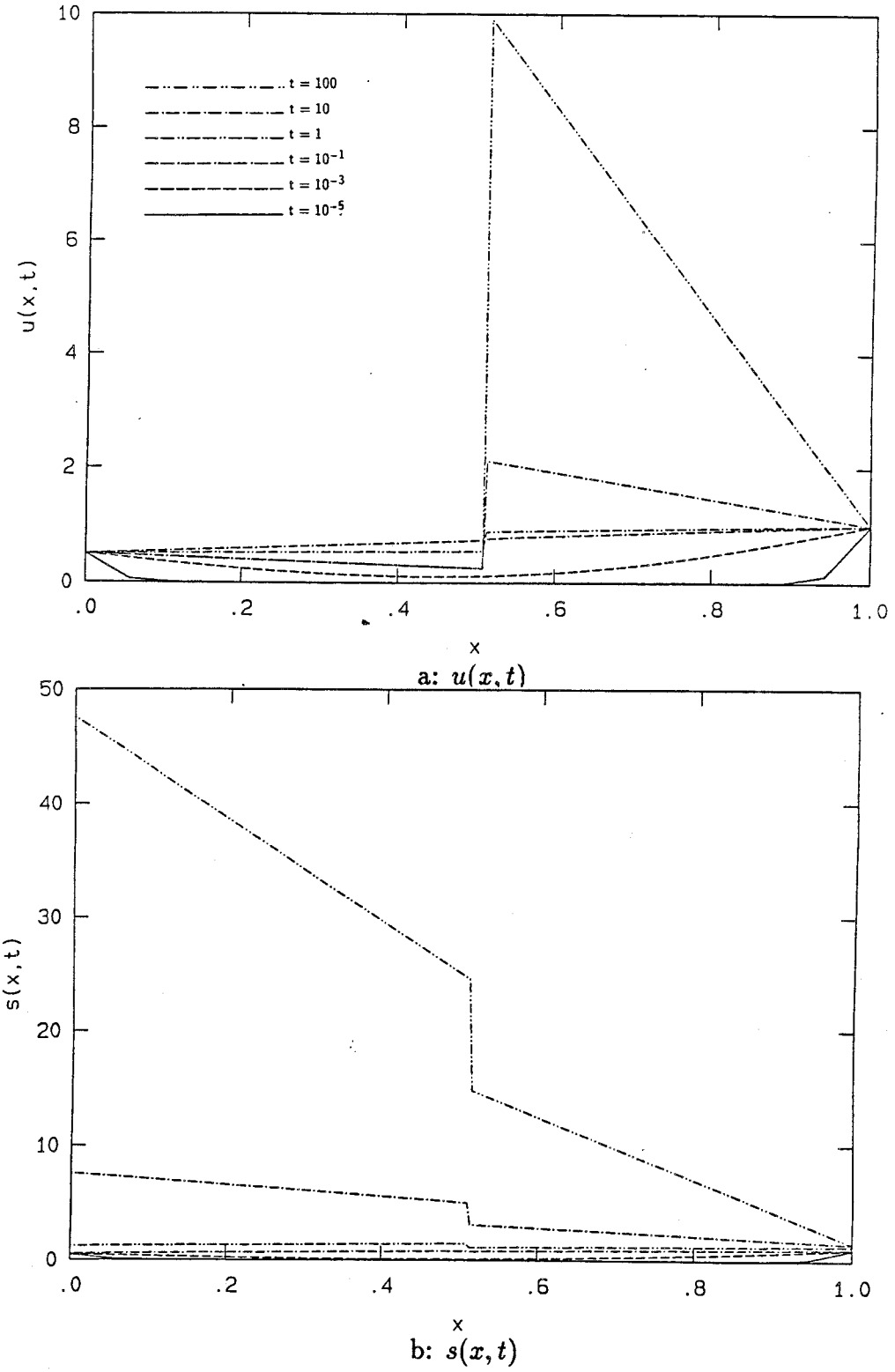

Figure 3.13: Profiles of u and s for small and large t; $p = 1.5$; $\alpha = 0.5$

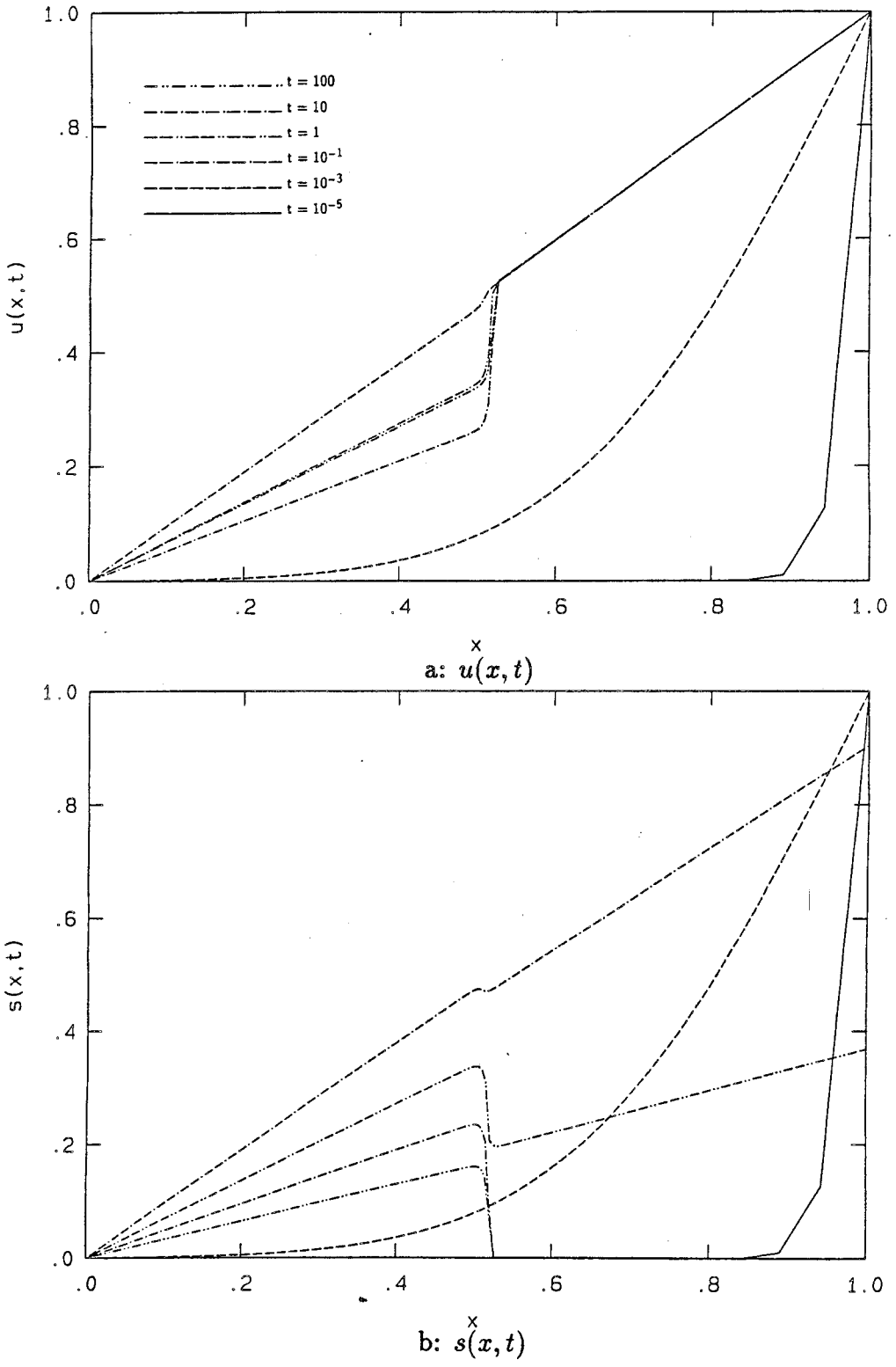

Figure 3.14: Profiles of u and s for small and large t; $p = 0.001$; $\alpha = 0$

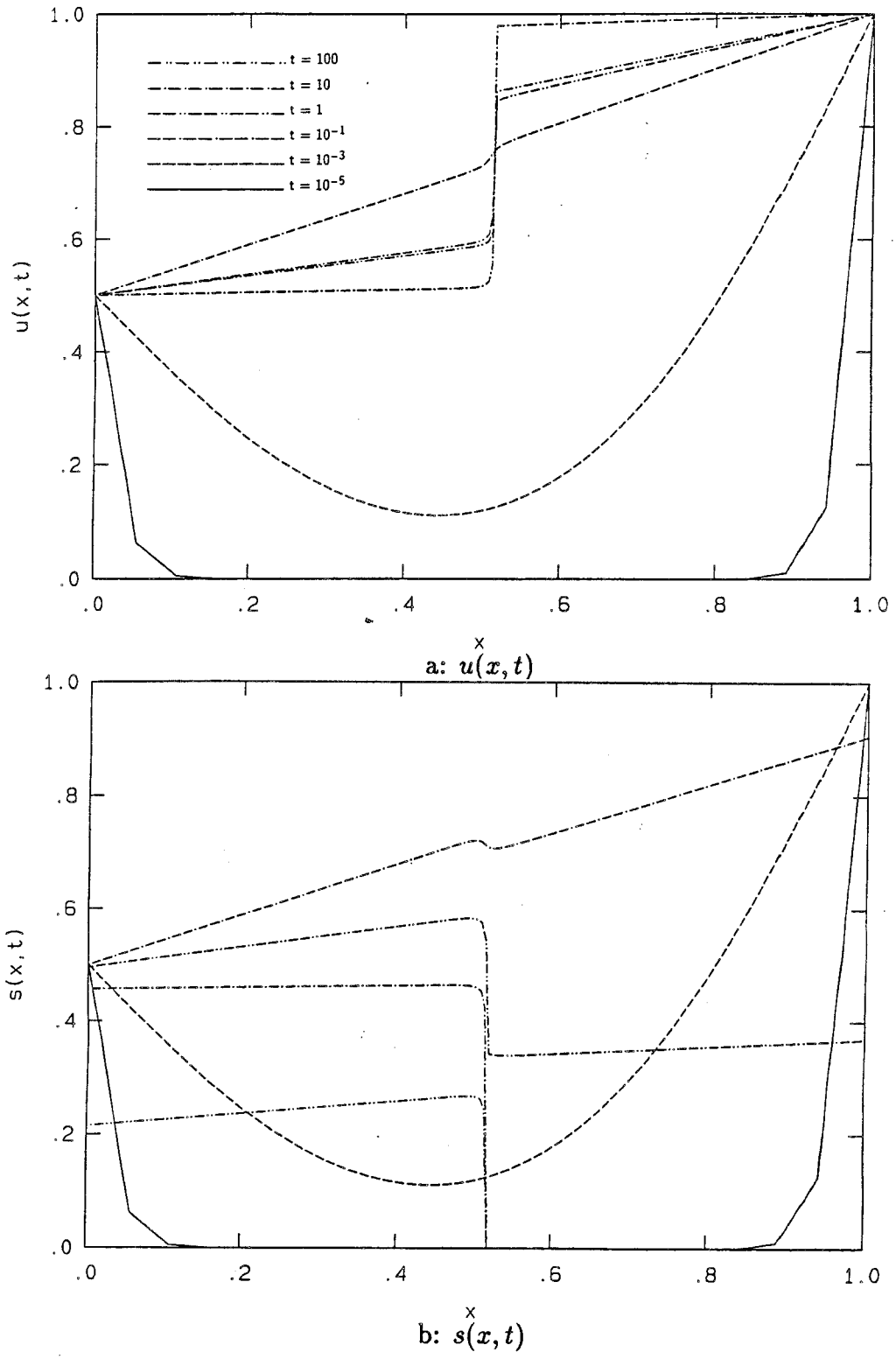

Figure 3.15: Profiles of u and s for small and large t; $p = 0.001$; $\alpha = 0.5$

Equation (3.29) can be solved immediately to yield

$$u_s(x) + s_s(x) = \left[1 + \frac{p}{b(1)} - \alpha - \frac{p\alpha}{b(\alpha)}\right] x + \alpha + \frac{p\alpha}{b(\alpha)}.$$

From equation (3.30) we have

$$s_s(x) = \frac{p u_s(x)}{b(u_s(x))} \tag{3.32}$$

so that

$$u_s(x)\left[1 + \frac{p}{b(u_s(x))}\right] = \left[1 + \frac{p}{b(1)} - \alpha - \frac{p\alpha}{b(\alpha)}\right] x + \alpha + \frac{p\alpha}{b(\alpha)}. \tag{3.33}$$

(Note that, in the original, dimensional variables, relation (3.32) becomes $\sigma = bC/\beta(C)$, the relation which we expected to find in regions where σ and C evolve slowly.)

The formula (3.33) cannot be used to express u_s explicitly as a function of x, but it can be inverted to give x as a function of u_s:

$$x(u_s) = \frac{u_s\left[1 + \frac{p}{b(u_s)}\right] - \alpha\left[1 + \frac{p}{b(\alpha)}\right]}{1 + \frac{p}{b(1)} - \alpha\left[1 + \frac{p}{b(\alpha)}\right]}. \tag{3.34}$$

Since we are looking for shocks in $u_s(x)$, we want to know whether $x(u_s)$ possesses any extrema in $0 < x < 1$; an extremum in $x(u_s)$ will correspond to a multivalued "solution" $u_s(x)$ whose true form will be a shock (see Figure 3.16). $x(u_s)$ exhibits an extremum at any point where $x'(u_s)$ changes sign. Now,

$$x'(u_s) = (\text{const})\left(1 + \frac{p}{b(u_s)} - \frac{p u_s b'(u_s)}{[b(u_s)]^2}\right),$$

where

$$(\text{const}) \equiv \left(1 + \frac{p}{b(1)} - \alpha\left[1 + \frac{p}{b(\alpha)}\right]\right)^{-1}.$$

Since $b(u)$ is nearly constant except near $u = u_{RG}$, the third term in the expression for $x'(u_s)$ can be neglected near $u_s = \alpha$ and $u_s = 1$, so that $x'(u_s)$ will be proportional to the positive quantity $1 + p/b(u_s)$ near these points. Near $u_s = u_{RG}$, $b'(u_s)$ may be

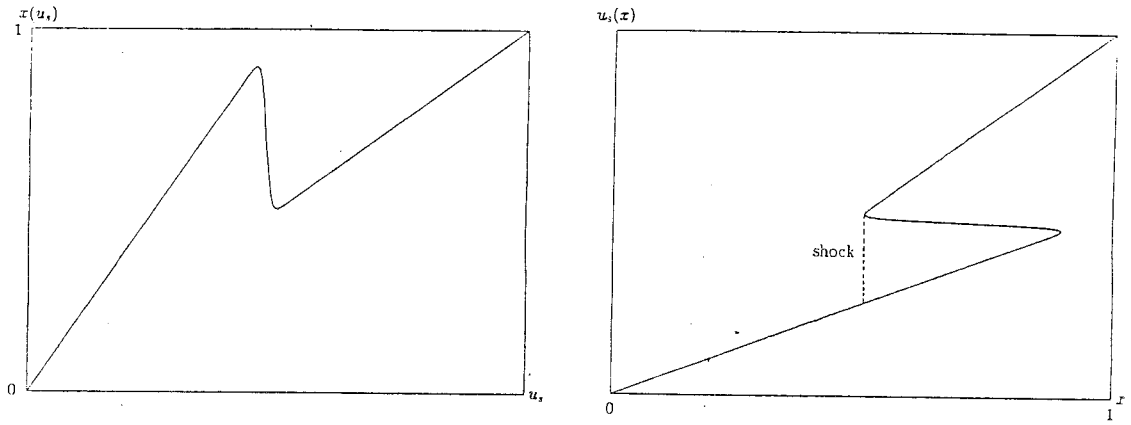

a: $x(u_s)$ b: $u_s(x)$

Figure 3.16: $x(u_s)$ and corresponding $u_s(x)$ with shock

large enough so that the third term in the expression for $x'(u_s)$ will force $x'(u_s)$ to be proportional to a negative quantity. Therefore, it is indeed possible for $u_s(x)$ to contain a shock.

To get a clearer idea of the form of $u_s(x)$, as well as some indication of the form of $s_s(x)$, we examine the limiting case $\Delta u = 0$. In this case, we can solve equation (3.34) for $u_s(x)$, finding

$$u_s < u_{RG}\text{: } u_s(x) = \alpha + \left[\frac{\omega(1+p)}{\omega+p} - \alpha\right] x \tag{3.35}$$

$$u_s > u_{RG}\text{: } u_s(x) = \frac{\alpha(\omega+p)}{\omega(1+p)} + \left[1 - \frac{\alpha(\omega+p)}{\omega(1+p)}\right] x, \tag{3.36}$$

so that $u_s(x)$ consists of two distinct line segments; these functions are, in fact, the $t \to \infty$ limit of (3.23) and (3.24), the time-dependent, first-order, $\Delta u = 0$, outer approximations to the solution u of equations (3.3) and (3.4). If

$$\alpha < \frac{\omega(1+p)}{\omega+p}, \tag{3.37}$$

then both segments have positive slopes, as in Figure 3.17a; if

$$\alpha > \frac{\omega(1+p)}{\omega+p}, \tag{3.38}$$

then both segments have negative slopes, as in Figure 3.17b. With ω set to 0.01, as in sections 3.1 and 3.2, relation (3.37) holds in three of the cases studied in those sections: $\alpha = 0$, $p = 1.5$; $\alpha = 0$, $p = 0.001$; and $\alpha = 0.5$, $p = 0.001$. Relation (3.38) holds in the case $\alpha = 0.5$, $p = 1.5$. We saw in the previous sections that, as t grows large, $u(x,t)$ tends toward a shape with two widely separated smooth curves (or, to first order in ε, two line segments) connected over a short distance in x by a curve with a steep gradient. The sign of the derivatives of these curves (to first order in ε, the slopes of the line segments) is, in all four of the parameter cases, as predicted by (3.37) and (3.38).

When $\Delta u = 0$, we can find an expression for $s_s(x)$ directly from (3.32), (3.35), and (3.36):

$$u_s < u_{RG}\text{: } s_s(x) = \frac{p\alpha}{\omega} + \frac{p}{\omega}\left[\frac{\omega(1+p)}{\omega+p} - \alpha\right]x \tag{3.39}$$

$$u_s > u_{RG}\text{: } s_s(x) = \frac{p\alpha(\omega+p)}{\omega(1+p)} + p\left[1 - \frac{\alpha(\omega+p)}{\omega(1+p)}\right]x. \tag{3.40}$$

$s_s(x)$ thus consists of two line segments with the same-signed slopes as $u_s(x)$.

We note that there are two special cases in which u_s and s_s do not contain shocks. When $p = 0$, so that the stress model is forced by the concentration rate only, the steady-state solutions are simply

$$u_s(x) = \alpha(1-x) + x$$

$$s_s(x) = 0.$$

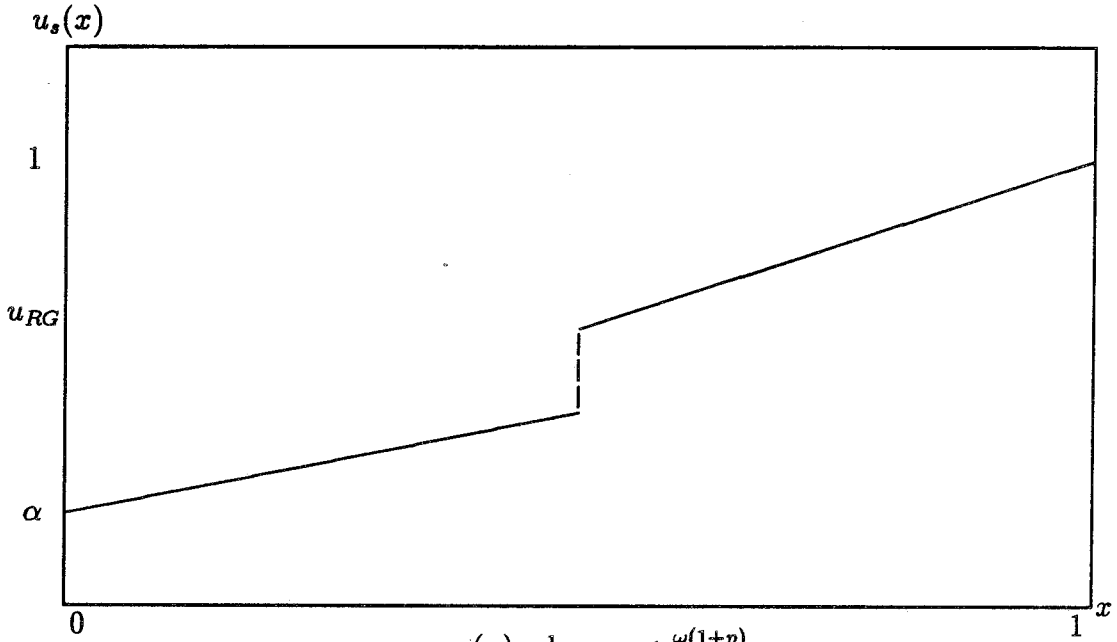

a: $u_s(x)$ when $\alpha < \frac{\omega(1+p)}{\omega+p}$

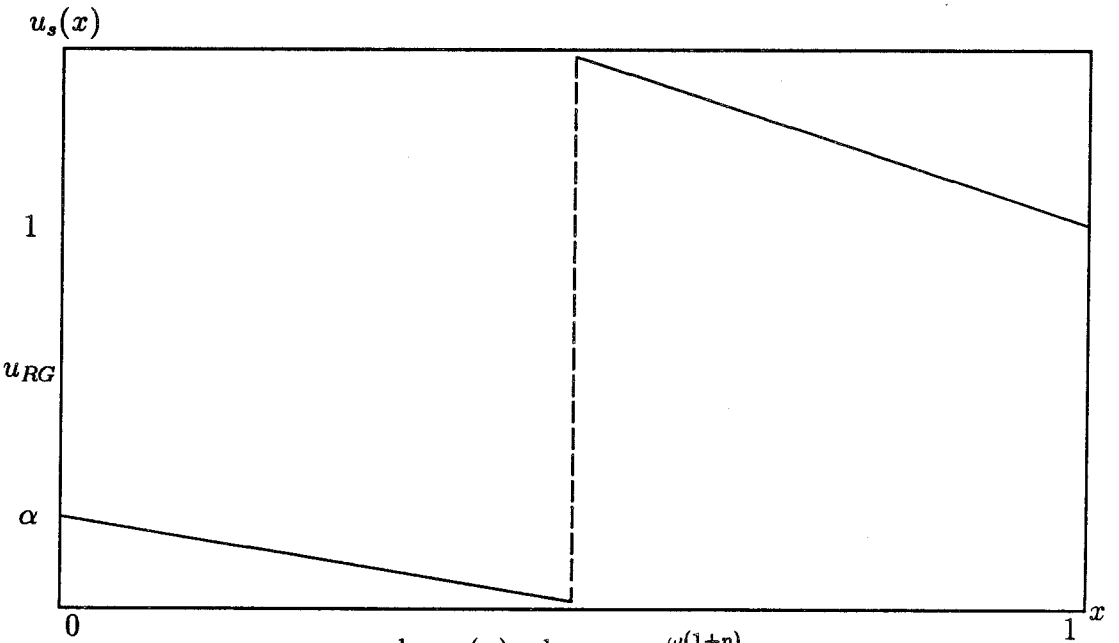

b: $u_s(x)$ when $\alpha > \frac{\omega(1+p)}{\omega+p}$

Figure 3.17: Two steady-state forms for $u_s(x)$

When $\omega = 1$, so that the relaxation time $1/b(u)$ is identically equal to 1 and the system (3.3), (3.4) is linear, the steady-state solutions are

$$\begin{aligned} u_s(x) &= \alpha(1-x)+x \\ s_s(x) &= p[\alpha(1-x)+x]. \end{aligned}$$

In all other cases, u_s and s_s contain shocks.

3.4 Conclusions

When $\varepsilon = \beta_R L^2/D$ is taken to be small, the polymer-penetrant system goes through two very different phases as time elapses. When the penetrant has been moving through the polymer for only a short time, the concentration and stress show smooth, diffusive profiles. After a longer time has elapsed, the concentration and stress profiles are no longer smooth, but instead possess steep gradients at the point where the polymer undergoes its glass–rubber transition. The steady-state solutions contain shocks at the glass–rubber transition point.

We can write approximate representations of the concentration and stress as explicit functions of distance and time when ε is taken to be small and the polymer's relaxation time is taken as piecewise constant, dropping where the polymer undergoes its glass–rubber transition. While these explicit functions are only approximations to the actual concentration and stress profiles, they provide correct information about both the short-time and the long-time behavior of the concentration and stress. For small times, the explicit functions predict correctly that the concentration and stress evolve diffusively; for longer times, they predict the evolution of steep gradients in the concentration and stress, and, in steady state, they can be used to derive a relation among several of the problem's parameters which predicts the correct shapes of the concentration and stress profiles.

Chapter 4

Conclusions and Future Research Suggestions

We have presented analysis of a mathematical model of non-Fickian polymer-penetrant drug-delivery systems. The model is composed of evolution equations for the penetrant concentration $C(X,T)$ and the viscoelastic stress $\sigma(X,T)$:

$$\frac{\partial C}{\partial T} = \frac{\partial}{\partial X}\left(D(C)\frac{\partial C}{\partial X} + E\frac{\partial \sigma}{\partial X}\right) + \mu C(k-C) \tag{4.1}$$

$$\frac{\partial \sigma}{\partial T} = -\beta(C)\sigma + a\frac{\partial C}{\partial T} + bC. \tag{4.2}$$

We have taken the diffusivity $D(C)$ and the relaxation time $\beta(C)^{-1}$ to be either constants or smoothed step functions with positive slopes. We defined these step functions to change value near C_{RG}, the concentration at which glass–rubber transition occurs.

This model accounts for the non-Fickian behavior of the polymer-penetrant system by adding stress-induced flux to the Fickian flux and by modeling the interaction of penetrant molecule with polymer site as a bimolecular reaction. The glassy polymer's resistance to diffusion and its slow relaxation after deformation are modeled by taking $D(C)$ and $\beta(C)$ to be small in $C < C_{RG}$.

We used perturbation analysis and numerical integration to examine the equations on two different domains. In Chapter 2, we took $X \in (-\infty, +\infty)$ and found traveling-wave solutions C and σ as functions of $X - VT$, V constant, under the assumption that the nondimensional analogue of k was small. In Chapter 3, we took $\mu = 0$ and D constant, and assumed that the nondimensional analogue of D and E was a single large parameter. We examined the evolution in time of C and σ on the finite domain $X \in [0, L]$, taking as boundary conditions infinite penetrant reservoirs of constant concentration at $X = 0$ and $X = L$. We took the concentration in the $X = 0$ reservoir to be less than C_{RG} and the concentration in the $X = L$ reservoir to be greater than C_{RG} in order to find interesting behavior.

Results

In Chapter 2, we presented traveling-wave results of our study of the model. We studied two cases for equation (4.2), $a = 0$ and $b = 0$. In both cases we started by analyzing the equations with $D(C)$ and $\beta(C)$ both constant. Regular perturbation expansion then showed that in both cases there was a solution C which dropped smoothly from $C(-\infty) = k$ to $C(+\infty) = 0$. When we took $b = 0$, we found that σ was very small over most of the range $-\infty < X - VT < +\infty$. Only where C was markedly different from either k or zero did σ rise far above zero; even at its largest, the nondimensional analogue of σ was much smaller than the nondimensional analogue of C. On the other hand, when we took $a = 0$, we found that, to first order, C and σ were equal.

We analyzed the stability of C to small perturbations in both cases. In the case $b = 0$, we found a restricted range of parameter values within which C was stable. In the case $a = 0$, we found that C was always stable.

We proceeded to study both cases under the assumption that $D(C)$ and $\beta(C)$

were smoothed step functions. We discovered that the problem was no longer solvable by a regular perturbation expansion; the expansion broke down near the glass–rubber transition concentration C_{RG}. We found the behavior of C near C_{RG} by approximating $D(C)$ and $\beta(C)$ as true step functions which changed values at C_{RG}. We discovered that the slope of C steepened near $C = C_{RG}$ in the *diffusion-driven* instance $DC_X > E\sigma_X$; in the *stress-driven* instance $DC_X < E\sigma_X$, the slope of C flattened near $C = C_{RG}$. We found that we could approximate σ by a regular perturbation expansion to first order and that, both for $a = 0$ and for $b = 0$, σ reached larger values when D and β were not constant than when they were constant. We successfully tested our analytical results by integrating the equations numerically, using a multiple shooting scheme.

In Chapter 3, we presented results of a singular perturbation analysis of the model equations on a finite domain. We found an initial layer near $T = 0$. In this layer, C and σ evolved according to a Fickian diffusion equation with diffusivity $D + aE$. Outside the initial layer, σ could be solved for as a function of C, and C evolved according to a nonlinear ordinary differential equation in T, in which X appeared only as a parameter. This ordinary differential equation could be solved under the assumption that $\beta(C)$ was a true step function. The resulting solutions C and σ each consisted of two distinct line segments, with a jump at a fixed internal value of X. When $\beta(C)$ was taken to be a smoothed step function and the equation for C was integrated numerically, the jumps in C and σ were replaced by steep, but not infinitely steep, fronts. The full set of equations was then solved numerically; the results were found to bear out the predictions of the perturbation analysis fully. Finally, the steady states of C and σ were examined and found to contain shocks.

In Appendix A, we presented traveling-wave solutions of Fisher's equation

$$\frac{\partial u}{\partial t} = \frac{\partial}{\partial x}\left(d(u)\frac{\partial u}{\partial x}\right) + u(1-u),$$

where we took the diffusivity $d(u)$ to be a smoothed step function like our $D(C)$. We found a qualitatively new traveling-wave solution u of the equation, one exhibiting steepening of its slope near the value of u at which the diffusivity rose sharply.

Suggestions for Future Research

We begin the suggestions for future research with points about the particular model that we studied. The existence and stability of traveling-wave solutions under the assumptions of constant diffusivity, constant relaxation time, and small saturation concentration have been demonstrated in Chapter 2. General existence and stability results for the variable diffusivity, variable relaxation time cases remain to be found. In addition, the equations have not yet been studied with both a and b nonzero in the traveling-wave frame.

The model itself could be modified. For example, changes could be made to the coefficients in the equations. The coefficient which we have called E ought to be a function of C satisfying $E(0) = 0$; when there is no penetrant present, there cannot be any penetrant flux, no matter how large the stress gradient is. Our coefficients a and b could also be taken as functions of C.

The model would probably produce quite different results if different relationships held among the various nondimensional parameters. In both chapters we have performed perturbation analyses about one small parameter and assumed that all other parameters were $O(1)$; taking the small parameter to be $O(1)$, or taking some of the others small as well, would change the results greatly. This consideration leads immediately to the most pressing need for further study: quantitative comparison of the mathematical results presented here to experimental results from the polymer-penetrant drug-delivery field.

Appendix A

Traveling-Wave Solutions of Fisher's Equation

Fisher's equation

$$u_t = (d(u)u_x)_x + u(1-u) \tag{A.1}$$

arises in many biological and physical systems [10,11,19]. It has been studied extensively with many different linear and nonlinear functional forms for $d(u)$ [10,11, 19,20,21]. Although a rather complete theory for traveling-wave solutions exists, we believe that we have produced a novel traveling-wave profile u. This profile emerges when we study equation (A.1) with

$$d(u) = \frac{1+\omega}{2} + \frac{1-\omega}{2}\tanh\frac{u-u_0}{\Delta u}. \tag{A.2}$$

Here $0 < \omega < 1$, $0 < u_0 < 1$, and $0 < \Delta u \ll 1$.

We were motivated to take $d(u)$ in this form because of our interest in traveling-wave solutions of the system (1.5), (1.6), which contains coefficient functions of the same shape as $d(u)$. In fact, the analysis of Fisher's equation presented in this appendix led us to the correct method of attack on our polymer-penetrant problem. Of particular interest to us is the work that has been done on existence of traveling-wave solutions of equation (A.1). Since the equation is second-order,

its traveling-wave solutions can be tracked easily in the phase plane. By making use of the already existing, large body of knowledge on Fisher's equation and the well-understood method of phase plane analysis, we obtain traveling-wave solutions of equation (A.1) with our choice for $d(u)$. We can then apply our knowledge and methods to the solution of equations (1.5) and (1.6).

We put equation (A.1) into the traveling-wave frame by setting

$$z \equiv x - vt, \ v \text{ constant.}$$

The resulting equation is

$$(d(u)u')' + vu' + u(1-u) = 0. \tag{A.3}$$

We look for monotonically decreasing solutions of equation (A.3) satisfying $0 \leq u(z) \leq 1$ and apply the boundary conditions

$$u(-\infty) = 1, \ u(+\infty) = 0.$$

For $d(u) \equiv A$, A a positive constant, a traveling-wave solution satisfying these boundary conditions has been found by Canosa [3] as a power series in the small parameter $1/v^2$:

$$u(z) = \frac{1}{1+C_0e^{z/v}} + \frac{1}{v^2}\frac{AC_0e^{z/v}}{(1+C_0e^{z/v})^2}\left[\ln\frac{C_0e^{z/v}}{(1+C_0e^{z/v})^2} + C_1\right] + O\left(\frac{1}{v^4}\right),$$

where C_0 and C_1 are constants. Furthermore, for $d(u) \equiv A > 0$, traveling-wave solutions of equation (A.3) have been searched for in the (u, u') phase plane, with results as in Figure A.1. Since u must lie between zero and one, we cannot accept the solution graphed in Figure A.1b, and, therefore, we require $v \geq 2\sqrt{A}$. We note that the unacceptable solution shown in Figure A.1b looks quite reasonable near $u = 1$; its deficiency becomes apparent only as it approaches $u = 0$.

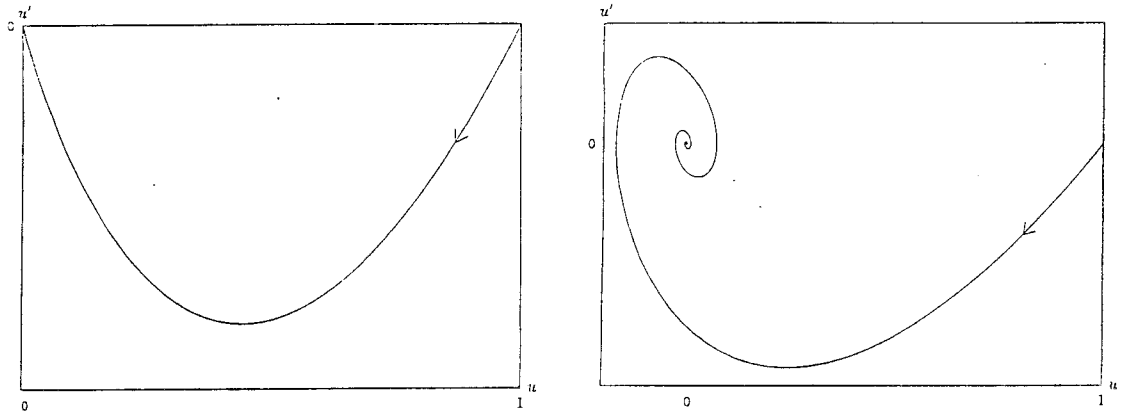

a: $v \geq 2\sqrt{A}$ b: $v < 2\sqrt{A}$

Figure A.1: (u, u') phase plane for $d(u) \equiv A$

To study the behavior of equation (A.3) with $d(u)$ as in equation (A.2), we first consider the extreme case $\Delta u \equiv 0$. $d(u)$ is piecewise constant in this case, so that equation (A.3) becomes

$$u > u_0: \quad u'' + vu' + u(1-u) = 0 \tag{A.4}$$

$$u < u_0: \quad \omega u'' + vu' + u(1-u) = 0. \tag{A.5}$$

If we require continuity of the flux J for all z, where

$$J \equiv -d(u)u_x = -d(u)u',$$

then at $u = u_0$ we set the condition

$$u'_R = \frac{u'_L}{\omega},$$

where the subscripts R and L refer respectively to the right and left halves of the (z, u)-plane. Since $\omega < 1$ and $u'(z) \leq 0$ for all z, we see that

$$|u'_R| > |u'_L| \iff u'_R < u'_L \text{ at } u = u_0,$$

so that the profile of $u(z)$ against z is as in Figure A.2.

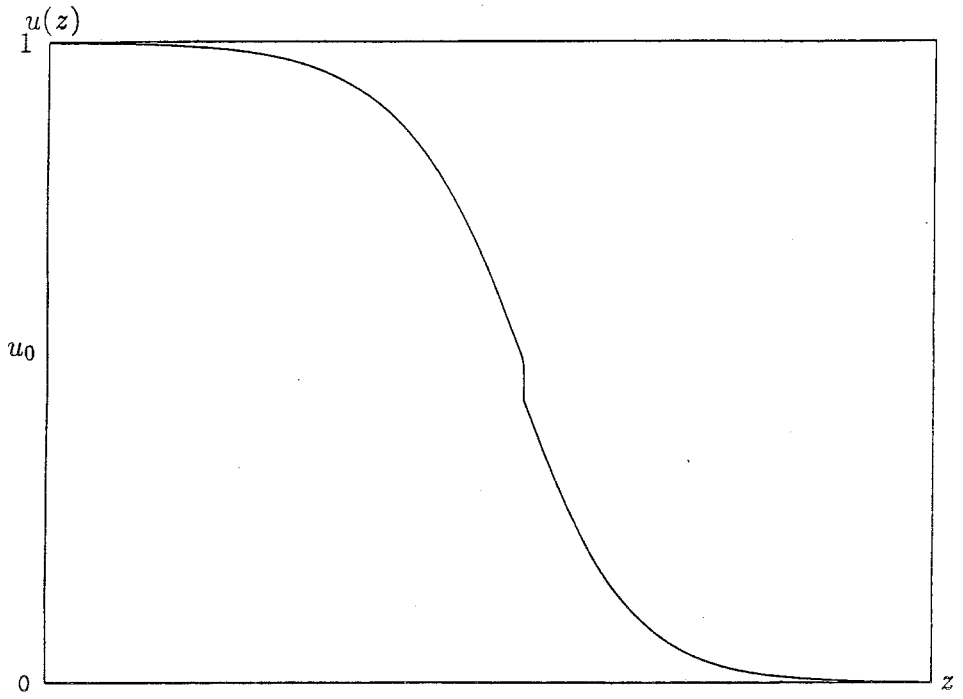

Figure A.2: $u(z)$ when $\Delta u = 0$

Strictly speaking, the "function" $u(z)$ thus defined is not a solution of equation (A.3). As we will see later, however, $u(z)$ is the relation obtained from a true solution of equation (A.3) in the limit $\Delta u \to 0$, so that study of the relation $u(z)$ is worthwhile.

We have not yet, in fact, proved the existence of a solution $u(z)$ satisfying (A.4), (A.5), and the boundary conditions $u(-\infty) = 1$, $u(+\infty) = 0$. We prove the existence of $u(z)$ by locating it in the (u, u') phase plane.

The stationary points of both equation (A.4) and equation (A.5) are the same: $(u, u') = (1, 0)$ and $(u, u') = (0, 0)$. The point $(1, 0)$ is a saddle point in both systems, and has an outgoing arm that moves through $u < 1$, $u' < 0$. Therefore, in the region $u > u_0$ where equation (A.4) holds, we have the first part of the monotonically decreasing solution, satisfying $u(-\infty) = 1$, that we want.

When the curve we are following reaches $u = u_0$, it must link up to a solution

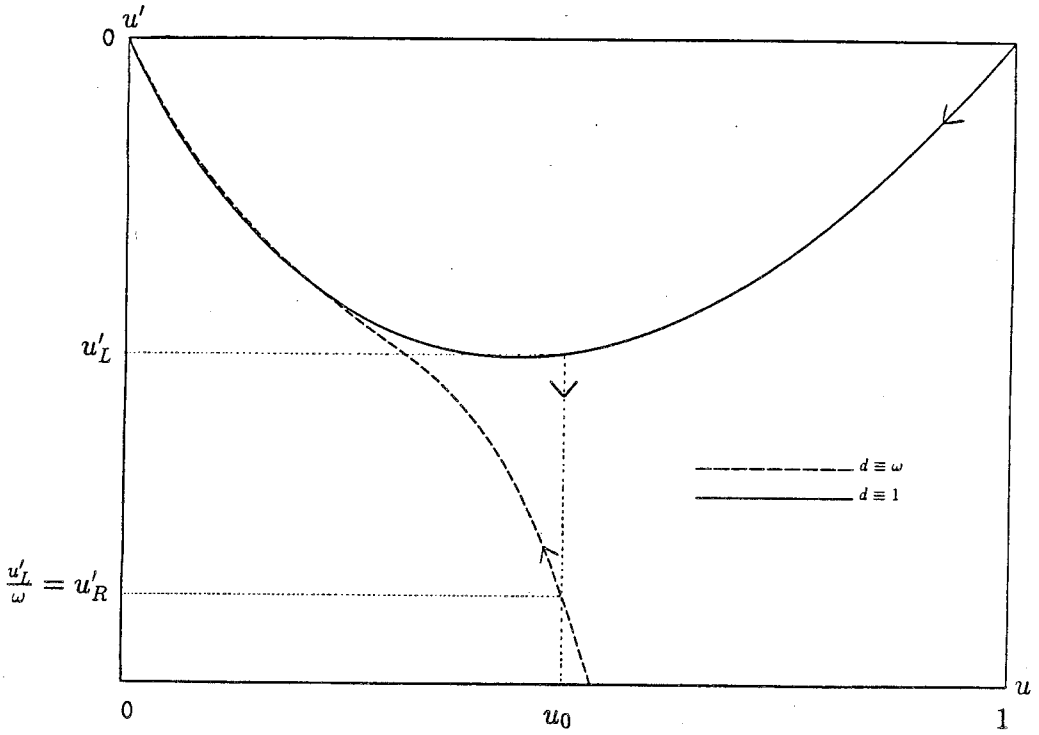

Figure A.3: (u, u') phase plane displaying $\Delta u = 0$ solution trajectories

of equation (A.5). When $v \geq 2\sqrt{\omega}$, the stationary point $(u, u') = (0, 0)$ of equation (A.5) is a stable node. (As we see from Figure A.1b, taking $v < 2\sqrt{\omega}$ leads to unacceptable behavior near $(u, u') = (0, 0)$.) Our solution $u(z)$ can, if $v \geq 2\sqrt{\omega}$, drop from its position $(u, u') = (u_0, u'_L)$ to the solution curve of (A.5) containing the point $(u, u') = (u_0, u'_L/\omega)$ and follow this curve into the node $(u, u') = (0, 0)$.

In Figure A.3, we display a sketch of the (u, u') phase plane containing the trajectories discussed above. The solid curve is the solution of equation (A.4) that satisfies $u(-\infty) = 1$. At $(u, u') = (u_0, u'_L)$, u drops onto the dashed curve, a solution of equation (A.5) which contains the point $(u, u') = (u_0, u'_L/\omega)$; $u(z)$ then follows this curve into $(u, u') = (0, 0)$.

We note that the relationship between v and ω which must obtain in order that a meaningful solution $u(z)$ may exist is $v \geq 2\sqrt{\omega}$. Whatever the relationship between v and ω, the stationary point $(u, u') = (1, 0)$ is a saddle point with an outgoing

arm in the direction we desire. Only as our solution $u(z)$ approaches $u = 0$, in the region where u is a solution of equation (A.5), must we place any restriction on the relationship between v and ω.

If Δu is not identically zero, but is very small, we must solve equation (A.3) numerically. Using a fourth-order accurate Runge-Kutta method with step size control [2], we find that the solution $u(z)$ is very similar to the $\Delta u = 0$ solution found above, except in the region near $u = u_0$. We display phase-plane graphs showing solutions of equation (A.3) for several values of Δu in Figure A.4. We use the parameter values $v = 1.5$, $u_0 = 0.5$, and $\omega = 0.5$, and decrease Δu steadily toward zero in order to compare the plots to the $\Delta u = 0$ plot in Figure A.4d. The $\Delta u = 0$ analysis proves to be useful in predicting the form of the traveling-wave solutions of equation (A.1).

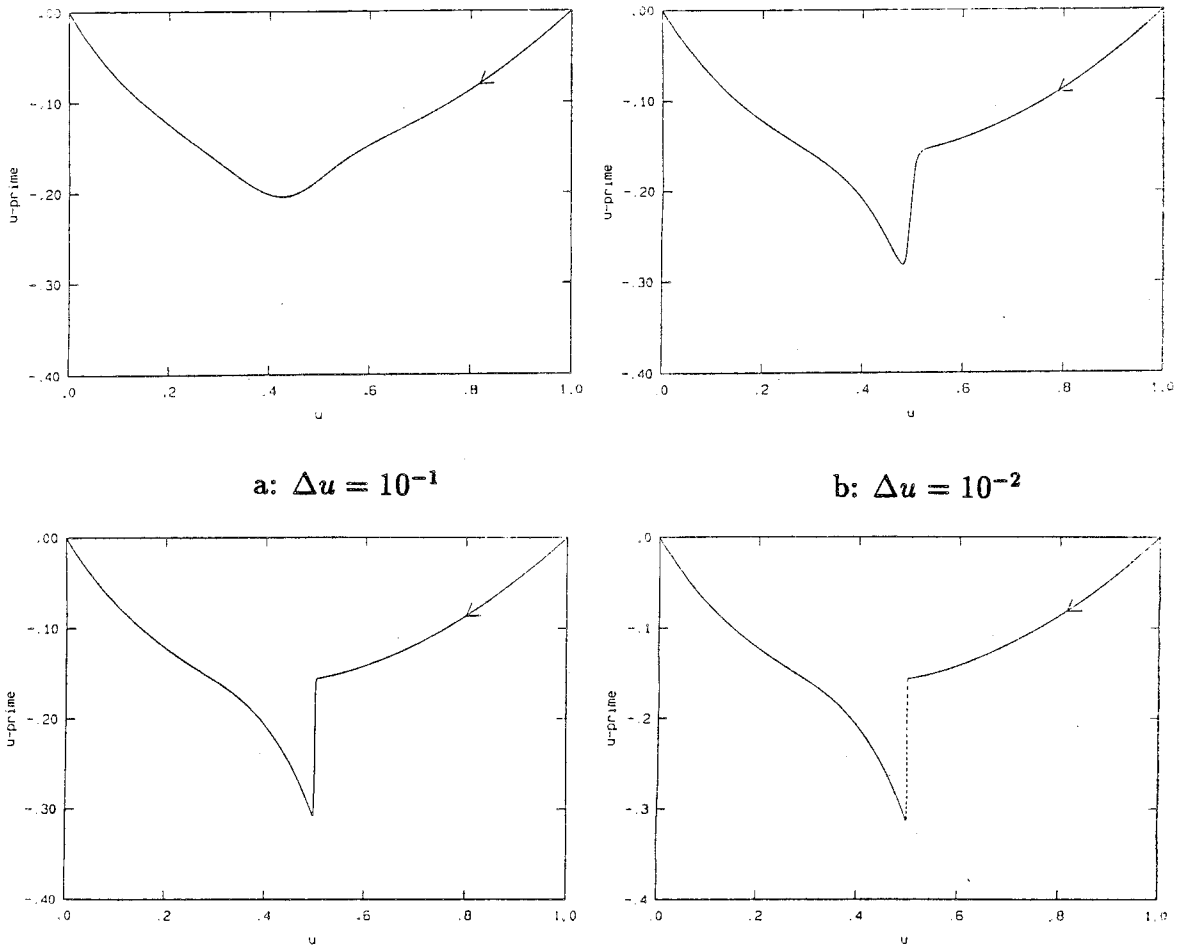

a: $\Delta u = 10^{-1}$

b: $\Delta u = 10^{-2}$

c: $\Delta u = 10^{-3}$

d: $\Delta u = 0$

Figure A.4: (u, u') phase plane showing effect of decreasing Δu

Bibliography

[1] T. Alfrey, E. F. Gurnee, and W. G. Lloyd, "Diffusion in glassy polymers," *Journal of Polymer Science C*, 12:249–261 (1966).

[2] C. T. H. Baker and C. Phillips, eds., *The Numerical Solution of Nonlinear Problems* (Clarendon Press, Oxford, 1981).

[3] J. Canosa, "On a nonlinear diffusion equation describing population growth," *IBM Journal of Research and Development,* 17:307–313 (1973).

[4] D. S. Cohen and A. B. White, Jr., "Sharp fronts due to diffusion and stress at the glass transition in polymers," *Journal of Polymer Science, Polymer Physics Edition,* 27:1731–1747 (1989).

[5] R. W. Cox, "Stress-assisted diffusion: a free boundary problem," submitted to *SIAM Journal of Applied Mathematics.*

[6] R. W. Cox and D. S. Cohen, "A mathematical model for stress-driven diffusion in polymers," *Journal of Polymer Science, Polymer Physics Edition,* 27:589–602 (1989).

[7] J. Crank, *The Mathematics of Diffusion,* 2nd edition (Clarendon Press, Oxford, 1975).

[8] C. J. Durning, "Differential sorption in viscoelastic fluids," *Journal of Polymer Science, Polymer Physics Edition,* 23:1831–1855 (1985).

[9] J. D. Ferry, *Viscoelastic Properties of Polymers,* 3rd edition (John Wiley and Sons, New York, 1980).

[10] P. C. Fife, *Mathematical Aspects of Reacting and Diffusing Systems* (Springer-Verlag, Berlin, Heidelberg, New York, 1979).

[11] R. A. Fisher, "The wave of advance of advantageous genes," *Annals of Eugenics,* 7:355–369 (1937).

[12] H. L. Frisch, "Sorption and transport in glassy polymers—a review," *Polymer Engineering and Science,* 20:2–13 (1980).

[13] C. Garcia-Reimbert, *Stable synchronization waves in neural networks and traveling waves in glassy polymers,* Ph.D. thesis, Department of Mathematics, University of Utah, Salt Lake City, 1986.

[14] E. A. Guillemin, *The Mathematics of Circuit Analysis* (John Wiley and Sons, New York, 1949).

[15] E. Kálnay de Rivas, "On the use of nonuniform grids in finite-difference equations," *Journal of Computational Physics,* 10:202–210 (1972).

[16] J. Kevorkian and J. D. Cole, *Perturbation Methods in Applied Mathematics* (Springer-Verlag, New York, 1981).

[17] R. S. Langer and D. S. Wise, eds., *Medical Applications of Controlled Release, Volume I* (CRC Press, Boca Raton, 1984).

[18] J. M. McKelvey, *Polymer Processing* (John Wiley and Sons, New York, 1962).

[19] J. D. Murray, *Lectures on Nonlinear-Differential-Equation Models in Biology* (Clarendon Press, Oxford, 1977).

[20] J. D. Murray, "A simple model for obtaining approximate solutions for a class of diffusion-kinetics enzyme problems: I. General class and illustrative examples," *Mathematical Biosciences,* 2:379–411 (1968).

[21] T. Nagylaki, "Conditions for the existence of clines," *Genetics,* 80:595–615 (1975).

[22] N. L. Thomas and A. H. Windle, "A theory of Case II diffusion," *Polymer,* 23:529–542 (1982).

[23] N. L. Thomas and A. H. Windle, "Transport of methanol in poly(methylmethacrylate)," *Polymer,* 19:255–265 (1978).

[24] G. B. Whitham, *Linear and Nonlinear Waves* (John Wiley and Sons, New York, 1974).